Study of ion cyclotron heating of plasma(Dissertation_全文)

AUTHOR(S):

Mohri, Akihiro

Study of Ion Cyclotron Heating of Plasma

Akihiro MOHRI

S T U D Y O F I O N C Y C L O T R O N H E A T I N G O F P L A S M A

Doctor Thesis of Kyoto University

A k i h i r o M O H R I

1 9 6 5

SYNOPSIS

Time varying electromagnetic field, produced by electrodes or coils with configuration that has a central axis and azimuthal and axial periodicities, is analyzed in general. As special cases of such a configuration, many types of electromagnetic fields, such as helical type, line cusp type and mirror type are found. Many configurations of electromagnetic fields used for plasma heating can be reduced to these special cases.

Ion motions, rf power absorption and other cooperative phenemena of plasma in the helical type field and the picket fence field are investigated. It can be found that these rf fields are suitable for ion cyclotron heating of plasma, when a strong axial magnetic field is externally imposed. If the plasma density is considerably higher, circularly polarized fields rotating in the same sense as would ions are shielded by the reacting ion currents. Reversely polarized field , however, penetrates into the plasma without considerable change in its magnitude. The peak of the rf power absorption curve drawn as a function of the external magnetic field or the rf frequency is expected to shift from the corresponding ion cyclotron resonance position, when the plasma is beam-like. This theoretically predicted shift

was experimentally verified by using a plasma generator "Heliotron-B". The helical type field was attempted and could raise electron temperature up to 7×10^5 ^{o}K in helium discharge.

Ion cyclotron waves with nonaxisymmetric modes are generally analyzed, where an ion beam is flowing. A boundary condition, that a cylindrical plasma is coaxially immersed in a cylindrical sheet current and has a vacuum clearance with the sheet, is taken into account. The resulting inner field, the ion current, the electron current are also discussed. As special cases of this general mode, dispersion relations for axisymmetric mode given by Stix or for nonaxisymmetric mode without axial ion current given by Bernstein and Trehan are found.

It can be found that momentum transfer of ions to neutral molecules causes a broadening of the absorption curve of ion cyclotron resonance. Rf field penetration and power dissipation in slightly ionized gas are also analyzed under the boundary condition of a cylindrical configuration. Experimentally, this broadening could be verified. Some collision frequencies for different conditions were determined.

Experiments on theion cyclotron heating of plasma was made by using the Heliotron-B device. The plasma generated by a Joule heating was supplied with rf

power of 100 kilowatts, and ion cyclotron waves was excited in a rf coil region and then damped in the slopes of the Heliotron magnetic field. As a result, ion temperature could be raised up to 4×10^5 ^{o}K. Electron temperature was insensible to this heating.

PREFACE

The successful release and utilization of the nuclear fusion energy of deuterium will serve the human being an inexhaustible energy source. In order to realize this controlled fusion reaction, we must first investigate the generation of deuterium plasma of extremely high temperature. Many procedures to get such a plasma may be considered. One of them is that, in the first stage, deuterium gas is brought to a fully ionized plasma and then heated and confined in a strong magnetic vessel. The heating method in this case, of course, much concerns the confining field itself. A plasma generator named "Heliotron-B" of Kyoto University belongs to this type. "Ion cyclotron heating" is one of the heating methods applicable to the confining field of the Heliotron-B device.

This thesis is the record of the investigation of ion cylotron heating of plasma, which was carried out by the author as a member of Kyoto University High Temperature Plasma Researching System called "Helicon Project".

It should be noted that Gauss units are used throughout this thesis, except for a description of electric currents in the magnetic coils of the device. Because it is convenient to the treatment of plasma behaviours, such as phase velocity, plasma density,

and wave length of spectral line.

The author would like to express his appreciation to Professor Shigenori Hayashi of Kyoto University for his kind guidance and continuous encouragement through this work. The late Professor Shūjiro Kunii and Professor Goro Kamimoto kindly gave the author a chance to receive the guidance of Professor S. Hayashi. Professor Tsunehiko Shidei and Dr. Shukuro Yano first drew the author's attention to the subject of ion cyclotron heating of plasma. The author is also indebted to Dr. Koji Uo and Dr. Ryohei Itatani for valuable discussion and advice. Mr. Hiroshi Oshiyama helped with the experiment in the chapters VI and VII and contributed valuable discussion. Dr. Riso Kato and Mr. Keishi Ishii suggested optical measurements of plasma, while Mr. Makoto Takahashi and Mr. Seiichi Ariga also helped with the experiment. The author is also grateful of other colleagues of Helicon Project of Kyoto University.

CONTENTS

I High Frequency Coil for Plasma Heating

1.1 Introduction

Many configurations of time varying electromagnetic field for plasma heating have been proposed and applied to experimental devices. However, it seems that such configurations have not been generally analyzed. Difficulties of general treatment of these fields may be due to the fact that the configuration of field for plasma heating must concern itself with the configuration of magnetic field for plasma confinement. Behaviours of plasma induced by the heating field, such as charge separation, must also be taken into account.

If it is able to find the common properties between the configurations of field for plasma heating and those for plasma confinement, then the way of the general treatment will be revealed. These common properties essentially originate from human nature and technical facilities, since human kind lives in three dimensional space and can make things only of three dimensional geometry. Furthermore, it should be remembered that plasma under fusion reaction must be confined in a bounded volume with a closed surface, as torus, ellipsoid, spheroid, wheel limniscoid, etc. Generally these have geometrically three axes. From the viewpoint of engineering, configurations with an axis are easy to

e realized. Therefore it should be concluded that we ıst deal with the configuration which has at least one ‹is.

In fact, most of the devices for plasma experiment ıve a configuration with an axis or more. For instance, ɔellarators[1] of Princeton University and Heliotron[2] of ɣoto University are of race-track shape and have two ‹es. Mirror machines, as DCX[3] of Oak Ridge, FELIX[4] or ƧRL, etc., have a central axis. As far as the small ɛction of a torus or race-track is concerned, its ɔnfiguration may be regarded as that with an axis.

On the basis of the above mentioned facts, configu- ıtions with a central axis are dealt with in this ıapter.[61] Electric field for plasma heating may be Lassified into two types according to their production ɛchanism; one is electrostatic field and the other ıduced field. However, in many practical cases, both ɣpes of fields coexist and produce a complicated ɔnfiguration.

In the next section 1.2, we deal with electrostatic ield with a central axis. And electric field induced ɣ time varying magnetic field will be discussed in a ɛction 1.3. Combined field of both types is also ɛalt with in a section 1.4.

Since relatively low frequency field is of interest ı the case of magnetic pumping or ion cyclotron heating

of plasma, displacement current is neglected in the analyses through these sections. As the special case of this general configuration, many types of electromagnetic fields, such as helical type, line cusp type and mirror type, are found. Many configurations of electromagnetic fields used for plasma heating can be reduced to these special cases.

1.2 Electric Field Produced by Electrodes

In order to treat the problem generally, we consider time varying electric field in vacuum produced by electrodes with the configuration that has a central axis and azimuthal and axial periodicities. Let us assume that the frequency of the field is sufficiently low enough for displacement current to be neglected. In other words, we treat the case in which the characteristic length of the machine under consideration is very short in comparison with the electromagnetic wave length with that frequency. Whence, the problem can be reduced to solve the Laplacian equation:

$$\nabla^2 \phi = 0, \qquad (1\text{-}1)$$

under given conditions, where ϕ is a scalar electric potential. Electric field $\vec{E}$ can be obtained from the potential ϕ by using the relation as

$$\vec{E} = -\vec{\nabla}\phi. \qquad (1\text{-}2)$$

Since we are interested in configurations with an axis, it is suitable to use cylindrical co-ordinates (r, θ, z). Equation (1-1) is expressed in cylindrical co-ordinates as

$$\frac{1}{r}\frac{\partial}{\partial r}\left(r\frac{\partial\phi}{\partial r}\right) + \frac{1}{r^2}\frac{\partial^2\phi}{\partial\theta^2} + \frac{\partial^2\phi}{\partial z^2} = 0. \qquad (1\text{-}3)$$

To solve the above equation, we shall seek the solution such as

$$\phi = R(r)F(\theta)Z(z)f(t). \qquad (1\text{-}4)$$

Here $F(\theta)$ and $Z(z)$ are periodic functions of θ and z, respectively, and $f(t)$ is a function of time t. Therefore we can express $Z(z)$ by means of a Fourier series:

$$Z(z) = \sum_{\nu=1}^{\infty} Z_\nu = \sum_{\nu=1}^{\infty}\left\{c_\nu \cos(\nu kz) + d_\nu \sin(\nu kz)\right\}. \qquad (1\text{-}5)$$

Substituting equations (1-4) and (1-5) into equation (1-3), we have

$$\sum_{\nu=1}^{\infty}\left[FZ_\nu\left\{\frac{\partial^2 R}{\partial r^2} + \frac{1}{r}\frac{\partial R}{\partial r} - \nu^2 k^2 R\right\} + \frac{RZ_\nu}{r^2}\frac{\partial^2 F}{\partial\theta^2}\right] = 0. \qquad (1\text{-}6)$$

From the fact that equation (1-6) must be held for any value of z, we obtain

$$R(r) = \sum_{n=0}^{\infty} \left\{ A_n I_n(\nu kr) + B_n K_n(\nu kr) \right\} \qquad (1\text{-}7)$$

and

$$F(\theta) = \sum_{n=0}^{\infty} \left\{ P_n \cos n\theta + Q_n \sin n\theta \right\} , \qquad (1\text{-}8)$$

where I_n and K_n are the modified Bessel functions of the first kind and of second kind, respectively, and A_n, B_n, P_n and Q_n are constants which should be determined from boundary conditions. On the other hand, a particular solution of equation (1-3) is found to be

$$\Phi = f(t)\left\{ e_1 \log r + e_2 \theta + e_3 z \right\} . \qquad (1\text{-}9)$$

Again e_1, e_2 and e_3 are constants. Thus we get the general solution of equation (1-3):

$$\Phi = f(t)\left[e_1 \log r + e_2 \theta + e_3 z + \sum_{\nu=1}^{\infty} \sum_{n=0}^{\infty} \left\{ c_\nu \cos(\nu kz) + d_\nu \sin(\nu kz) \right\} \times (P_n \cos n\theta + Q_n \sin n\theta) \left\{ A_n I_n(\nu kr) + B_n K_n(\nu kr) \right\} \right] . \qquad (1\text{-}10)$$

The analytical procedures introducing equation (1-10) was first developed by Uo.[5] He adopted this method so as to analyze the static magnetic field such as the Heliotron field.

Imposing following boundary conditions on equation (1-10), that is,

$$|E| \text{ is finite at } r=0$$
$$E_r = 0 \quad \text{when} \quad n\theta + \nu kz = m\pi, \quad m=0,1,2,\ldots \quad , \tag{1-11}$$

we obtain finally

$$\Phi = f(t)\left[e_3 z + \sum_{\nu=-\infty}^{+\infty}\sum_{n=0}^{\infty} A_{n\nu} I_n(\nu kr)\sin(n\theta + \nu kr)\right] . \tag{1-12}$$

Substituting equation (1-12) into equation (1-2), we obtain the expressions of the electric field

$$\left.\begin{aligned} E_r &= -f(t)k\sum_{\nu=-\infty}^{+\infty}\sum_{n=0}^{\infty}\nu A_{n\nu} I_n'(\nu kr)\sin(n\theta + \nu kz), \\ E_\theta &= -f(t)\frac{1}{r}\sum_{\nu=-\infty}^{+\infty}\sum_{n=0}^{\infty} nA_{n\nu} I_n(\nu kr)\cos(n\theta + \nu kz), \\ E_z &= -f(t)\left[e_3 + k\sum_{\nu=-\infty}^{+\infty}\sum_{n=0}^{\infty}\nu A_{n\nu} I_n(\nu kr)\cos(n\theta+\nu kz)\right]. \end{aligned}\right\} \tag{1-13}$$

Needless to say, each constant in equation (1-13) should be determined from boundary conditions. However, these boundary conditions are much concerned with the configuration of electrodes in a given special case. Therefore, let us consider several special cases in following small sections.

1.2.1 Case that n=0 and ν=1

The condition n=0 corresponds to an axisymmetric configuration. When n=0, equations (1-12) and (1-13)

become

$$\Phi = f(t)\left[e_3 z + \sum_{\nu=-\infty}^{+\infty}{}' A_{0\nu} I_0(\nu kr)\sin(\nu kz)\right] \qquad (1\text{-}14)$$

and

$$\left.\begin{aligned} E_r &= -f(t)k\sum_{\nu=-\infty}^{+\infty}{}' \nu A_{0\nu} I_1(\nu kr)\sin(\nu kz), \\ E_\theta &= 0, \\ E_z &= -f(t)\left[e_3 + k\sum_{\nu=-\infty}^{+\infty}{}' \nu A_{0\nu} I_0(\nu kr)\cos(\nu kz)\right]. \end{aligned}\right\} \qquad (1\text{-}15)$$

Clearly equation (1-15) gives exact solutions of any given configuration of axisymmetric field.

On the other hand, the approximate field expressions of the configuration of electrodes shown in Fig. 1-1 are found, by putting $\nu=1$, to be

$$\Phi = f(t)\left[e_3 z + A_{01} I_0(kr)\sin(kz)\right], \qquad (1\text{-}16)$$

$$\left.\begin{aligned} E_r &= -f(t)\, kA_{01} I_1(kr)\sin(kz), \\ E_\theta &= 0, \\ E_z &= -f(t)\left[e_3 + kA_{01} I_0(kr)\cos(kz)\right]. \end{aligned}\right\} \qquad (1\text{-}17)$$

If the potential diference between neighbouring electrodes where $r=r_0$ is Φ_0 when $t=t_0$, the constant A_{01} is determined to be

$$A_{o1} = - \frac{\phi_o}{2f(t_o) I_o(kr_o)} \quad .$$

Furthermore, the condition

$$\int_0^{\frac{2\pi}{k}} E_z \, d_z = 0$$

introduces

$$e_3 = 0.$$

Thus under these conditions, we have

$$\left.\begin{aligned} E_r &= \frac{1}{2} \frac{f(t)}{f(t_o)} k\phi_o \frac{I_1(kr)}{I_o(kr_o)} \sin(kz), \\ E_\theta &= 0, \\ E_z &= \frac{1}{2} \frac{f(t)}{f(t_o)} k\phi_o \frac{I_o(kr)}{I_o(kr_o)} \cos(kz). \end{aligned}\right\} \qquad (1\text{-}18)$$

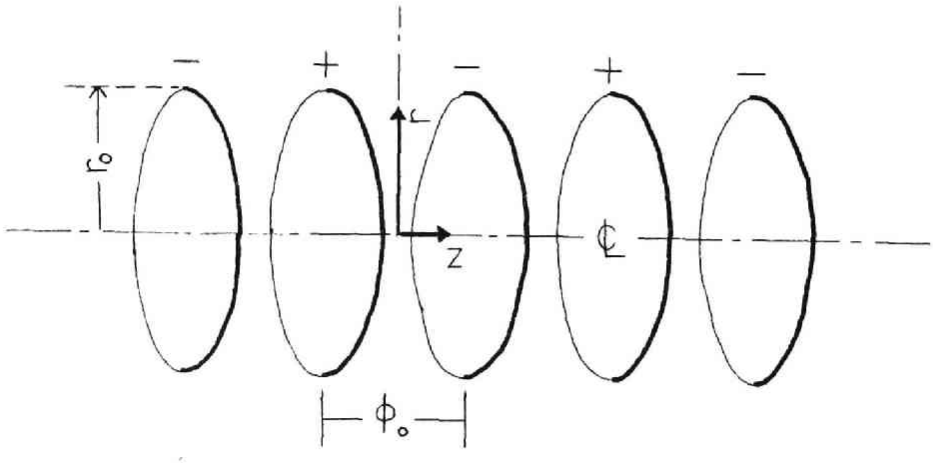

Fig. 1-1 Configuration of ring electrodes when n=0 and p=1.

It is clarified from equation (1-18) that, when ϕ_o is constant, the axial field on the z-axis decreases as $\frac{1}{k}$ or r_o decreases.

This field configuration is the same as linear accelerators for heavy ions. If an external magnetic field is present parallel to the z-axis, one may expect the axial acceleration of charged particles along the magnetic lines of force. However, all particles are not always in phase with the electric field. Some particle may be subject to a trapping similar to that in longitudinal electrostatic plasma oscillations.

Some trials to adopt this kind of acceleration had been done by K. Watanabe and his coworkers (1963)[6]. Their experimental device had a discharge tube of a eight-figure shape, which consisted of ring electrodes of Alminium and insulator rings of epoxi-regin. The external magnetic field was energized by the currents in coils set around the discharge tube. As a result, a rotational transform would be acheived as Stellarator machines. But, unfortunately, they could not have fully ionized gases at high temperature inside the discharge tube.

One more example of the configuration of this type is also seen in a L-C resonant circuit shown in Fig. 1-2a. Voltage between the terminals of the inductive coil causes a electric field inside the coil. Stix's coil[7]

for ion cyclotron heating as shown in Fig.1-2b generates similar electric field inside the coil, which damages the excitation of ion cyclotron waves.

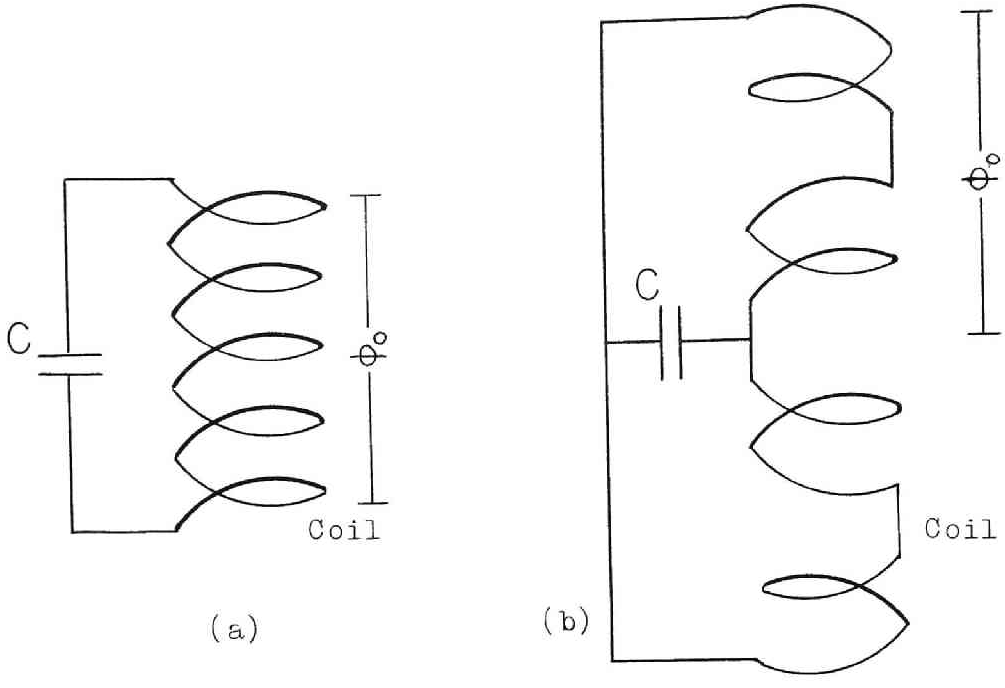

Fig. 1-2 Potential difference occurring in a resonance circuit.
(a) Ordinary induction coil
(b) Exciting coil of ion cyclotron waves

1.2.2 Case that $\nu=1$ and $kz\to 0$

This case corresponds to the situation that electrodes are set parallel to the axis at a constant interval where $r=r_0$ and their potential are periodic in the azimuthal direction.

In a region of small kr, equations (1-12) and (1-13) are put in the form, approximately, as

$$\Phi = f(t)\left[e_3 z + \sum_{n=0}^{\infty} A_{n1} \frac{k^n r^n}{2^n n!} \sin n\theta\right] , \qquad (1\text{-}19)$$

$$\left.\begin{aligned} E_r &= -f(t) \sum_{n=0}^{\infty} A_{n1} \frac{k^n r^{n-1}}{2^n (n-1)!} \sin n\theta , \\ E_\theta &= -f(t) \sum_{n=0}^{\infty} A_{n1} \frac{k^n r^{n-1}}{2^n (n-1)!} \cos n\theta , \\ E_z &= -e_3 . \end{aligned}\right\} \qquad (1\text{-}20)$$

Under the condition that the potential difference between the neighbouring electrodes is Φ_o when $t=t_o$ and only the terms where n=m in equations (1-19) and (1-20) are taken into account, we get

$$\Phi = -\frac{\Phi_o}{2} \frac{f(t)}{f(t_o)} \left(\frac{r}{r_o}\right)^m \sin m\theta , \qquad (1\text{-}21)$$

$$\left.\begin{aligned} E_r &= \frac{m\Phi_o}{2r_o} \frac{f(t)}{f(t_o)} \left(\frac{r}{r_o}\right)^{m-1} \sin m\theta , \\ E_\theta &= \frac{m\Phi_o}{2r_o} \frac{f(t)}{f(t_o)} \left(\frac{r}{r_o}\right)^{m-1} \cos m\theta , \\ E_z &= 0. \end{aligned}\right\} \qquad (1\text{-}22)$$

These equations give approximately the electric field of the configuration of electrodes shown in Fig. 1-3. It becomes evident from equation (1-22) that an increase of m is associated with a large decrease in the electric

field near the axis. The directions of the field is parpendicular to the axis, so that some parpendicular accelerations of charged particles may be expected when an externally applied magnetic field exists.

A trial to trap particles in a similar field has been made by T. Suita and his coworkers.[8)]

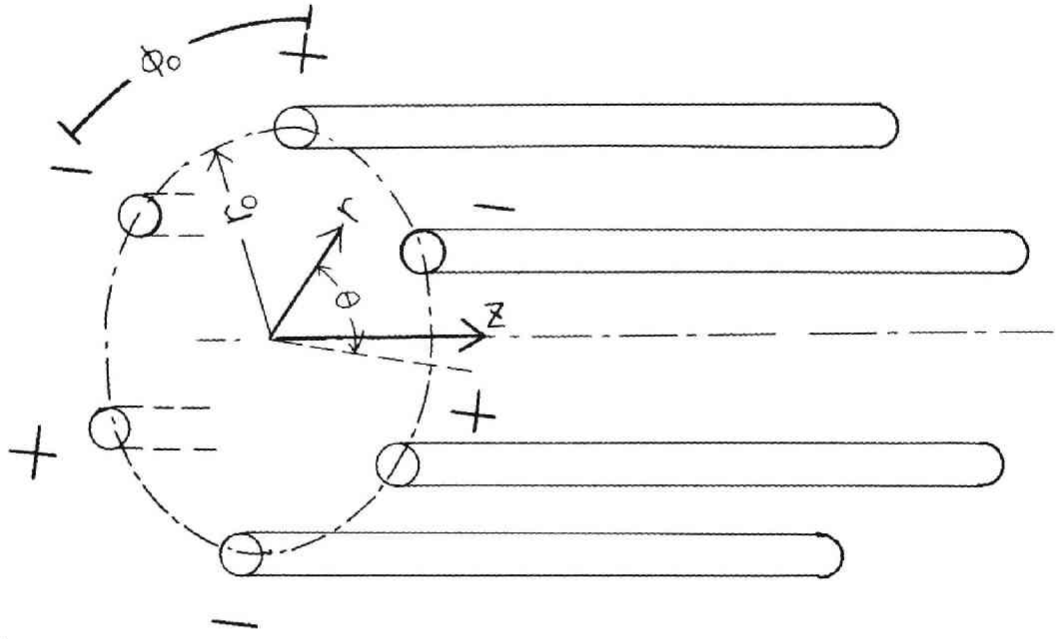

Fig. 1-3 Configuration of bar electrodes when n=m and kz→0. Here m=3 case is shown.

1.2.3 Helical Electrodes

Next we investigate the electric field of the configuration such that electrods are helical and set at a constant azimuthal interval where $r=r_o$. Fig.1-4 shows this configuration.

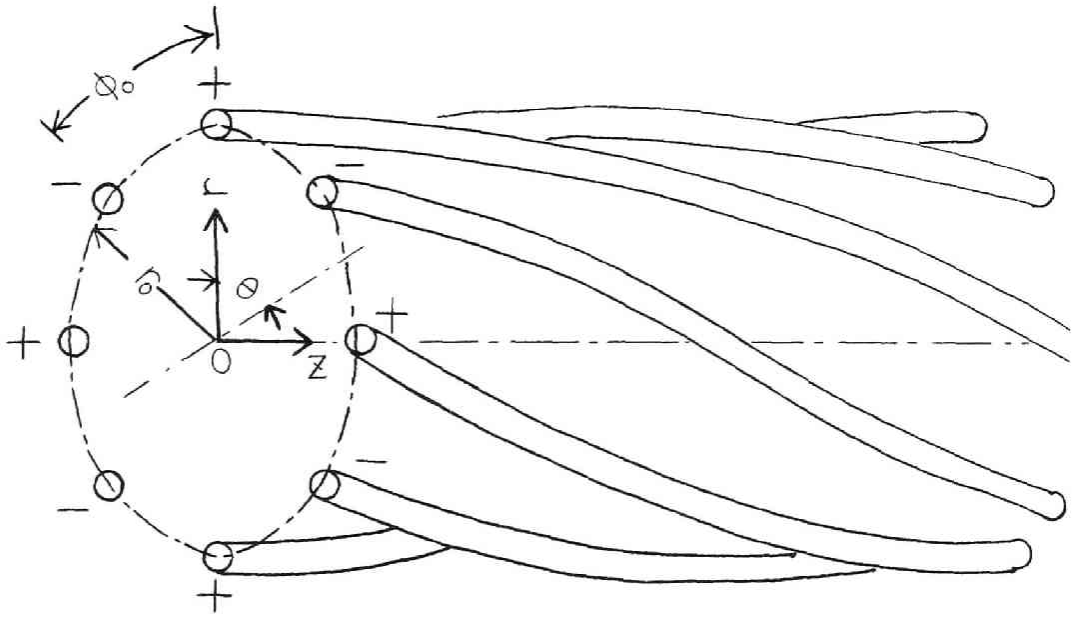

Fig. 1-4 Configuration of helical electrodes when n=m and =1. Here m=4 case is shown.

Whence approximate formulae of equations (1-12) and (1-13) are

$$\phi = f(t)\left[e_3 z + A_{ml} I_m(kr)\sin(m\theta + kz)\right], \qquad (1\text{-}23)$$

$$\left.\begin{aligned} E_r &= -f(t)kA_{ml} I_m'(kr)\sin(m\theta + kz), \\ E_\theta &= -f(t)\frac{m}{r}A_{ml} I_m(kr)\cos(m\theta + kz), \\ E_z &= -f(t)\left[e_3 + kA_m I_m(kr)\cos(m\theta + kz)\right]. \end{aligned}\right\} \qquad (1\text{-}24)$$

Under the condition that, when $t=t_o$ and $z=0$,

$$\phi_{\theta=\frac{\pi}{2m}(2p+1)} - \phi_{\vartheta=\frac{\pi}{2m}(2p)} = -\phi_o ,$$

(p: integer)

we have

$$\left.\begin{aligned} E_r &= \frac{f(t)}{f(t_o)} \frac{k\phi_o}{2I_m(kr_o)} I_m'(kr)\sin(m\vartheta+kz), \\ E_\theta &= \frac{f(t)}{f(t_o)} \frac{m\phi_o}{2I_m(kr_o)} \frac{1}{r} I_m(kr)\cos(m\vartheta+kz), \\ E_z &= \frac{f(t)}{f(t_o)} \frac{k\phi_o}{2I_m(kr_o)} I_m(kr)\cos(m\vartheta+kz). \end{aligned}\right\} \quad (1\text{-}25)$$

Especially, when m=1, equation (1-25) becomes

$$\left.\begin{aligned} E_r &= \frac{f(t)}{f(t_o)} \frac{k\phi_o}{4I_1(kr_o)} \sin(\theta+kz), \\ E_\theta &= \frac{f(t)}{f(t_o)} \frac{k\phi_o}{4I_1(kr_o)} \cos(\theta+kz), \end{aligned}\right\} \quad (1\text{-}26)$$

$$E_z = 0.$$

Equation (1-26) indicates that this field is a circularly polarized travelling field.

If we adopt complex co-ordinates perpendicular to the z-axis and assume that f(t) varies sinusoidally with time, then we can express the field by, instead of equation (1-26),

$$E = E_o \, (e^{i\omega t} + e^{-i\omega t}) e^{i(kz-\theta)} \quad (1\text{-}27)$$

where $E = E_r + iE_\theta$.

It becomes evident from equation (1-27) that this configuration of electrodes (i.e. m=1 mode) produces an effective field to heat charged particles by means of cyclotron resonance under the existence of an externally applied magnetic field. Discussions of the heatin by such a field is to be given in detail in the next chapter. Also the last chapter is devoted to describe an experiment of this field.

1.3 Induced Electric Field

When magnetic configuration are given beforehand, induced electric field can be found from Maxwell's equations. We shall analyze here the electric field induced by current flows whose configurations are similar to those of electrodes discussed in the previous section. Namely its configuration has a central axis and periodicities in both the axial and the azimuthal directions. K. Uo analized static magnetic fields which have similar configurations as will be discussed here. We are now interested in field with time variation, the frequency of which is sufficiently low so that displacement current can be neglected. Therefore, we can apply his method to the analyses of the magnetic field. Neglecting a displacement current, we have Maxwell's equations as

$$\vec{\nabla} \times \vec{E} = 0 \qquad (1\text{-}28)$$

$$\vec{\nabla} \cdot \vec{B} = 0 \qquad (1\text{-}29)$$

Thus we can express $\vec{B}$ in terms of a scalar potential φ, that is,

$$\vec{B} = \nabla\varphi \, . \qquad (1\text{-}30)$$

Substituting equation (1-30) into equation (1-28), we obtain

$$\nabla^2\varphi = 0 \, , \qquad (1\text{-}31)$$

which is to be solved under given boundary conditions.

The same procedure as in the previous section yields the general solution of equation (1-31). This solution is written in the cylindrical co-ordinates in the form:

$$\left.\begin{aligned} B_r &= f(t)k\sum_{\nu=-\infty}^{+\infty}\sum_{n=0}^{\infty}\nu A_{n\nu}I_n'(\nu kr)\sin(n\theta + \nu kz), \\ B_\theta &= f(t)\frac{1}{r}\sum_{\nu=-\infty}^{+\infty}\sum_{n=0}^{\infty}nA_{n\nu}I_n(\nu kr)\cos(n\theta + \nu kz), \\ B_z &= f(t)\left[e_1 + k\sum_{\nu=-\infty}^{+\infty}\sum_{n=0}^{\infty}A_{n\nu}I_n(\nu kr)\cos(n\theta + \nu kz)\right]. \end{aligned}\right\} \qquad (1\text{-}32)$$

Where $A_{n\nu}$ and e_1 are determined from boundary conditions. Induced electric field is readily obtained by using a Maxwell's equation:

$$\nabla \times \vec{E} = -\frac{1}{c}\frac{\partial \vec{B}}{\partial t}. \qquad (1\text{-}33)$$

Once a configuration of currents is given, the constant in equation (1-32) are determined and then the analysis of induced electric field is straightforward. Therefor in following small sections let us consider the several special configurations of currents and the correspondin electric fields.

1.3.1 Axisymmetric Configuration ($n=0$, $\nu=1$)

The condition $n=0$ means an axisymmetric configuration. In this case, equation (1-32) becomes

$$\left.\begin{aligned} B_r &= f(t)\ k\sum_{\nu=-\infty}^{+\infty} \nu A_{o\nu} I_1(\nu kr)\sin(\nu kz), \\ B_\theta &= 0, \\ B_z &= f(t)\left[e_1 + \sum_{\nu=-\infty}^{+\infty} \nu A_{o\nu} I_o(\nu kr)\cos(\nu kz)\right]. \end{aligned}\right\} \qquad (1\text{-}34)$$

The magnetic field produced by current flows as shown in Fig. 1-5 is approximately expressed in the form, by taking $\nu=1$,

$$\left.\begin{aligned} B_r &= f(t)\ kA_{o1} I_1(kr)\sin(kz), \\ B_\theta &= 0, \\ B_z &= f(t)\left[e_1 + kA_{o1} I_o(kr)\cos(kz)\right]. \end{aligned}\right\} \qquad (1\text{-}35)$$

Strictly speaking, equation (1-35) expresses the field configuration such that neighbouring ring currents are mutually opposite in their directions and arranged periodically along the z-axis. (Needless to say, equation (1-35) is also valid for the case that all currents are flowing in the same direction.)

Let the coil interval be a, the radius of the coils b and the ratio of the larger current to the opposite neighbouring smaller current λ. Then we can determine k, e_1 and A_{01} in equation (1-35). Many special configurations are found, according as different values of λ and a/b.

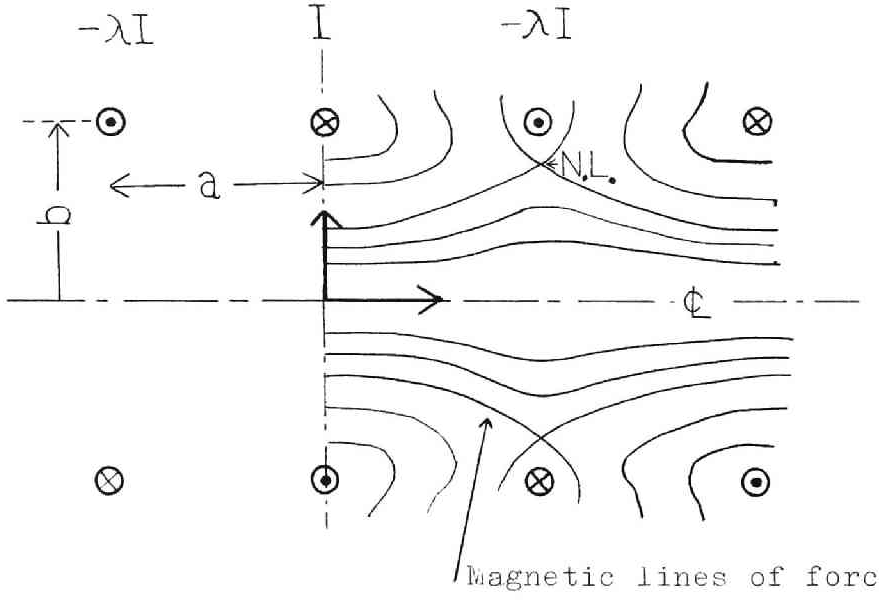

Fig. 1-5 Configuration of axisymmetric currents.

When the currents vary with time as $I \cdot f(t)$, we can determine the constants in equation (1-35) in terms of λ, a and b. Thus we obtain

$$B_e = kA_{o1} = \frac{\pi}{c} \frac{b^2 I}{a^3} (S_1 - S_2)(1+\lambda), \tag{1-36}$$

$$e_1 = \frac{\pi}{c} \cdot \frac{b^2 I}{a^3} (S_1 + S_2)(1-\lambda), \tag{1-37}$$

where

$$\left.\begin{aligned} S_1 &= \frac{a^3}{b^3} \left[1 + \frac{b^3}{4a^3} \frac{1}{\sqrt{\left(1+\frac{b^2}{4a^2}\right)^3}} + \cdots \right], \\ S_2 &= \frac{2}{\sqrt{\left(1+\frac{b^2}{a^2}\right)^3}} + \cdots . \end{aligned}\right\} \tag{1-38}$$

Equations (1-36) and (1-37) were introduced by K. Uo. Some configurations have circles N. L. (i.e. neutral line), at which magnetic field vanishes. Let the position of N. L. be at $(r_o, (2n+1)a)$, then we have

$$I_o(kr_o) = \frac{1-\lambda}{1+\lambda} \frac{S_1+S_2}{S_1-S_2} . \tag{1-39}$$

In terms of the above constants, equation (1-35) is rewritten to be

$$\left.\begin{aligned} B_r &= f(t)\ I_1(kr)\ \sin(kz), \\ B_\theta &= 0, \\ B_z &= f(t)\ B_e\left[I_0(kr_o) + I_0(kr)\cos(kz)\right]. \end{aligned}\right\} \quad (1\text{-}40)$$

Whence, equation (1-33) yields an induced electric field as

$$E_\theta = -f'(t)\ \frac{B_e}{kc}\left[\frac{1}{2}krI_0(kr_o) + I_1(kr)\cos(kz)\right]. \quad (1\text{-}41)$$

A number of induced field configurations of our interest can be derived from equation (1-41) for different λ and a/b.

(i) Case that $\lambda = S_2/S_1$

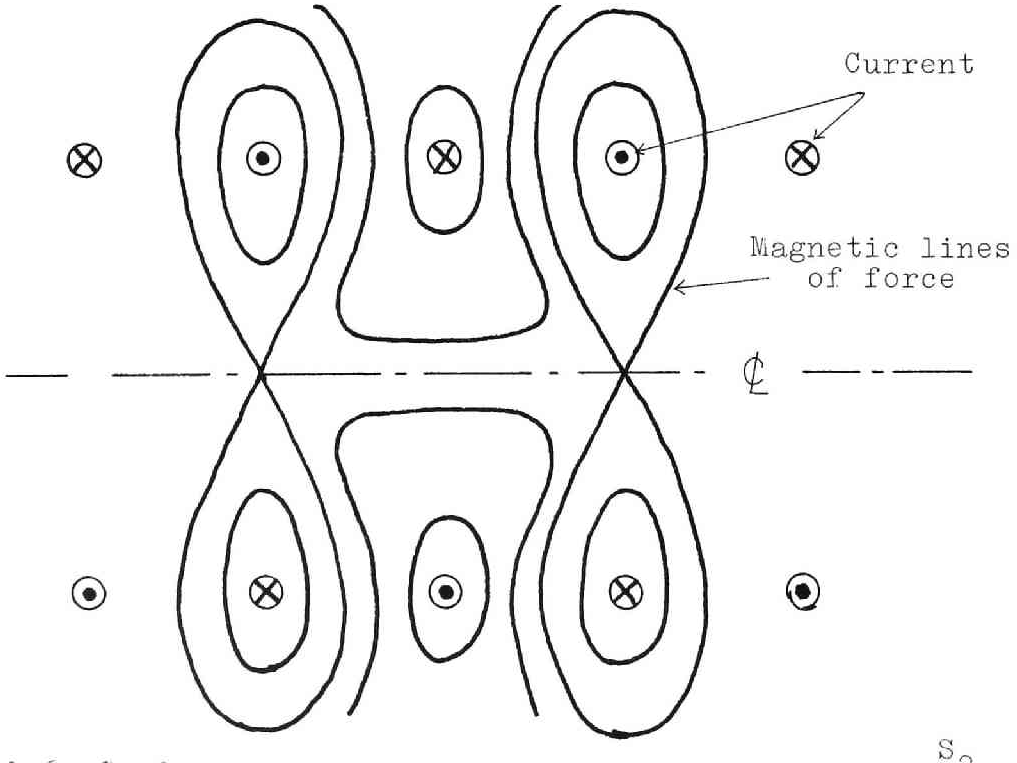

Fig. 1-6 Configuration of axisymmetric currents when $\lambda = \frac{S_2}{S_1}$.

Whence, $I_0(kr_0)=1$. The magnetic field in this case is as shown in Fig. 1-6. N. L. is reduced to a point on the axis. The induced electric field is expressed by

$$E_\theta = -f'(t)\ \frac{B_e}{kc}\left[\frac{1}{2}kr + I_1(kr)\ \cos(kz)\right]. \qquad (1\text{-}42)$$

(ii) Case that $\lambda=1$ (Picket Fence type)

From equation (1-37), e_1 must vanish. Hence we have

$$E_\theta = -f'(t)\ \frac{B_e}{kc}\ I_1(kr)\ \cos(kz). \qquad (1\text{-}43)$$

The magnetic field of this configuration may be regarded as a series of linecusps which are arranged along the z-axis. Fig. 1-7 shows the magnetic lines of force in this case.

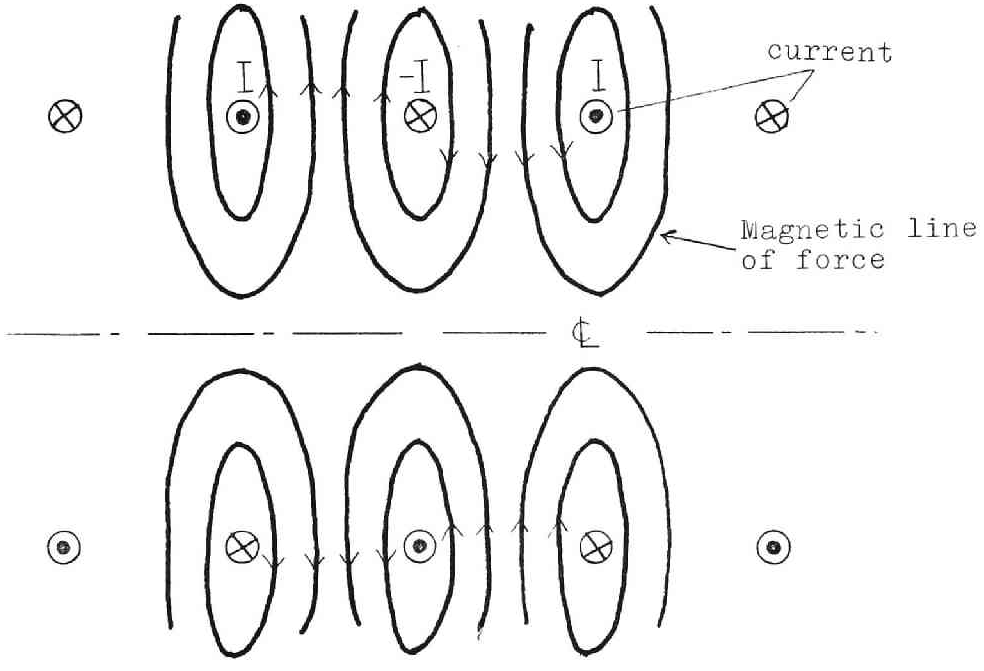

Fig. 1-7 Configuration of axisymmetric currents when $\lambda=1$.

The induced electric field is perpendicular to the axis and periodic along the axis. Therefore, this field has been applied to a plasma heating of ion cyclotron resonance. Stix (1958)[7] used this m=o mode field to excite ion cyclotron waves. In this thesis, the experiment of plasma heating by this field is to be described in a latter chapter.

(iii) Case that $\lambda<1$

When λ is suitable value less than 1, so-called Heliotron type is found, whose magnetic lines of force were shown in Fig. 1-5. Also the expression describing the induced field were given by equation (1-41).

No application of this type of field have been tried up to the present, but projected by Mohri and his collaborators in order to heat plasma by adiabatic compression. Let B_z at $kz=2n\pi$ be B_o when $t=t_o$, then we obtain another expression for equation (1-41) as

$$E_\theta = -f'(t)\frac{B_o r_o}{c}\,\frac{I_o(kr_o)}{1+I_o(kr_o)}\,\frac{1}{kr_o}\left[\frac{1}{2}kr + \frac{I_1(kr)}{I_o(kr_o)}\cos(kz)\right]. \qquad (1\text{-}44)$$

To clarify the dependence of E_θ on kr and kz, a term in equation (1-44):

$$\frac{I_o(kr_o)}{1+I_o(kr_o)}\,\frac{1}{kr_o}\left[\frac{1}{2}kr + \frac{I_1(kr)}{I_o(kr_o)}\cos(kz)\right],$$

is shown graphically in Fig. 1-8 as a function of kr for different kz when $kr_0 = \frac{\pi}{2}$.

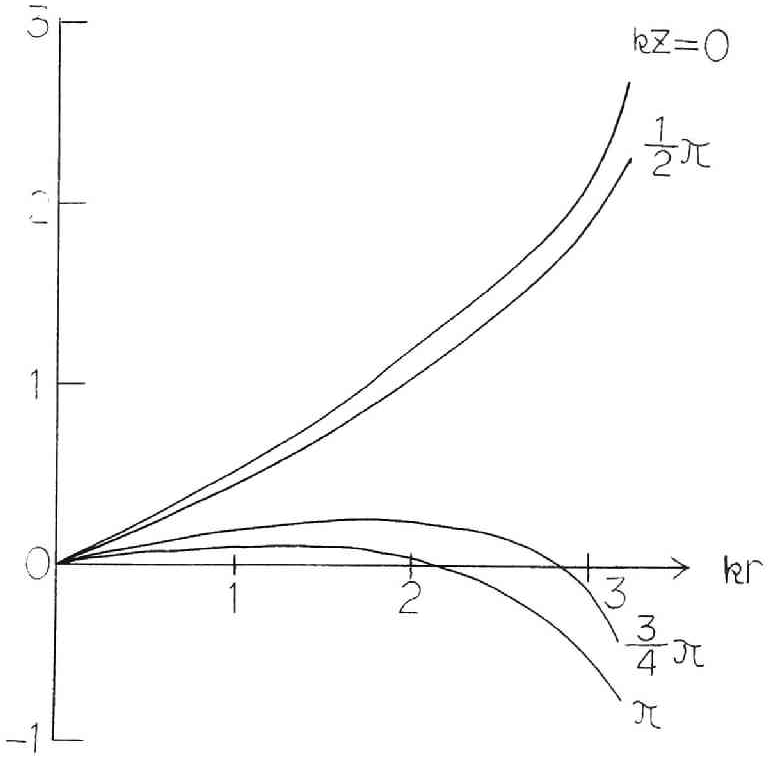

Fig. 1-8 Radial and axial variations of the azimuthal electric field when n=0 and $kr_0=\pi/2$.

(iv) Case that $\lambda=0$ (Mirror type)

This case corresponds to a corrugated magnetic field. Whence the induced electric field is given by

$$E_\theta = -f'(t)\,\frac{B_e}{kc}\left[\frac{1}{2}\,\frac{S_1+S_2}{S_1-S_2}\,kr + I_1(kr)\cos(kz)\right]. \quad (1\text{-}45)$$

For instance, M-S[9] (a plasma pinch machine) belongs to this type.

1.3.2 Line Cusp Configuration

Next let us investigate the configuration that current flows are parallel to the axis with azimuthal periodicity and neighbouring currents are opposite in their direction. This type corresponds to the case that $\nu=1$ and $kz\to 0$. If only a region near the axis is concerned, an approximate expression of the magnetic field is readily obtained to be

$$\left.\begin{aligned} B_r &= f(t)\sum_{n=1}^{\infty} \frac{k^n A_{n1}}{2^n(n-1)!}\, r^{n-1} \sin(n\theta), \\ B_\theta &= f(t)\sum_{n=0}^{\infty} \frac{k^n A_{n1}}{2^n(n-1)!}\, r^{n-1} \cos(n\theta), \\ B_z &= f(t)e_1 . \end{aligned}\right\} \qquad (1\text{-}46)$$

The magnetic field with a configuration as shown in Fig. 1-9 can be given approximately by

$$\left.\begin{aligned} B_r &= f(t)\, C_m\, r^{m-1} \sin(m\theta), \\ B_\theta &= f(t)\, C_m\, r^{m-1} \cos(m\theta), \\ B_z &= f(t)e_1 , \end{aligned}\right\} \qquad (1\text{-}47)$$

where

$$C_m = \frac{k^m A_{m1}}{2^m(m-1)!} \quad .$$

Combination of (1-47) and (1-33) yields

$$E_z = -f'(t)\,\frac{C_m}{mc}\,r^m \cos(m\theta) \qquad (1\text{-}48)$$

where $e_1=0$ case is only considered.

Heating and confinement of plasma by this field have been tried by E. M. Little and W. E. Quinn[10] of University of California. They have adopted a m=3 configuration (so-called Hexapole field), where e_1 in equation (1-47) is not zero. This configuration has a stalization effect for plasma, that is, so-called minimum B configuration. However their experimental results were not always as what might have been expected. On the other hand, Kondo[11] proposed a method for trapping plasma by a similar type of field, any experiment on his proposal has not been made.

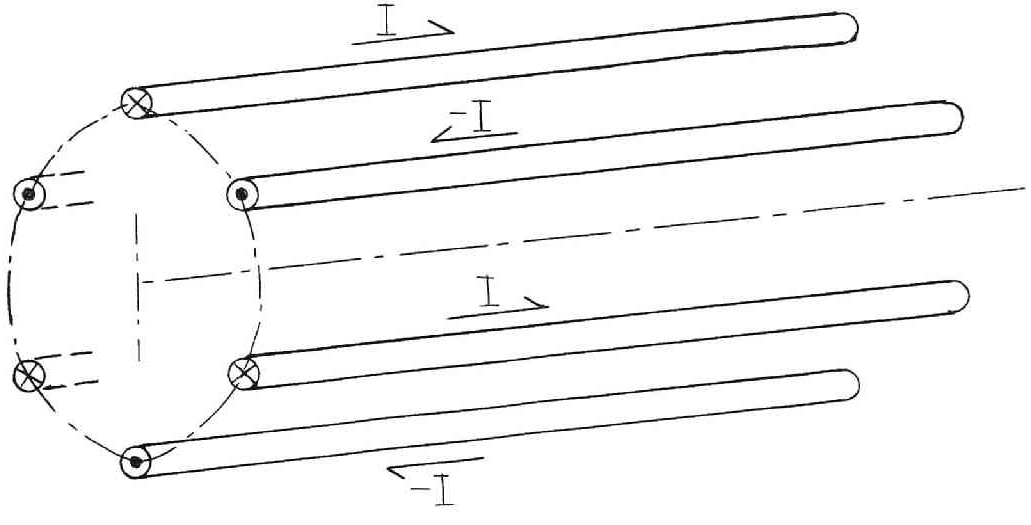

Fig. 1-9 Line cusp configuration of currents when m=3.

1.3.3 Helical Type Configuration

Here we consider the configuration which is achieved by twisting the current flows around the axis as shown in Fig. 1-9. This magnetic field is expressed by equation (1-32).

Let us consider the configuration as shown in Fig. 1-10. Again this type is approximately described, when $n=m$ and $\nu=1$. Once we know the axial magnetic field at a given point and time as

$$B_z = B_o \qquad \text{where} \quad \begin{cases} m\theta + kz = 0 \\ r = r_o \\ t = t_o \end{cases}, \qquad (1\text{-}49)$$

then we can obtain the approximate expressions of the magnetic field

$$\left.\begin{aligned} B_r &= \frac{f(t)}{f(t_o)}\, B_o\, \frac{I_m(kr)}{I_m(kr_o)}\, \sin(m\theta + kz) \\ B_\theta &= \frac{f(t)}{f(t_o)}\, B_o\, \frac{m}{kr}\, \frac{I_m(kr)}{I_m(kr_o)}\, \cos(m\theta + kz) \\ B_z &= \frac{f(t)}{f(t_o)}\, B_o\, \frac{I_m(kr)}{I_m(kr_o)}\, \cos(m\theta + kz) \end{aligned}\right\} \qquad (1\text{-}50)$$

Combination of equations (1-50) and (1-33) yields an approximate expression of the induced field near axis as

$$\left.\begin{aligned} E_r &= -\frac{f'(t)}{f(t_o)}\frac{B_o}{c}\frac{mr_o}{4(m+1)}\left(\frac{r}{r_o}\right)^{m+1}\sin(m\theta+kz), \\ E_\theta &= -\frac{f'(t)}{f(t_o)}\frac{B_o}{c}\frac{(m+2)r_o}{4(m+1)}\left(\frac{r}{r_o}\right)^{m+1}\cos(m\theta+kz), \\ E_z &= \frac{f'(t)}{f(t_o)}\frac{B_o}{kc}\left(\frac{r}{r_o}\right)^{m}\cos(m\theta+kz). \end{aligned}\right\} \quad (1\text{-}51)$$

Under another condition such as

$$B_\vartheta = B_o \quad \text{where} \quad \begin{cases} m + kz = 0 \\ r = r_o \\ t = t_o \end{cases}, \quad (1\text{-}52)$$

equation (1-51) can be rewritten to be

$$\left.\begin{aligned} E_r &= -\frac{f'(t)}{f(t_o)}\frac{B_o}{c}\frac{kr_o^2}{4(m+1)}\left(\frac{r}{r_o}\right)^{m+1}\sin(m\vartheta+kz), \\ E_\vartheta &= -\frac{f'(t)}{f(t_o)}\frac{B_o}{c}\frac{(m+2)kr_o^2}{4m(m+1)}\left(\frac{r}{r_o}\right)^{m+1}\cos(m\vartheta+kz), \\ E_z &= \frac{f'(t)}{f(t_o)}\frac{B_o}{c}\frac{r_o}{m}\left(\frac{r}{r_o}\right)^{m}\cos(m\vartheta+kz). \end{aligned}\right\} \quad (1\text{-}53)$$

Needless to say, equation (1-51) can be reduced to the approximate formula of equation (1-43) when m=0. Also equation (1-53) is able to be reduced to equation (1-48) when k=0.

From equation (1-51) or (1-52), it becomes evident that all directional components of the electric field are finite and the axial electric field becomes dominant at small r, especially when k is small. Provided that an external magnetic field is applied parallel to the axis, and heating of electrons in plasma is desired, this axial field may desirably work for this purpose. Because electrons stick to the magnetic lines of force and easily move along the lines. Therefore, this configuration will be applicable to a preheating of plasma. In contrast to this effect, the axial field will lead to a trapping of charged particles in the potential wall of the field. Thus accelerations of charged particles perpendicular to the magnetic field have to be followed by charge separation, since electrons of small mass would cansel the charge separation unless the trapping does not take place. In this case, plasma neutrality is no longer retained and undesirable co-operative phenomena for plasma confinement may arise.

Also it is a noticeable characteristic of the field that the induced electric field becomes very weak when m is sufficiently large. If a combined type of electrostatic and induced fields is set up, the induced field in the case with large m will be negligible frequently compared with the electrostatic field.

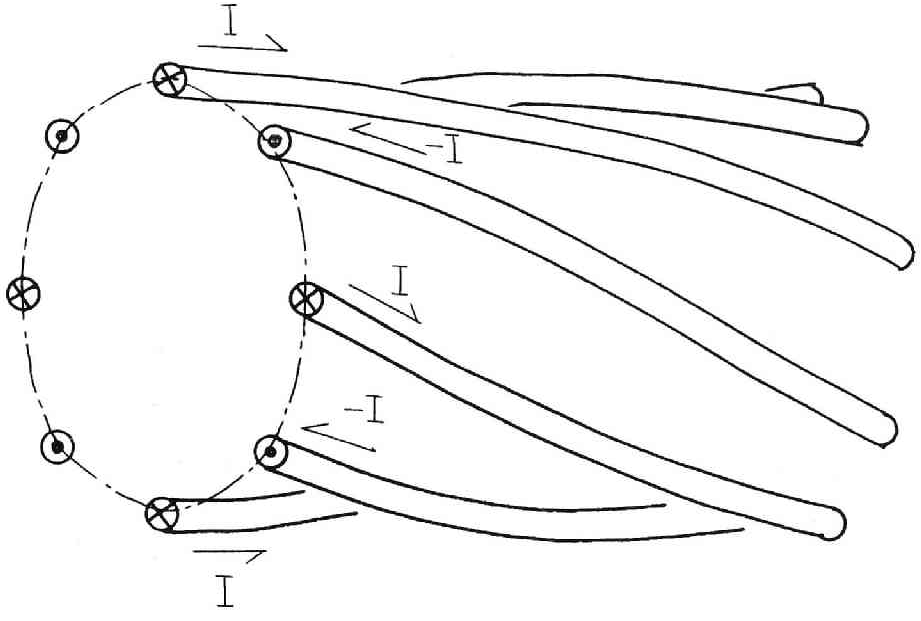

Fig. 1-10 Configuration of helical currents when m=4.

1.4 Combined Electric Field

Electrostatic and induced electric fields described in sections 1.2 and 1.3 coexist frequently in practical devices. The configurations shown in Fig. 1-2 are examples. Here we investigate another example.

Let us consider a resonant circuit of L-C as shown in Fig. 1-11a. Resultant fields are an electrostatic field in the diametral direction and an induced field in the axial direction. As described in the section 1.3.2 the induced field with large m is very weak near the axis. On the other hand, the electrostatic field is not negligible, since the field corresponds the case when m=1 in equation (1-22).

Furthermore, twisting the conducting bar as shown in Fig. 1-11b, we have a combined helical electric field that is described by equations (1-26) and (1-51) for electrostatic and induced electric fields, respectively. It is to be explained in the next chapter that this configuration of field is suitable and applicable to an ion cyclotron heating of plasma with a finite m mode. A. Mohri and S. Hayashi (1964)[12] made the experiment on such a heating of plasma. Many other combined fields may be considered, but these fields have not been used yet for plasma heating, except several cases.

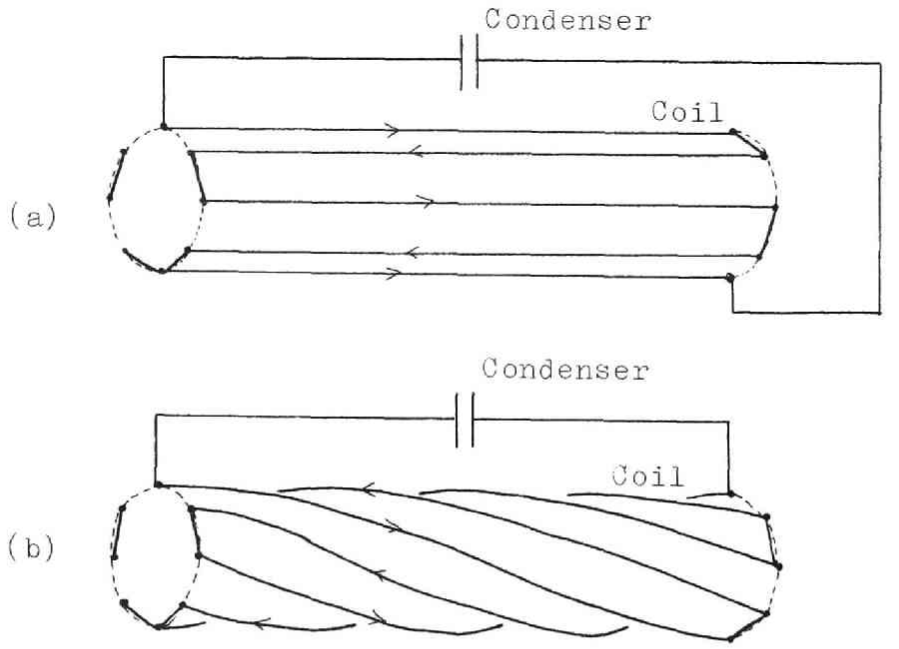

Fig. 1-11 Resonant circuits producing a combined field.
(a) Line cusp type
(b) Helical type

II. Particle Treatment of Ion Cyclotron Heating of Plasma

2.1 Introduction

A time varying electric field perpendicular to a strong static magnetic field can directly accelerate ions of plasma at or near their ion cyclotron frequency. This mechanism is similar to the acceleration in ordinary cyclotron accelerators. It is considered that this heating of ions would be one of the most prominent methods to raise quickly ion temperature from zero to an appropriate reacting temperature for fusion. In this chapter, this ion cyclotron heating will be discussed theoretically from a microscopic point of view.

Tenuous plasma at a sufficiently high temperature may be regarded as a collisionless plasma. K. M. Watson[13] demonstrated the equivalence of the Boltzman equation in the absence of collisions and the particle orbit theorem within the accuracy of the adiabatic theorem. Therefore, we can deal with the mechanism by means of particle orbits in the field.

Necessary properties of the electric field for ion cyclotron heating are as follows.

(i) The field has no axial component, if static magnetic field is imposed along the axis.

(ii) Its perpendicular components are periodic along the

axis. This condition comes from the requirement that space charge neutrality of plasma is maintained under the heating, so as to make the heating efficiency high.

Appropriate configurations of electric field for the above stated conditions should be picked out from those given in the chapter I. The electric fields given by equation (1-43) and (1-26) are found to be suitable for this purpose, because of their simple configuration and easy realization in practice. One is a Picket Fence type of the induced electric field and another a helical type of the electrostatic field.

It is convenient to rewrite the above fields according to a complex notation:

$$\mathcal{E} = E_r + iE_\theta . \tag{2-1}$$

Then we obtain for the Picket Fence type field

$$\mathcal{E} = (\mathcal{E}_+ e^{i\omega t} + \mathcal{E}_- e^{-i\omega t}) \sin(kz). \tag{2-2}$$

And for the helical type field we may write

$$\mathcal{E} = (\mathcal{E}_+ e^{i\omega t} + \mathcal{E}_- e^{-i\omega t})\, e^{-i\theta} e^{ikz}. \tag{2-3}$$

In equations (2-2) and (2-3), we decomposed the field into two components, each of which revolves with time on a circle at a given point. A term $e^{-i\omega t}$ expresses a circularly polalized field in the same sense as ion

cyclotron gyration. Therefore, this term much contributes to the ion cyclotron heating as seen below. Needless to say, in the absence of plasma reaction (i.e. in vacuum field), ε_+ should be equal to ε_-.

Many analyses of the ion cyclotron heating by the field given by equation (2-2) were reported,[14)15)16)] but the heating by the helical type field given by equation (2-3) has not been discussed up to the present. This helical field will be discussed in the next section 2.2, where frequency spectra of energy flux ejected from a heating region are to be discussed in detail in comparison with those in the case of the Picket Fence field. Through this comparison, it will be found that a remarkable difference between the frequency spectra of energy flux in both cases is present. Also it will be revealed that these spectra have a kind of Doppler shift when the velocity distribution is shifted Maxwellian. This result could be confirmed experimentally by the auther as described in a Chapter VII. Thus we can have a method to determine the macroscopic velocity of anion beam from the measurement of this Doppler shift. In a section 2,3, the frequency spectra of energy flux in the case of the Picket Fence field are to be given.

2.2 Ion Cyclotron Heating by the Helical Field

In this section, the ion cyclotron heating by the

helical field expressed by equation (2-3) will be dealt with. The physical situation under consideration is as follows. An infinitely long cylindrical plasma is confined in a strong static magnetic field $\vec{B}_0$ parallel to its axis (the z-axis). A small oscillating electric field expressed by equation (2-3) is superimposed on a finite heating section of the cylinder. In this heating region, ions feels the electric field as they travel parallel to the z-axis with their thermal velocity. If the frequency of oscillation is near the ion cyclotron frequency, so-called ion cyclotron heating will be achieved and their velocity perpendicular to the z-axis will increase. On the other hand, the parallel velocity component will not be changed, since the accelerating field has no parallel component. Such ion motions will give rise to large ion currents and then the oscillation in the ionic charge density.. On the contrary, electrons are sticked to the magnetic lines of force, and can move freely along the lines in consequence of their small mass. Therefore, electric neutrality of plasma will be retained by such a neutralization effect of electron flow, provided that the oscillation of the ionic charge separation is periodic along the z-axis. This is the reason why we must use an axially periodic electric field for accelerating. The electron flows will produce induced fields. This suggests that we must treat the situation by a self-consistent method.

Consequently, in the next small section 2.2.1, let an electric field be assumed given, and the resulting ion behaviours are found. An energy flux ejected from the heating region is also introduced. Section 2.2.2 is devoted to give physical picture of the properties of the energy flux. An energy flux averaged over velocity space, which was calcurated by a digital computer, is also given in a section 2.2.3. In a section 2.2.4, co-operative phenomena will be discussed by means of a self-consistent method. Finally, it should be noted that the analytical method applied in this section is the same in several points as that developed by A.Lenard and R. Kulsrud.[14] They dealt with the case of the Picket Fence Type.*

2.2.1 Ion Motion

As above stated, the electric field for acceleration of ions is assumed given as the equation (2-3). The basic equation to be solved is a familiar equation of motion of a particle of charge q and mass M in a region in an

---

* They analyzed only the case of the ordinary Maxwellian distribution of ionic velocity.

electric field $\vec{E}$ and a magnetic field $\vec{B}$. This is

$$M \frac{d\vec{w}}{dt} = q \left(\vec{E} + \frac{1}{c} \vec{w} \times \vec{B} \right), \qquad (2\text{-}4)$$

where $\vec{w}$ and c are the velocities of the particle and light, respectively.

For the sake of simplification of the analysis, we shall make four approximations:

(i) We neglect the oscillating component of magnetic field so that $\vec{B} = \vec{B}_0 = \text{const}$, which is parallel to the z-axis.

(ii) We assume electrical neutrality, which may be achieved by freely movable electrons along the magnetic lines of force, if the resulting phenomena are periodic in the z-axis.

(iii) We neglect the variation of the transverse electric field over the Larmor radius of the ion.

(iv) We neglect the axial electric field. That is,

$$E_z = 0. \qquad (2\text{-}5)$$

We are now interested in the field with frequency near the ion cyclotron frequency, so electron inertia can be neglected and then electrons cansel the axial field by their free motions along the magnetic lines of force. In other words, equation (2-5) corresponds to an approximation as

$$\frac{m(\text{electron mass})}{M(\text{ion mass})} \ll 1. \qquad (2\text{-}6)$$

We assume a finite heating section, where the accelerating field is working. This heating region may be expressed by

$$-L \leqq z \leqq L \ . \qquad (2\text{-}7)$$

We also assume that the length of the heating region is an integer times as large as the axial wave length of the accelerating field.

Then, we note

$$L = \frac{\pi N}{k} \ , \qquad N : \text{integer} \qquad (2\text{-}8)$$

where k is the same notation as used in equation (2-3).

Combination of equations (2-4) and (2-5) yields, in our approximations,

$$\frac{dw_z}{dt} = 0. \qquad (2\text{-}9)$$

According to the approximation (iii), it is no longer necessary to consider the radial and the azimuthal variation of the accelerating field in equation (2-4).

It is convenient to rewrite the velocity of particle $\vec{w}$ in the complex formula, likewise in equation (2-3); that is,

$$w = w_r + iw_\theta . \tag{2-10}$$

Then equation (2-4) can be rewritten by

$$\frac{dw}{dt} + i\omega_i w = \frac{q}{M}\varepsilon , \tag{2-11}$$

where

$$\omega_i = \frac{qB_o}{Mc} \quad \text{(ion cyclotron angular frequency).}$$

The general solution of equation (2-11) is readily obtained by using a Laplace transformation. If t_1 is the incident time of the particle into the heating region, then the solution is

$$w(t) = w(t_1)e^{i\omega_i(t-t_1)} + \frac{q}{M}\int_{t_1}^{t} ds\ \varepsilon(s)e^{i\omega_i(s-t)} . \tag{2-12}$$

In order to carry out the integration in equation (2-12), the axial position z of the particle in question need to be expressed as a function of t. Equation (2-9) now yields this relation

$$\begin{aligned} z(t) &= \pm w_o (t-t_1) \mp L \\ w_o &= \pm w_z \qquad (w_o > 0) , \end{aligned} \tag{2-13}$$

where the upper (lower) sign corresponds to ions moving in the directions of increasing (decreasing) z.

With this transformation, the solution (2-12) then becomes

$$w_{\pm}(t) = w_{\pm}(t_1)e^{i\omega_i(t-t_1)} + (-1)^N \frac{q\varepsilon_- e^{-i\theta}}{iM} \left[\frac{\varepsilon_+ e^{i\omega t}}{\omega_i + \omega \pm kw_o} \times \right.$$

$$\left\{ e^{ik(L\pm z)} - e^{\frac{-i(\omega_i+\omega)(L\pm z)}{w_o}} \right\} + \frac{\varepsilon_- e^{-i\omega t}}{\omega_i - \omega \pm kw_o} \times$$

$$\left. \left\{ e^{\pm ik(L\pm z)} - e^{\frac{-i(\omega_i-\omega)(L\pm z)}{w_o}} \right\} \right] . \qquad (2\text{-}14)$$

The first term on the right hand side of equation (2-12) (or equation (2-14)) represents the undisturbed cyclotron gyration, whereas the second represents the increase in velocity due to the acceleration. If we consider the mean ion velocity averaged over the phase between the randomly incoming particle and the accelerating field, this first term vanishes. The second term on the right hand side of equation (2-14) may be decomposed into two terms; one including $e^{i\omega t}$ and the other $e^{-i\omega t}$. If the frequency of the accelerating field is near the cyclotron frequency, the term including $e^{-i\omega t}$ becomes predominant. Therefore, near ion cyclotron resonance, the mean velocity $\overline{w_{\pm}}$ may be given approximately by

$$\overline{w_{\pm}(t)} = \frac{q\varepsilon_- e^{-i\theta}}{iM} \frac{(-1)^N e^{-i\omega t}}{\omega_i - \omega \pm kw_o} \times$$

$$\left\{ e^{\pm ik(L\pm z)} - e^{-\frac{i(\omega_i-\omega)(L\pm z)}{w_o}} \right\} . \qquad (2\text{-}15)$$

Next let us consider the energy gain W of the ion at the exit end of the heating section. This is obtained from equation (2-15), which becomes

$$W_{\pm} = \frac{1}{2}M \left| \overline{w_{\pm}} \right|^2 = \frac{2q^2\varepsilon_-^2}{Mk^2w_o^2} \frac{\sin^2(\pi N \frac{\omega_i - \omega}{kw_o})}{(1 \pm \frac{\omega_i - \omega}{kw_o})^2} \quad . \qquad (2\text{-}16)$$

Equation (2-16) can introduce an energy flux ejected from the end of the heating section. This energy flux may be regarded as the energy flow, carried out by ions moving parallel to the axis, per unit time per unit area. If E.F. denotes the energy flux, we obtain

$$\begin{aligned} E.F._{\pm} &= n_i w_z W_{\pm} \\ &= \pm \frac{2n_i q^2 \varepsilon_-^2}{Mk^2 w_o} \frac{\sin^2(\pi N \frac{\omega_i - \omega}{kw_o})}{(1 \pm \frac{\omega_i - \omega}{kw_o})^2} \quad , \end{aligned} \qquad (2\text{-}17)$$

where n_i is the number density of ions. Physical meanings brought out from equation (2-17) will be given in the next small section.

Equation (2-17) denotes only the energy flux carried out by ions of a mono-energy. In practice, however, ionic velocity is distributed. Thus we must consider a mean energy flux averaged over ionic velocities. If we assume the shifted (or drifted) maxwellian distribution of ionic velocity, this normalized distribution function is writted by

$$f(w_z) = \frac{1}{V_T\sqrt{\pi}} e^{-\frac{(w_z-u)^2}{V_T^2}}, \qquad (2\text{-}18)$$

$$V_T = \sqrt{\frac{2kT}{M}},$$

u : beam velocity,

k : Boltzmann constant.

An energy dissipation per unit time per unit area from the heating region may also be defined by the relation

$$E.D. = |< E.F._+ >| + |< E.F._- >|, \qquad (2\text{-}19)$$

where $< x >$ denotes to average x over velocity space. From equations (2-17) and (2-18), we find

$$E.D. = \frac{2n_i q^2 \mathcal{E}_-^2}{\sqrt{\pi} M k^2 V_T} \int_{-\infty}^{+\infty} \frac{\sin^2(\pi N \frac{\omega_i-\omega}{kw_z})}{|w_z|(1+\frac{\omega_i-\omega}{kw_z})^2} e^{-\frac{(w_z-u)^2}{V_T^2}} dw_z. \qquad (2\text{-}20)$$

In order to carry out the integration in equation (2-20) by a digital computer, we rewrite the integrand in a non-dimensional form, and we get

$$E.D. = \frac{2n_i q^2 \mathcal{E}_-^2}{\sqrt{\pi} M k^2 V_T} \int_{-\infty}^{+\infty} \frac{\sin^2(\pi N \frac{\alpha}{S})}{S\,(1+\frac{\alpha}{S})^2} e^{-(S-\delta)^2} ds, \qquad (2\text{-}21)$$

where

$$\frac{\omega_i - \omega}{kV_T} = \alpha,$$

$$\frac{u}{V_T} = \delta \ . \qquad (2\text{-}22)$$

The parameter δ indicates the deviation in velocity distribution from the ordinary Maxwellian distribution (i.e. u=0). Accordingly, we can get frequency spectra of the energy dissipation for different δ. In the section 2.2.3, this frequency spectra, which are computed numerically by a electronic digital computer KDC-1 of Kyoto University, are to be given.

Next let us give the average transverse ion velocity over the longitudinal ionic velocities. This average transverse velocity at any given point in the heating section is derived from the equations (2-15) and (2-18), according to the relation

$$\langle w \rangle = \frac{1}{2} \int_{-\infty}^{+\infty} f(w_z) \ (\overline{w_+} + \overline{w_-}) dw_z . \qquad (2\text{-}23)$$

After some algebra, we have

$$\overline{w_+} + \overline{w_-} = e^{-i\omega t} \frac{q\varepsilon_- e^{-i\theta}}{iM} \frac{2(-1)^N}{kw_o \left\{ \left(\frac{\omega_i - \omega}{kw_o} \right)^2 - 1 \right\}} \times$$

$$\left[\frac{\omega_i - \omega}{kw_o} e^{ikz} (-1)^N - e^{-i(\omega_i - \omega)\frac{L}{w_o}} \times \right.$$

$$\left. \left\{ \frac{\omega_i - \omega}{kw_o} \cos\left\{ (\omega_i - \omega)\frac{z}{w_o} \right\} + \sin\left\{ (\omega_i - \omega)\frac{z}{w_o} \right\} \right] . \qquad (2\text{-}24)$$

Then we find, under the condition u = 0,

$$\langle w \rangle_{-} = \frac{q\mathcal{E}_{-}e^{-i\theta}}{MV_T k} e^{-i\omega t} \underline{I}(kz; \frac{\omega_i - \omega}{kV_T}) \quad , \tag{2-25}$$

where

$$\underline{I}(kz,\alpha) = \frac{2\ sg(\alpha)}{i\sqrt{\pi}} \int_0^{\infty} \frac{e^{-\alpha^2/x^2}}{x^2-1} \left[e^{ikz} - (-1)^N \times e^{-ix\pi N sg(\alpha)} \left\{ \cos xkz + \frac{1}{x} \sin xkz \right\} \right] dx \ ,$$

$$\alpha = \frac{\omega_i - \omega}{kV_T} \quad , \tag{2-26}$$

$$sg(\alpha) : \text{sign of } \alpha \quad .$$

In the section 2.2.4, co-operative phenomena, induced by the mean ion velocity $\langle w \rangle$ in equation (2-25), will be discussed.

2.2.2 Physical Picture of the Energy Flux of Mono-energy Ions

When the energy flux of mono-energy ions, given by equation (2-17), is contemplated in detail, many physical pictures of ion cyclotron heating may be clarified. Therefore, let us examine equation (2-17) in this small section.

Taking the term of plus sign in equation (2-17),

we have

$$E.F._{+} = \frac{2n_i q^2 \varepsilon_-^2}{Mk^2 w_o} \frac{\sin^2(\pi N - \frac{\omega_i - \omega}{kw_o})}{(1 + \frac{\omega_i - \omega}{kw_o})^2} \qquad (2\text{-}27)$$

$$= \frac{2n_i q^2 \varepsilon_-^2}{Mk^2 w_o} \frac{\sin^2(\pi N \alpha')}{(1+\alpha')^2} \qquad (2\text{-}28)$$

$$= \frac{2n_i q^2 \varepsilon_-^2}{Mk(\omega_i - \omega)} \frac{\alpha' \sin^2(\pi N \alpha')}{(1+\alpha')^2} \quad , \qquad (2\text{-}29)$$

where $\alpha' = \frac{\omega_i - \omega}{kw_o}$.

The prime of α' is employed to distinguish α' from α in equation (2-22).

If w_o is assumed constant, the frequency spectrum of $E.F._{+}$ is found from the consideration of behaviours of a term in equation (2-28), which is

$$\frac{\sin^2(\pi N \alpha')}{(1+\alpha')^2} = Y(\alpha') \ . \qquad (2\text{-}30)$$

Readily, we find

$$Y(\alpha') = 0 \text{ (minimum value) , when } \alpha' = \frac{s}{N} \qquad (2\text{-}31)$$

(s : integer but $s \neq -N$)

$$Y(\alpha') = \frac{\pi^2 N^2}{\pi^2 N^2 (\alpha'+1)^2 + 1} \text{ (maximum values), } (2\text{-}32)$$

$$\text{when } \tan(\pi N \alpha') = \pi N(\alpha' + 1). \ (2\text{-}33)$$

When α is large, roots of equation (2-33) are given approximately by

$$\alpha \approx \frac{2s + 1}{2N} \qquad (2\text{-}34)$$

and $\alpha = -1$ is also a root. As a result, we can trace the variation of $Y(\alpha')$ with α' as shown in Fig. 2-1. This curve is the frequency spectrum for mono-energy ions, which is just to be obtained.

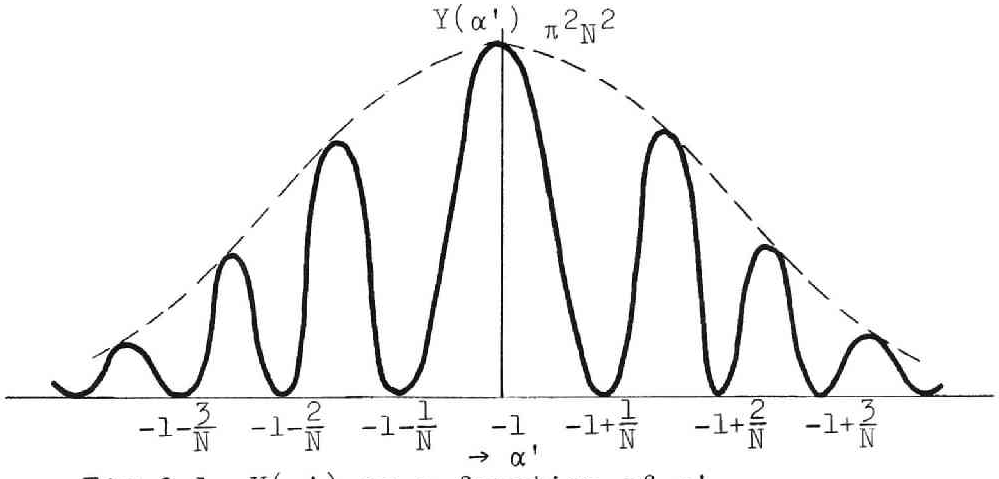

Fig.2-1 $Y(\alpha')$ as a function of α'.

It should be noted that the spectrum shown in Fig. 2-1 is remarkably different from the spectrum in the accelerating field expressed by equation (2-2). $Y(\alpha')$ in Fig. 2-1 has a maximum value where $\alpha = -1$. On the other hand, the spectrum* in the field of the

---

* In this case, spectrum is given by

$$E.F._{+} = \frac{2n_i q^2 \mathcal{E}_-^2}{Mk^2 w_o} \cdot \frac{\sin^2 \pi N \alpha'}{(1-\alpha'^2)^2}$$

Picket Fence type has two identical muxima where $\alpha = \pm 1$.

From the curve in Fig. 2-1, we may say that this spectrum has a fine structure, which underlies in the envelope shown by a dashed line. If the beam velocity is slightly distributed by Δw_o, according as

$$1 \gg \frac{\Delta w_o}{w_o} \gtrsim \frac{1}{N} \quad , \tag{2-35}$$

We can only observe the spectrum similar to the dashed line.

In practice, this dushed line may be verified from the measurement of power absorption of plasma under Joule (or Ohmic) heating with high accelerating field. In high accelerating field, ions will become beamlike as well as electrons. Therefore, we can determine the beam velosity by measuring the shift of the absorption peak from the ion cyclotron frequency. This method can be applied in the case of the Picket Fence field.

Again return to equation (2-27) (or(2-30)), and let us examine the physical picture of this fine structure. The frequency that ions feel in the heating region is

$$w_f = w - kw_o \ .$$

Therefore the beat frequency between w_f and w_i is given by

$$\omega_b = \omega_f \sim \omega_i = |(\omega - kw_o) - \omega_i| \ .$$

Substituting equation (2-31) into the above equation, we have

$$\omega_b = \frac{s + N}{N} kw_o \quad , \tag{2-36}$$

when $E.F._+$ vanishes. The transit time through the heating section is also given by

$$t_t = \frac{2L}{w_o} = \frac{2\pi N}{kw_o} \ .$$

Thus we have the relation

$$t_t = (s + N) \frac{2\pi}{\omega_b} \ . \tag{2-37}$$

From equation (2-37), it is clarified that the transit time becomes integer times as large as the period of the beat, when $E.F._+$ vanishes. Intuitively, this fact may be explained as follows.

Particle may be accelerated in phase with the field at a moment, but, in the next instance, deaccelerated out of phase. This process is periodic with the beat frequency ω_b. Fig. 2-2 is given for explaining this phenomenon schematically.

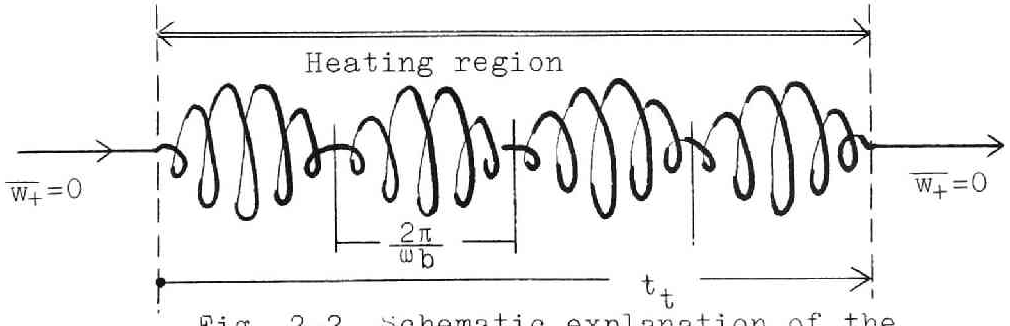

Fig. 2-2 Schematic explanation of the fine structure of $Y(\alpha')$.

Finaly let us consider extreme cases and explain the result intuitively.

(i) $E.F._{+} \rightarrow 0$ as $\alpha' \rightarrow \infty$.

This case is decomposed into two extreme cases.

(a) $w_o \rightarrow 0$

, whence there is no out flow from the heating region.

(b) $\omega \rightarrow \infty$

At high frequency, ions can not follow the field, due to their mass inertia.

(ii) $E.F. \rightarrow 0$ as $\alpha' \rightarrow 0$.

This case is also decomposed into three.

(a) $w_o \rightarrow \infty$

, whence the transite time become zero, that is equivalent to the nonexistence of the accelerating field.

(b) $k \rightarrow \infty$

This corresponds to the zero wave length, so there is no heating field.

(c) $\omega_i = \omega$

This case is included in the $\alpha' = \frac{S}{N}$ case.

2.2.3 Frequency Spectra of the Energy Flux for Distributed Ion Velocities

In order to examine the dependence of the energy

dissipation E.D. in equation (2-21) on parameters α and δ, the integration in this equation was carried out numerically by using an electronic digital computer KDC-1 of Kyoto University.

For convenience' sake, we define

$$I(\alpha, \delta) = \int_{-\infty}^{+\infty} \frac{\sin^2(\pi N \frac{\alpha}{s})}{|s|(1+\frac{\alpha}{s})^2} e^{-(s-\delta)^2} ds, \qquad (2\text{-}38)$$

where α and δ are given by equation (2-22). If $I(\alpha, \delta)$ is calculated for different values of α and for a given δ, a frequency spectrum of E.D. will be obtained as a function of α. This process gives a number of spectra for different δ.

A comparatively accurate result was obtained by using an integration method of Simpson's rule* in the case that $\delta = 0$, where the integration was made to an accuracy of an absolute value of 0.01

---

* refer to KDC-1 Manual of Kyoto University, Vol. 3, p. 68; Routine No. : I 1-002

The numerical values computed in this way are shown in Table 2-1.

Table 2-1 $I(\alpha,0)$ for different α

α	$I(\alpha,0)$	α	$I(\alpha,0)$
-5.0	2.19×10^{-2}	-1.2	4.3715×10^{0}
-4.8	2.45×10^{-2}	-1.0	6.6175×10^{0}
-4.6	2.64×10^{-2}	-0.8	9.4758×10^{0}
-4.4	3.33×10^{-2}	-0.6	1.27655×10^{1}
-4.2	3.46×10^{-2}	-0.4	1.60864×10^{1}
-4.0	4.18×10^{-2}	-0.2	1.92488×10^{1}
-3.8	4.30×10^{-2}	-0	0
-3.6	4.78×10^{-2}	+0.2	1.92488×10^{1}
-3.4	6.57×10^{-2}	+0.4	1.60864×10^{1}
-3.2	6.92×10^{-2}	+0.6	1.27355×10^{1}
-3.0	8.99×10^{-2}	+0.8	9.4703×10^{0}
-2.8	1.206×10^{-1}	+1.0	6.5693×10^{0}
-2.6	1.666×10^{-1}	+1.2	4.3453×10^{0}
-2.4	2.449×10^{-1}	+1.4	2.7534×10^{0}
-2.2	3.857×10^{-1}	+1.6	1.6910×10^{0}
-2.0	6.240×10^{-1}	+1.8	1.0204×10^{0}
-1.8	1.0217×10^{0}	+2.0	6.213×10^{-1}
-1.6	1.6949×10^{0}	+2.2	3.790×10^{-1}
-1.4	2.7684×10^{0}	+2.4	2.405×10^{-1}

However, Simpson's method in this case takes long time for the calculation of $I(\alpha, \delta)$. Therefore, it is more suitable to use Legendre-Gauss 16 point* method for the computation, in order to see the shapes of the frequency spectra for different δ. This computed results are given in Fig. 2-3. From the results, we can obtain the following information ;

(i) When $\delta = 0$, E.D. becomes maximum where α is equal to about zero. Namely, if the velocity distribution is the ordinary Maxwellian, the

* News of Electronic Computer Laboratory of Kyoto Univ., No.1, Subroutine No.: I1-007A

most efficient heating may be achieved when $\omega = \omega_i$.

(ii) Each spectrum for a given δ, has only a peak, which should be compared with the case of the Picket Fence field.

(iii) In the region of high value of δ, the corresponding peak of E.D. is situated near the position where $\delta = \alpha$ (i.e. $\omega_i - \omega = ku$). In addition to this property, the shape of the spectrum becomes to resemble the dashed line shown in Fig. 2.1. Needless to say, these properties of the spectrum are due to the physical situation that the macroscopic velocity of ions becomes so high that plasma can be regarded as a beam of charged particle. Therefore, if plasma is beamlike, we can determine the beam velocity and its direction from the measurement of the shift of the E.D. peak. This method will become a useful one to decide a ion beam energy, since we have only a few method for determing the ion energy of high temperature plasma.

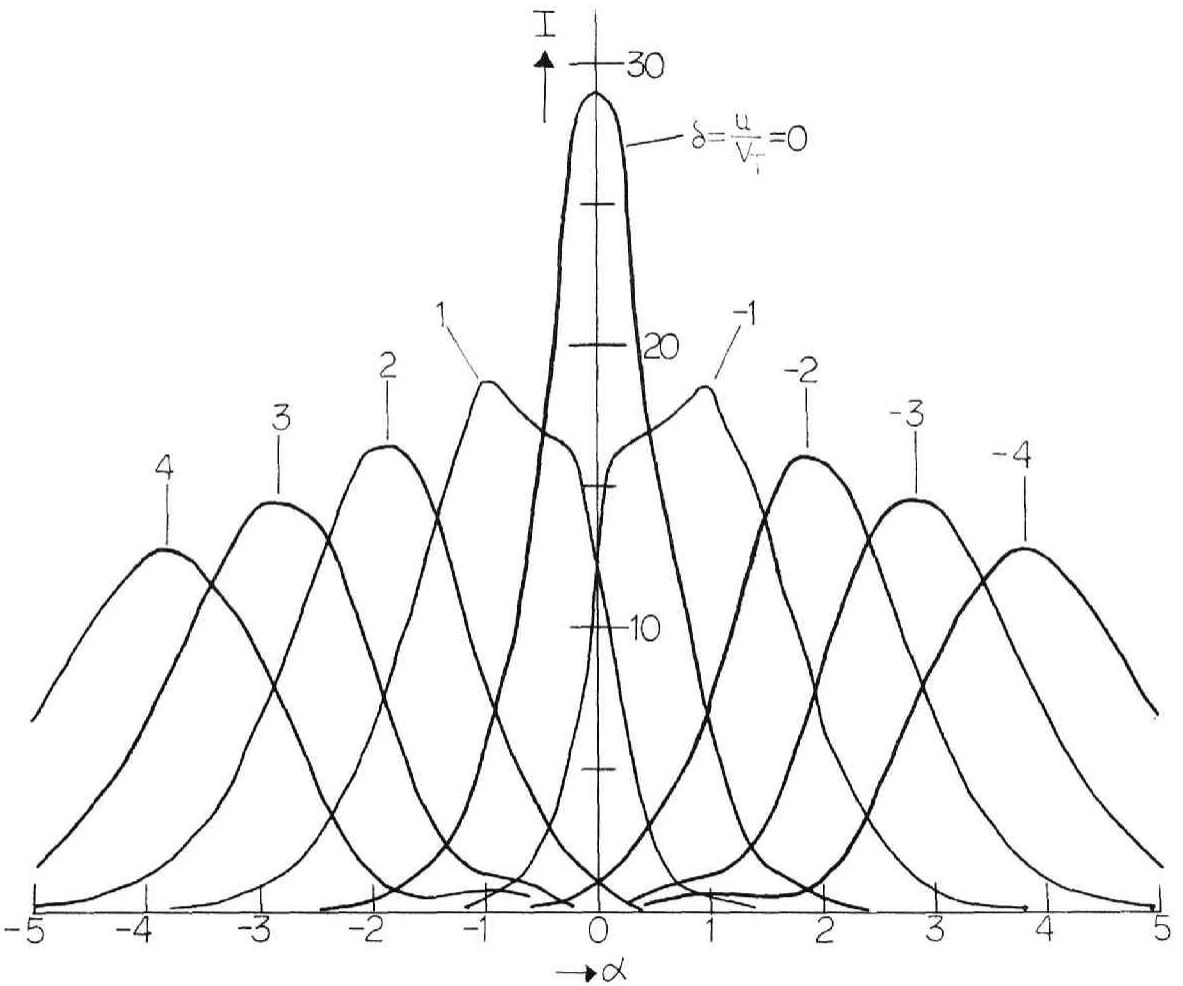

Fig. 2-3 $I(\alpha,\delta)$ as a function of α for different δ in the case of the helical type field.

2.2.4 Penetration of the Accelerating Field into Plasma

Next we shall examine the cooperative phenomena of the plasma as a whole, especially the penetration of the accelerating field. The ion motion induced by the oscillating field produces ion currents perpendicular to the axial direction, as shown in the small section 2.2.1. The resulting ion charge fluctuations are neutralized by electron motion along the magnetic lines of force, owing to the negligibly small mass of electrons compared with ion mass. These oscillating currents induce an oscillating electric field by induction. Hence, we must solve the phenomena by a self-consistent method.

Maxwell's equations without displacement current are

$$\vec{\nabla} \times \vec{B} = \frac{4\pi}{c} \vec{J} , \qquad (2\text{-}39)$$

$$\vec{\nabla} \times \vec{E} = - \frac{1}{c} \frac{\partial \vec{B}}{\partial t} , \qquad (2\text{-}40)$$

where $\vec{J}$ is the current density in the plasma. In our approximation, $\vec{\nabla} \times \vec{E}$ should vanish in vacuum. The field in vacuum, which is expressed by the form of equation (2-3), is solenoidal but not irrotational. This originates in that we have neglected the axial component of the accelerating field compared with other

two components, but $\frac{1}{r}\frac{\partial E_z}{\partial \theta}$ and $\frac{\partial E_z}{\partial r}$ are not negligible compared with $\frac{\partial E_\theta}{\partial z}$ and $\frac{\partial E_r}{\partial z}$. Therefore, a compensating term $\vec{S}$ must be introduced into equation (2-40) in this case, which is in complex form

$$S_r + iS_\theta = 2\varepsilon_0 k \cos \omega t \, e^{i(kz-\vartheta)}, \qquad (2\text{-}41)$$

where we have used the relation $\varepsilon_+ = \varepsilon_- = \varepsilon_0$ in vacuum. In cylindrical coordinates, equations (2-39) and (2-40) are expressed by

$$\begin{aligned}
&\frac{1}{r}\frac{\partial B_z}{\partial \theta} - \frac{\partial B_\theta}{\partial z} = \frac{4\pi}{c} J_r \\
&\frac{\partial B_r}{\partial z} - \frac{\partial B_z}{\partial r} = \frac{4\pi}{c} J_\theta \\
&\frac{1}{r}\frac{\partial}{\partial r}(rB_\theta) - \frac{1}{r}\frac{\partial B_r}{\partial \theta} = \frac{4\pi}{c} J_z
\end{aligned} \qquad (2\text{-}42)$$

and

$$\begin{aligned}
&-\frac{\partial E_\theta}{\partial z} + S_r = -\frac{1}{c}\frac{\partial B_r}{\partial t} \\
&\frac{\partial E_r}{\partial z} + S_\theta = -\frac{1}{c}\frac{\partial B_\theta}{\partial t} \\
&\frac{1}{r}\frac{\partial}{\partial r}(rE_\theta) - \frac{1}{r}\frac{\partial E_r}{\partial \theta} = -\frac{1}{c}\frac{\partial B_z}{\partial t}
\end{aligned} \qquad (2\text{-}43)$$

where we have introduced the compensating term $\vec{S}$. From equations (2-1) and (2-3), we readily get the relation

$$\frac{\partial E_r}{\partial \zeta} = E_\zeta$$

and

$$\frac{\partial E_\zeta}{\partial \zeta} = -E_r \quad . \tag{2-44}$$

Combining equations (2-41) to (2-44), finally we have

$$\left[\frac{1}{r}\frac{d}{dr} - k^2\right] E_r + \frac{\partial S_\zeta}{\partial z} = \frac{4\pi}{c^2}\frac{\partial J_r}{\partial t} \quad , \tag{2-45}$$

$$\left[\frac{d^2}{dr^2} - k^2\right] E_\zeta - \frac{\partial S_r}{\partial z} = \frac{4\pi}{c^2}\frac{\partial J_\zeta}{\partial t} \quad . \tag{2-46}$$

As described in the next chapter, the contribution of electron flow to the transverse current is negligible. Then the transverse current is expressed by equation (2-25). Lenard and Kulsrud[14] showed that $I(kz, \alpha)$ given by equation (2-26) has an oscillatory behaviour with the approximate wavelength $2\pi/k$. Therefore,

$$I_-(kz, \alpha) \simeq I_- e^{ikz}$$

is qualitatively an approximate form. Then we get

$$\langle w \rangle_- = \frac{q\varepsilon_-}{MV_T k} I_- e^{i(kz-\vartheta)} e^{-i\omega t} \quad . \tag{2-47}$$

The transverse current components are obtained by using above equation and they are

$$J_{-r} = qn_i \mathrm{Re}\langle w\rangle_-$$

$$= \frac{q^2 n_i}{MkV_T}\left[\mathrm{Re}\left\{\varepsilon_- e^{i(kz-\theta)} I_-\right\}\cos\omega t + \mathrm{Im}\left\{\varepsilon_- e^{i(kz-\theta)} I_-\right\}\sin\omega t\right] \tag{2-48}$$

$$J_{-\theta} = qn_i \mathrm{Im}\langle w\rangle_-$$

$$= \frac{q^2 n_i}{MkV_T}\left[-\mathrm{Re}\left\{\varepsilon_- e^{i(kz-\vartheta)} I_-\right\}\sin\omega t + \mathrm{Im}\left\{\varepsilon_- e^{i(kz-\vartheta)} I_-\right\}\cos\omega t\right] \tag{2-49}$$

Similarly, we have

$$E_r = \mathrm{Re}\left[(\varepsilon_+ + \varepsilon_-)e^{i(kz-\theta)}\right]\cos\omega t - \mathrm{Im}\left[(\varepsilon_+ - \varepsilon_-)e^{i(kz-\theta)}\right]\sin\omega t, \tag{2-50}$$

$$E_\theta = \mathrm{Re}\left[(\varepsilon_+ - \varepsilon_-)e^{i(kz-\theta)}\right]\sin\omega t + \mathrm{Im}\left[(\varepsilon_+ + \varepsilon_-)e^{i(kz-\theta)}\right]\cos\omega t, \tag{2-51}$$

$$S_r = 2k\mathrm{Re}\left[\varepsilon_o e^{i(kz-\vartheta)}\right]\cos\omega t, \tag{2-52}$$

$$S_\theta = 2k\mathrm{Im}\left[\varepsilon_o e^{i(kz-\vartheta)}\right]\cos\omega t. \tag{2-53}$$

We can now rewrite equations (2-45) and (2-46) in terms of ε_+ and ε_-. Each equation is divided into two parts; one varying with $\sin\omega t$ and the other with $\cos\omega t$. Thus we obtain four equations for the complex amplitudes ε_+ and ε_-. These equations are

$$(\frac{1}{r}\frac{d}{dr}-k^2)Re(\varepsilon_+ + \varepsilon_-) + 2k^2 Re(\varepsilon_o) = \zeta Im(\varepsilon_- I_-), \qquad (2\text{-}54)$$

$$(\frac{1}{r}\frac{d}{dr}-k^2)Re(-\varepsilon_+ + \varepsilon_-) = -\zeta Re(\varepsilon_- I_-), \qquad (2\text{-}55)$$

$$(\frac{d^2}{dr^2}-k^2)Im(\varepsilon_+ + \varepsilon_-) - 2k^2 Im(\varepsilon_o) = -\zeta Re(\varepsilon_- I_-), \qquad (2\text{-}56)$$

$$(\frac{d^2}{dr^2}-k^2)Re(\varepsilon_+ - \varepsilon_-) = -\zeta Im(\varepsilon_- I_-), \qquad (2\text{-}57)$$

where

$$\zeta = \frac{4\pi n q^2 \omega}{Mk V_T c^2} \qquad (2\text{-}58)$$

In complex form, equations (2-54) to (2-57) are written as

$$(\frac{1}{r}\frac{d}{dr}-k^2)(\varepsilon_+^* + \varepsilon_-) + 2k^2 Re(\varepsilon_o) = -i\zeta\varepsilon_- I_- , \qquad (2\text{-}59)$$

$$(\frac{d^2}{dr^2}-k^2)(\varepsilon_+^* - \varepsilon_-) + 2k^2 i Im(\varepsilon_o) = i\zeta\varepsilon_- I_- , \qquad (2\text{-}60)$$

where x* denotes the conjugate of x. As assumptions $Im(\varepsilon_o)=0$ and $k>0$ do not violate the generality of equations (2-59) and (2-60), we shall solve the equations under these assumptions.

The field equations in vacuum can be get by setting $\zeta=0$, and their solutions are found to be

$$\varepsilon_+^{*v} - \varepsilon_-^{v} = c_1 e^{-kr} \quad , \tag{2-61}$$

$$\varepsilon_+^{*v} + \varepsilon_-^{v} = 2\varepsilon_0 \quad . \tag{2-62}$$

In order to distinguish the quantities in vacuum from those in plasma, we affix superscripts v and p to the symbols in vacuum and plasma, respectively. If $kr_p < 1$, we can express the general solutions of equations (2-59) and (2-60) in terms of power series of kr. These solutions can be found after some calculations, and they are

$$\varepsilon_+^{*p} = a + a_1 r + \frac{1}{2}(a-\varepsilon_0)(kr)^2 + \frac{1}{12}\left[2+\frac{i\zeta I_-}{k^2}\right]\frac{a_1}{k}(kr)^3 + \cdots\cdots\cdots + a_n r^n + \cdots, \tag{2-63}$$

$$\varepsilon_-^{p} = b - a_1 r + \frac{1}{2}\left\{(b-\varepsilon_0) - \frac{i\zeta I_-}{k^2} b\right\}(kr)^2 + \frac{1}{12}\left(-2+\frac{i\zeta I_-}{k^2}\right)\frac{a_1}{k}(kr)^3 + \cdots b_n r^n + \cdots, \tag{2-64}$$

where

$$\begin{aligned}
a_{2m+1} &= \frac{1}{4m(2m+1)}\left[k^2(2m+1)a_{2m-1} + (2m-1)(k^2 - i\zeta I_-)b_{2m-1}\right] \quad \text{for } m \geq 1, \\
a_{2m} &= \frac{1}{2m(2m-1)}\left[k^2 m a_{2m-2} + (m-1)(k^2 - i\zeta I_-)b_{2m-2}\right] \quad \text{for } m \geq 2, \\
b_{2m+1} &= \frac{1}{4m(2m+1)}\left[k^2(2m-1)a_{2m-1} + (2m+1)(k^2 - i\zeta I_-)b_{2m-1}\right] \quad \text{for } m \geq 1, \\
b_{2m} &= \frac{1}{2m(2m-1)}\left[k^2(m-1)a_{2m-2} + (m-1)(k^2 - i\zeta I_-)b_{2m-2}\right] \quad \text{for } m \geq 2.
\end{aligned} \tag{2-65}$$

The constants a, a_1, b and c_1 are determined from boundary conditions. Next we shall derive the boundary equations so as to determine the constants. From Maxwell's equations, we have

$$\Delta(\vec{r}\cdot\vec{B}) = 0, \tag{2-66}$$

$$-\Delta(\vec{r} \times \vec{B}) = \frac{4\pi}{c} \vec{J}^s , \tag{2-67}$$

$$\Delta(\vec{r} \times \vec{E}) = 0 , \tag{2-68}$$

$$\Delta(\vec{r}\cdot\vec{D}) = 0 , \tag{2-69}$$

where $\vec{J}^s$ and $\vec{D}$ are the surface current and the electric displacement. $\Delta(x)$ denotes the change of some quantity x across the plasma surface. Since there is no mass flow across the interface, a magneto-hydrodynamic equation

$$\rho \frac{\partial \vec{v}}{\partial t} = \frac{1}{c} \vec{J} \times \vec{B}$$

yields

$$\vec{J}^s \times \hat{z} = 0, \tag{2-70}$$

in the approximation of the first order. From equations (2-66) to (2-70), we finally get the first order boundary equations as

$$\frac{\partial E_\theta^p}{\partial z} = \frac{\partial E_\theta^v}{\partial z} , \tag{2-71}$$

$$\frac{\partial E_\theta^p}{\partial r} = \frac{\partial E_\theta^v}{\partial r} , \tag{2-72}$$

$$E_\theta^p = E_\theta^v , \tag{2-73}$$

$$D_r^p = D_r^v , \tag{2-74}$$

at $r=r_p$, where we have used equation (2-42).

From equation (2-51), we have

$$\frac{\partial E_\theta^p}{\partial z} = k\left[\mathrm{Re}\left\{(\varepsilon_+^p+\varepsilon_-^p)e^{i(kz-\theta)}\right\}\cos\omega t - \mathrm{Im}\left\{(\varepsilon_+^p-\varepsilon_-^p)e^{i(kz-\theta)}\right\}\sin\omega t\right] \tag{2-75}$$

and likewise $\frac{\partial E_\theta^v}{\partial z}$ is expressed. Then equation (2-71) is written by

$$\mathrm{Re}(\varepsilon_+^p+\varepsilon_-^p) = \mathrm{Re}(\varepsilon_+^v+\varepsilon_-^v) \ , \tag{2-76}$$

$$\mathrm{Im}(\varepsilon_+^p-\varepsilon_-^p) = \mathrm{Im}(\varepsilon_+^v-\varepsilon_-^v) \ . \tag{2-77}$$

In complex form, above equations become

$$\varepsilon_+^{*p} + \varepsilon_-^p = \varepsilon_+^{*v} + \varepsilon_-^v = 2\varepsilon_o \ , \tag{2-78}$$

where we have used equation (2-62). Analogously, the boundary conditions (2-72) and (2-73) can be expressed in terms of ε_+^* and ε_- as

$$\frac{d}{dr}(\varepsilon_+^{*p}-\varepsilon_-^p) = \frac{d}{dr}(\varepsilon_+^{*v}-\varepsilon_-^v) = -kc_1e^{-kr_p} \ , \tag{2-79}$$

$$\varepsilon_+^{*p} - \varepsilon_-^p = \varepsilon_+^{*v} - \varepsilon_-^v = c_1e^{-kr_p} \ . \tag{2-80}$$

In order to derive the electric displacement $\vec{D}$, the ion currents, induced by the field component varying with time as $e^{i\omega t}$, must be taken into account. This current $\vec{J}_+$ is given in complex form by

$$J_{+r} + iJ_{+\theta} = \frac{n_i q^2 \mathcal{E}_+}{MV_T k} I(kz;\beta) e^{-i\theta} e^{i\omega t} , \qquad (2\text{-}81)$$

where $I(kz;\beta)$ is defined by equation (2-26) and

$$\beta = \frac{\omega_i + \omega}{kV_T} . \qquad (2\text{-}82)$$

The term $I(kz;\beta)$ may be approximately expressed by

$$I(kz;\ \beta) \simeq I_+ e^{ikz} ,$$

similarly to equation (2-47). Thus the induced current $\vec{J}$ is given by

$$J_r + iJ_\theta = \frac{n_i q^2}{MV_T k} \left[\mathcal{E}_+^{\mathcal{P}} I_+ e^{i\omega t} + \mathcal{E}_-^{\mathcal{P}} I_- e^{-i\omega t} \right] e^{i(kz-\theta)} . \qquad (2\text{-}83)$$

The electric displacement $\vec{D}$ includes the vacuum displacement and the plasma current according to the relation

$$\vec{D} = \vec{E} + 4\pi \int \vec{J}\, dt . \qquad (2\text{-}84)$$

Combination of equations (2-3), (2-83) and (2-84) yields the displacement current in complex form

$$D_r + iD_\theta = \left[(\mathcal{E}_+^p e^{i\omega t} + \mathcal{E}_-^p e^{-i\omega t}) + i\zeta \frac{c^2}{\omega^2} (-\mathcal{E}_+^{\mathcal{P}} I_+ e^{i\omega t} + \mathcal{E}_-^{\mathcal{P}} I_- e^{-i\omega t}) \right] e^{i(kz---} \qquad (2\text{-}85)$$

Thus the last boundary equation (2-74) is expressed by

$$\mathcal{E}_+^{*p} I_+^* + \mathcal{E}_-^p I_- = 0 , \qquad (2\text{-}86)$$

where we have used equation (2-78). This relation implies there is no radial current at the interface. In the case of zero plasma density, equation (2-86) is no longer valid, but equation (2-80) acts as a substitute for this equation.

The constants a, a_1, b and c_1 can be determined from these four boundary equations (2-78), (2-79), (2-80) and (2-86). Finally we can write down the solutions as

$$\varepsilon_+^{*p} = \varepsilon_o\left[1+\xi+\eta(1-\xi k^2 r_o^2)-\xi(kr_o)(kr)+(\frac{\eta}{2}+\xi)(kr)^2+0\{(kr)^3\}\right] \tag{2-87}$$

$$\varepsilon_-^{p} = \varepsilon_o\left[1-\xi+\xi(kr_o)(kr)-\frac{1}{2}\eta(kr)^2+0\{(kr)^3\}\right] \tag{2-88}$$

and

$$\varepsilon_+^{*v} = \varepsilon_o(1+\xi e^{-kr}) , \tag{2-89}$$

$$\varepsilon_-^{v} = \varepsilon_o(1-\xi e^{-kr}) , \tag{2-90}$$

where

$$\eta = \frac{i\zeta I_-}{k^2} = i\omega_{pi}^2 \frac{\omega}{k^3 V_T c^2} , \tag{2-91}$$

$$\xi = \frac{1-\frac{1}{2}\eta k^2 r_o^2 - K\{1+\eta(1+\frac{1}{2}k^2 r_o^2)\}}{1-k^2 r_o^2+K\{1-\frac{1}{4}(1+2\eta)k^2 r_o^2\}} , \tag{2-92}$$

$$\omega_{pi} = \left(\frac{4\pi n_i q^2}{M}\right)^{1/2} : \text{ion plasma frequency,} \tag{2-93}$$

$$K = \frac{\varepsilon_-^p}{\varepsilon_+^{*p}} = -\frac{I_+^*}{I_-} \quad \text{at } r=r_p \quad \text{when } n_i \neq 0 , \tag{2-94}$$

$$=1 \quad \text{when } n_i=0, \tag{2-94}'$$

$$k > 0. \tag{2-95}$$

When n_i tends to zero, ξ vanishes and then $\varepsilon_+^{*p}=\varepsilon_-^p=\varepsilon_+^{*v}=\varepsilon_-^v=\varepsilon_0$. Needless to say, this implies the vacuum field. In the central region of the plasma, the field is approximately given by

$$\varepsilon_+^{*p} = \varepsilon_0 \left\{1 + \xi + \eta(1 - \xi k^2 r_0^2)\right\} , \tag{2-96}$$

$$\varepsilon_-^p = \varepsilon_0(1 - \xi). \tag{2-97}$$

Generally K is small quantity in the cyclotron resonance state $|\omega_i+\omega| \gg |\omega_i-\omega|$. Therefore, if $kr_0 \ll 1$ (i.e. the case of long axial wavelength), equations (2-96) and (2-97) approximately become

$$\varepsilon_+^{*p} \simeq 2\varepsilon_0(1 - K) , \tag{2-98}$$

$$\varepsilon_-^p \simeq 2\varepsilon_0 K. \tag{2-99}$$

That is $$|\varepsilon_+^{*p}| \gg |\varepsilon_-^p| . \tag{2-100}$$

The polarized field in the same sense as the ion gyration becomes very small in this case. As seen from equations (2-26), $I_+(kz,\beta)$ approaches $I_-(kz,\alpha)$ as kV_T tends to infinity; namely, $|I_+^*|$ approaches $|I_-|$. These facts mean that the axial wavelength of the heating field, $\frac{2\pi}{k}$, should be appropriately short in order to heat the plasma efficiently by this configuration of field. This is the reason why axially periodic heating fields are used for ion cyclotron heating of plasma.

2.3 Ion Cyclotron Heating by the Picket Fence Field

The ion cyclotron heating by the Picket Fence field expressed by equation (2-2) will be treated in this section. The analytical process is alike to that adopted in the section 2.2, so that only the results are given here.

We make the same approximations as in the section 2.2 and then solve the equation of motion (2-4). The mean velocity and mean energy flux averaged over all phase of incoming ions will be derived. Averaging these quantities over distributed velocities of ions, we have the energy dissipation from the heating region and the averaged ion velocity in this case.

2.3.1 Ion Motion and Physical Picture

After some algebra, we get the mean energy flux of mono-energy ions, which is, in the similar notations in the section 2.2,

$$E.F_{+} = \frac{2n_i q^2 \mathcal{E}_{-}^{2}}{Mk^2 w_o} \quad \frac{\sin^2 \pi N\alpha'}{(1-\alpha'^2)^2} \quad , \qquad (2\text{-}101)$$

where

$$\alpha' = \frac{\omega_i - \omega}{kw_o} \ .$$

Then we get the averaged energy dissipation from the heating section, which is

$$E.D. = \frac{2n_i q^2 \varepsilon_-^2}{\sqrt{\pi} M k^2 V_T} \int_{-\infty}^{\infty} \frac{\sin^2(\pi N \frac{\alpha}{s})}{|s|(1-\alpha^2)^2} e^{-(s-\delta)^2} ds, \quad (2\text{-}102)$$

where

$$\left.\begin{aligned} \frac{\omega_i - \omega}{k V_T} &= \alpha \ , \\ \frac{u}{V_T} &= \delta \ . \end{aligned}\right\}$$

Equation(2-101) corresponds to equation (2-28) and equation(2-102) to equation (2-21).

Now let us consider the physical picture introduced from equation (2-101). Similarly to the section 2.2, we have a curve of the frequency spectrum of $E.F_+$. For convenience' sake, we define

$$Y(\alpha') = \frac{\sin^2(\pi N \alpha')}{(1-\alpha'^2)^2} \quad , \qquad (2\text{-}103)$$

which again corresponds to equation (2-30). Then we find

$$Y(\alpha') = 0, \quad \text{when } \alpha = \frac{s}{N} \quad (s : \text{integer but } s \neq +1),$$

$$Y(\alpha') = \frac{\pi^2 N^2}{\pi^2 N^2 (1-\alpha'^2)^2 + 4\alpha'^2} \quad , \text{ when}$$

$$\tan(\pi N \alpha') = -\frac{\pi N (1-\alpha'^2)}{2\alpha'} \quad .$$

As a results, we have the frequency spectrum of $E.F_+$ as shown in Fig. 2-4.

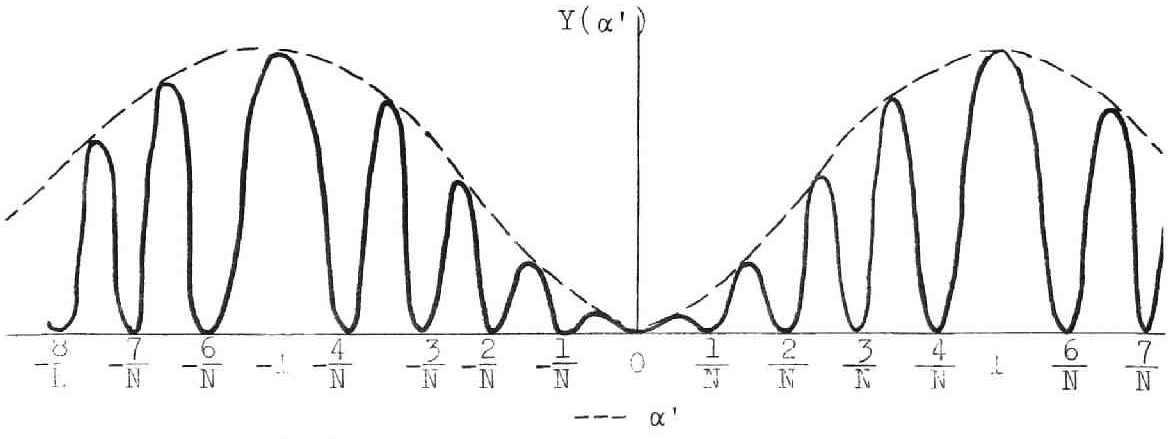

Fig. 2-4 $Y(\alpha')$ as a function of α' .

It is worth while noting that this frequency spectrum has two identical maxima where $\alpha = \pm 1$. On the other hand, the spectrum in the case of the helical field has only a maximum. This situation may be explained as follows.

A particle traveling in the heating region feels two frequencies at the same time; one is due to the field approaching to the particle (or $\omega'=\omega+kw_o$) and another due to the field going away from the particle (or $\omega'=\omega-kw_o$). In other words, the particle feels two shifted frequencies on account of a Doppler effect. If w_o is somewhat distributed by Δw_o, according as

$$\frac{1}{N} < \frac{\Delta w_o}{w_o} \ll 1 \quad ,$$

then the frequency spectrum has no longer fine structure and its shape becomes alike to the envelope shown in Fig. 2-4.

2.3.2 Frequency Spectra of the Energy Flux for Distributed Ion Velocities

Again, we shall see the frequency dependence of the energy dissipation from the heating region. For this sake, we shall examine a term in equation (2-102)

$$I(\alpha, \delta) = \int_{-\infty}^{+\infty} \frac{\sin^2(\pi N \frac{\alpha}{s})}{|s|\,(1-\alpha^2)^2}\, e^{-(s-\delta)^2}\, ds. \quad (2\text{-}104)$$

Computed values of $I(\alpha, \delta)$ by KDC-1 are given in Fig. 2-5 for different values of α and δ. Consequently, we can get information as follows.

(i) For large δ, the corresponding peak of $I(\alpha, \delta)$ (or E.D.) is situated near the position where $\alpha = \pm \delta$ (i.e. $\omega = \omega_i + ku$). In this case, the shape of the spectrum tends to resemble to the dashed line in Fig. 2-4. Therefore we can also determine the beam velocity of plasma, in a similar way described in the section 2.2.3.

(ii) For large δ, the spectrum tends to have double peaks on both the negative and the positive sides of α. This point is different from the case of the helical field.

(iii) The heating efficiency, which corresponds to $I(\alpha, \delta)$, rapidly decreases as δ becomes larger.

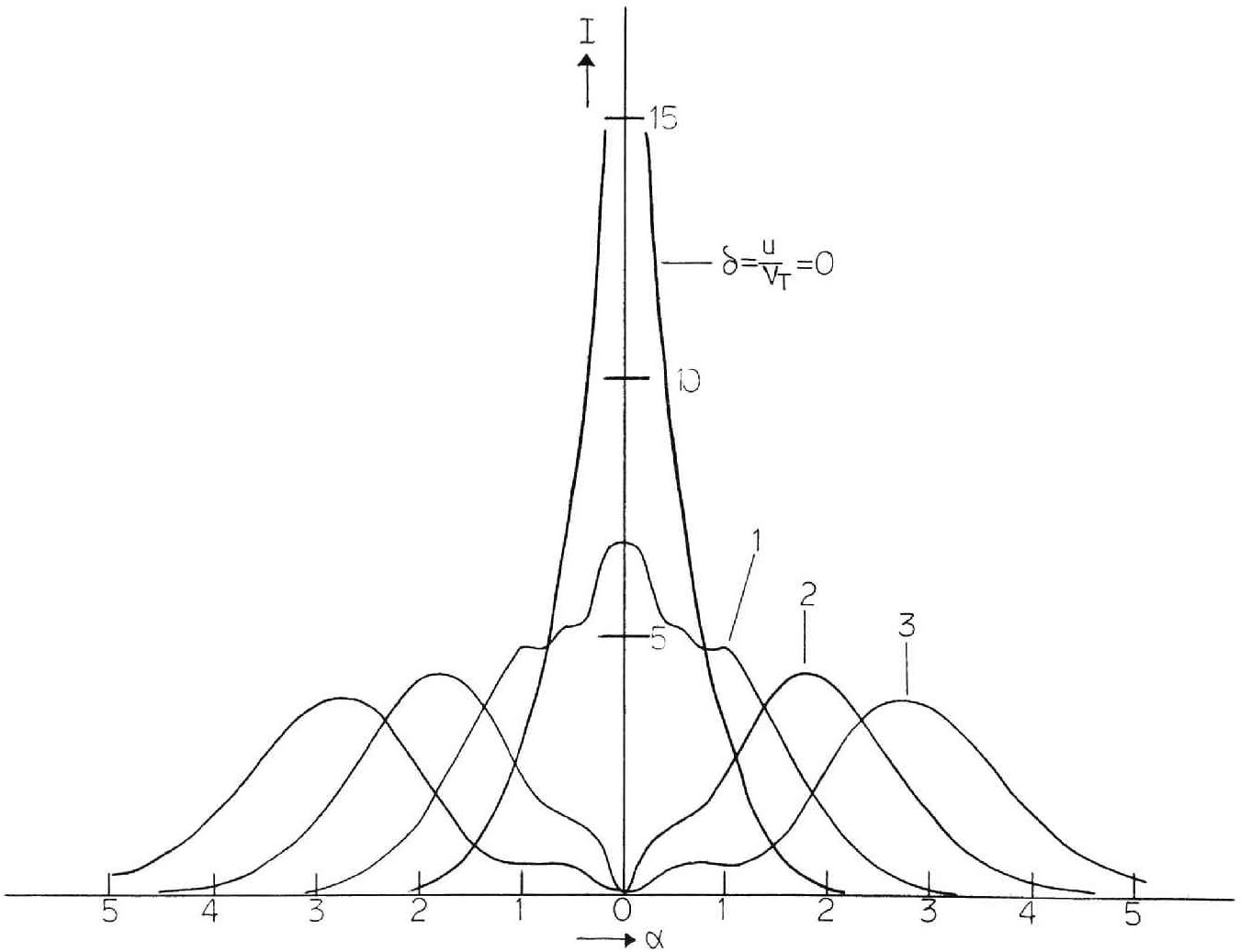

Fig. 2-5 $I(\sigma,\delta)$ as a function of α for different δ in the case of the Picket Fence type field.

2.3.3 Penetration of the Accelerating Field into Plasma

This problem is considerably simple in comparison with the case of the helical field, since the field configuration is axisymmetric and consequently its boundary condition is simple. There is only an azimuthal electric component at the boundary, so that the connection of the displacement as expressed by equation (2-69) is no longer required. Furthermore, differential field equations in the first order approximation are in simple form. Lenard and Kulsrud analyzed the radial dependence of the field and found

$$\varepsilon_+^{*p} = c_1 J_1\left(\frac{ikr}{\sigma}\right), \tag{2-105}$$

$$\varepsilon_+^{*p} + \varepsilon_-^{p} = \eta I(kz,\alpha)\varepsilon_- , \tag{2-106}$$

$$\varepsilon_+^{*v} = c_1 \sigma J_1(ikr), \tag{2-107}$$

$$\varepsilon_+^{*v} + \varepsilon_-^{v} = 0. \tag{2-108}$$

where

$$\sigma^2 = \frac{\eta I - 2}{2\eta I - 2},$$

η : defined by equation (2-91),

$$\alpha = \frac{\omega_i - \omega}{kV_T},$$

$$I(kz,\alpha) = -\frac{2sg(\alpha)}{i\sqrt{\pi}} \int_0^\infty dx\ e^{-\alpha^2/x^2} \frac{\sin kz - \frac{1}{x}(-1)^N e^{-N\pi i x sg(\alpha)} \sin xkz}{1 - x^2}$$

If we consider the extreme case $\eta I \ll 1$, we get to a good approximation

$$\mathcal{E}_+^* = -\mathcal{E}_- \qquad (2\text{-}109)$$

In this case the two circularly polarized electric field components have about the same amplitude. Above relation implies

$$E_r^p \ll E_\theta^p \qquad (2\text{-}110)$$

In the opposite case of sufficiently high density,

$$\mathcal{E}_+^{*p} = \eta I \mathcal{E}_-^p \qquad (2\text{-}111)$$

This shows that the component rotating in the opposite sense of ion gyration is predominant. In this case the circularly polarized field component rotating in the same sense as would ions becomes very small and ,as a result, the heating efficiency is low.

III Theory of Nonaxisymmetric Oscillation of Plasma near Ion Cyclotron Frequency in an External Magnetic Field

3.1 Introduction

After Alfven's discovery[17] of magnetohydrodynamic waves in 1942, many types of plasma oscillations have been found theoretically and also verified experimentally. In such waves, so-called in cyclotron waves were found useful for plasma heating by Stix (1957)[18], since then many investigations have been done on these waves. As stated in the chapterII, the direct heating of ions with the ion cyclotron resonance tends to be less efficient as plasma density increases, which is due to the shielding of accelerating field by the inductive ion currents. On the other hand, in such high density plasma, ion cyclotron waves can naturally exist and be resonantly excited by externally applied currents surrounding the plasma. The ion cyclotron wave, excited in such a way, may propagate along the magnetic lines of force through a region where the magnetic field decreases slowly in the direction of the wave propagation. In this region, the phase velocity of the wave will become slower and slower and finally subjects to cyclotron damping, which is a kind of phase mixing. As a result, the oscillation energy will be converted into random energy of ions (i.e. thermal energy). This is the heating mechanism.

Stix and his collaborators verified experimentally this thermalization mechanism by using Model B-65 Stellarator[19] and Model B-66 Stellarator[20]. Wilcox and his coworkers[21] observed the cyclotron damping of a torsional Alfvén wave. However, these theoretical and experimental results were only concerning axisymmetric modes of the waves, except for Bernstein and Trehan's theoretical work[22]. This reason is that there are lying many difficulties to solve nonaxisymmetric modes. Bernstein and Trehan found a way to obtain the dispersion relation of nonaxisymmetric modes of ion cyclotron waves. Neverthless, they treated the case without beam current, and did not give the detail physical picture of the waves.

In this chapter, nonaxisymmetric modes with an ionic beam current are to be generally analyzed by expanding the Bernstein and Trehan's analytical method. Furthermore, detail discussions of the physical picture and the boundary situation of the waves are also to be given. The dispersion relation will be derived in a section 3.2. The physical pictures, such as ion current, electron motion and plasma neutrality, are also discussed in a section 3.3. Discussions of bounded plasma oscillations are to be done in a section 3.4. Finally, in a section 3.5, application to plasma heating is to be briefly explained.

Since relatively low frequency oscillations are of interest for ion heating, we shall simplify the analysis with following approximations through this chapter.

(i) Oscillation frequency ω is sufficiently low compared with electron plasma frequency ω_{pe} and electron cyclotron frequency ω_e. That is,

$$\omega^2 \ll \omega_{pe}^2 , \quad \omega_e^2 \tag{3-1}$$

(ii) Electron mass m can be neglected in comparison with ion mass M. That is,

$$\frac{m}{M} \ll 1 \tag{3-2}$$

(iii) We assume electrical neutrality in equilibrium state.

(iv) Plasma is so tenuous that interparticle collision is negligible and that particles interact each other through long range electromagnetic interactions.

(v) We neglect the plasma pressure, but a beamlike motion parallel to the axis is assumed. Plasma with Maxwellian distribution of ions may be regarded as a ensemble of infinite number of ion beams. Therefore, we can expand our conclusion of an ion beam to plasma with distributed ions after some investigations.

3.2 Derivation of Dispersion Relation

Situations discussed in this section are schematically shown in Fig. 3-1.

In equilibrium state, an external static magnetic field $\vec{B}_o$ is imposed parallel to the z-axis of cylindrical co-ordinates (r, θ, z). An infintely long cylindrical uniform plasma is set up coaxially with the z-axis. The plasma pressure is assumed zero, but a beam of ions with velocity $\vec{u}$ is flowing parallel to the z-axis. A variety of boundary conditions may be considered, but these problem will be discussed again in the section 3.4.

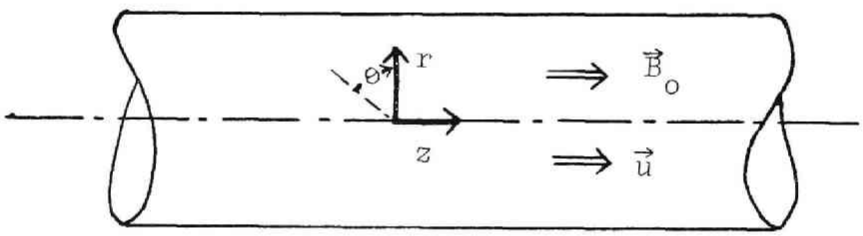

Fig. 3-1 Schematic drawing of plasma situation.

First-order perturbations from the equilibrium situation are considered. $\vec{B}$, $\vec{E}$, $\vec{J}$ and $\vec{v}$ are the first-order perturbed quantities of magnetic field, electric field, current and mean mass velocity, respectively.

In the next small section, basic equations valid for this situation are to be derived. Dispersion relations of general or special cases are both disccussed in the remaining small sections.

3.2.1 Basic Equations

The macroscopic quantities are determined by the transport equations of kinetic theory . In the approximations stated above, we have a linealized equation for ions

$$\frac{\partial \vec{v}_i}{\partial t} + (\vec{u}\cdot\vec{\nabla})\vec{V}_i = \frac{Z_i e}{M}(\vec{E} + \frac{1}{c}\vec{u}\times\vec{B} + \frac{1}{c}\vec{v}_i \times \vec{B}_o). \qquad (3\text{-}3)$$

For electrons, we get

$$-\frac{\partial \vec{v}_e}{\partial t} = \frac{e}{m}(\vec{E} + \frac{1}{c}\vec{v}_e \times \vec{B}_o). \qquad (3\text{-}4)$$

Where suffices i and e correspond to ion and electron, respectively, and $Z_i e$ and e are the charges of an ion and an electron. Equations (3-3) and (3-4) must be solved together with Maxwell's equations:

$$\nabla \times \vec{B} = \frac{4\pi}{c}(\vec{J} + \vec{J}_o), \qquad (3\text{-}5)$$

$$\nabla\cdot\vec{B} = 0, \qquad (3\text{-}6)$$

$$\nabla \times \vec{E} = -\frac{1}{c}\frac{\partial \vec{B}}{\partial t}, \qquad (3\text{-}7)$$

$$\nabla\cdot E = 4\pi\sigma', \qquad (3\text{-}8)$$

where

$$\vec{J} = n_i Z_i e\vec{v}_i - n_e e\vec{v}_e \simeq n_e e(\vec{v} - \vec{v}_e), \qquad (3\text{-}9)$$

$$\vec{J}_o \simeq n_e e\vec{u}. \qquad (3\text{-}10)$$

$$(\vec{v} = \frac{n_i M\vec{v}_i + n_e m\vec{v}_e}{n_i M + n_e m} \simeq \vec{v}_i)$$

and n_i and n_e are number densities of the ion and the electron, respectively. There is a relation in equilibrium state as

$$n_i Z_i = n_e. \qquad (3\text{-}11)$$

We have neglected the displacement current, since we are interested only in low frequency oscillations.

To obtain the dispersion relation, we derive some convenient formulae from above equations. Combination of equations (3-3) and (3-4) gives

$$\frac{1}{n_e e^2}\frac{\partial \vec{J}}{\partial t} + \frac{(\vec{u}\cdot\vec{\nabla})v_i}{e} = (\frac{Z_i}{M} + \frac{1}{m})\vec{E} + \frac{1}{c}\{\frac{Z_i}{M}(\vec{u}\times\vec{B} + \vec{v}_i \times \vec{B}_o) + \frac{1}{m}v_e \times \vec{B}_o\}$$

$$\simeq \frac{1}{m}\{\vec{E} + \frac{1}{c}\vec{v}_e \times \vec{B}_o\} \qquad (3\text{-}12)$$

$$\rho\{\frac{\partial \vec{v}}{\partial t} + (\vec{u}\cdot\vec{\nabla})\vec{v}\} = \frac{1}{c}\vec{J} \times \vec{B}_o + \frac{1}{c}\vec{J}_o \times \vec{B}_o , \qquad (3\text{-}13)$$

where we have adopted the approximation expressed by relation (3-2), and ρ is the mass density of plasma, which is

$$\rho \simeq n_i M. \tag{3-14}$$

From the definition of $\vec{J}$, we get

$$\vec{v}_e \simeq \vec{v} - \frac{1}{n_e e}\vec{J}. \tag{3-15}$$

Substituting equation (3-15) into equation (3-13), finally we have

$$4\pi\omega_{pe}^{-2}\frac{\partial \vec{J}}{\partial t} = \vec{E} + \frac{1}{c}\vec{v} \times \vec{B}_o - \frac{1}{cn_e e}\vec{J} \times \vec{B}_o - 4\pi\omega_{pe}^{-2}(\vec{J}_o \cdot \vec{\nabla})\vec{v}, \tag{3-16}$$

where

$$\omega_{pe}^2 = \frac{4\pi n e^2}{m} \text{ (electron plasma frequency).}$$

When $\omega \ll \omega_{pe}$ and $ku \ll \omega_{pe}$ (k: wave number), equation (3-16) can be rewritten as

$$\vec{E} + \frac{1}{c}\vec{v} \times \vec{B}_o - \frac{1}{cn_e e}\vec{J} \times \vec{B}_o = 0. \tag{3-17}$$

This is a linealized equation of the generalized Ohm's law when an ion beam is flowing.

Equations (3-13), (3-17) and Maxwell's equations are the basic equations for solving the problem. Also it should be noted that equation (3-17) shows the non-existence of the electric field parallel to the external magnetic field.

3.2.2 Dispersion Relation of Nonaxisymmetric Mode

In order to obtain the dispersion relation, we follow a normal mode analysis similar to that of Berstein and Trehan, though the situation in this case is different from in their case. We assume that variations of all quantities conform to a form $\exp\{i(m\theta + kz - \omega t)\}$. Combination of equations (3-7) and (3-17) yields

$$\frac{\partial \vec{B}}{\partial t} = \vec{\nabla} \times \left\{ \vec{v} \times B_o - \frac{1}{cn_e e} \vec{J} \times \vec{B}_o \right\} . \qquad (3\text{-}18)$$

Furthermore, differentiating equation (3-18) with respect to t, then we get

$$\frac{\partial^2 \vec{B}}{\partial t^2} = \vec{\nabla} \times \left\{ \frac{\partial \vec{v}}{\partial t} \times \vec{B}_o - \frac{1}{n_e e} \frac{\partial \vec{J}}{\partial t} \times B_o \right\} . \qquad (3\text{-}19)$$

Using equations (3-13) and (3-5), we find that equation (3-19) becomes

$$- \frac{\omega^2}{A^2} \vec{B} = \vec{\nabla} \times \left[\left\{ (\vec{\nabla} \times \vec{B}) \times \hat{z} \right\} \times \hat{z} + i \frac{\omega - ku}{\omega_i} \left\{ (\vec{\nabla} \times \vec{B}) \times \hat{z} \right\} + \frac{\omega_i u}{A^2} \vec{B} \right] , \qquad (3\text{-}20)$$

where we have assumed that the contribution of the electron motion to transverse plasma current is negligible compared with that of the ion motion. Also ω_i

is the ion cyclotron frequency and A is defined as

$$A^2 = \frac{B_o}{4\pi\rho} , \qquad (3\text{-}21)$$

which is the velocity of Alfven wave.

Each component of equation (3-20) is readily found to be

r-component:

$$(k^2 - \frac{\omega^2}{A^2})B_r = ik(k\Omega^* - \frac{\omega_i u}{A^2})B_\theta - i\left\{k\frac{\partial}{\partial r} + \frac{m}{r}(k\Omega^* - \frac{\omega_i u}{A^2})\right\} B_z . \qquad (3\text{-}22)$$

θ-component:

$$(k^2 - \frac{\omega^2}{A^2})B_\theta = -ik(k\Omega^* - \frac{\omega_i u}{A^2})B_r + \left\{(k\Omega^* - \frac{\omega_i u}{A^2})\frac{\partial}{\partial r} + \frac{m}{r}k\right\} B_z . \qquad (3\text{-}23)$$

z-component:

$$-(\frac{\partial^2}{\partial r^2} + \frac{1}{r}\frac{\partial}{\partial r} + \frac{\omega^2}{A^2} - \frac{m^2}{r^2})B_z = \left[k\frac{m}{r} - (k\Omega^* - \frac{\omega_i u}{A^2})(\frac{1}{r} + \frac{\partial}{\partial r})\right]B_\theta$$

$$-i\left[-(k\Omega^* - \frac{\omega_i u}{A^2})\frac{m}{r} + k(\frac{1}{r} + \frac{\partial}{\partial r})\right]B_r , \qquad (3\text{-}24)$$

where $\Omega^* = \frac{\omega - ku}{\omega_i}$, and the term $\exp\{i(m\theta + kz - \omega\tau)\}$ is supressed.

From equations (3-22), (3-23) and (3-24), we have, after some algebra,

$$B_r = \frac{-i}{F^2-k^2G^2}\left[\frac{m}{r}G(F-k^2)B_z + k(F-G^2)\frac{\partial B_z}{\partial r}\right], \qquad (3\text{-}25)$$

$$B_\theta = \frac{1}{F^2-k^2G^2}\left[\frac{m}{r}k(F-G^2)B_z + G(F-k^2)\frac{\partial B_z}{\partial r}\right], \qquad (3\text{-}26)$$

$$B_z = C\, J_m(hr)\, \exp i(m\theta + kz - \omega t), \qquad (3\text{-}27)$$

where

$$h^2 = -\frac{F^2-k^2G^2}{F-G^2}, \qquad (3\text{-}28)$$

$$\left.\begin{aligned} G &= k\Omega^* - \frac{\omega_i u}{A^2}, \\ F &= k^2 - \frac{\omega^2}{A^2}, \\ \Omega^* &= \frac{\omega - ku}{\omega_i}, \end{aligned}\right\} \qquad (3\text{-}29)$$

and J_m is the Bessel Function of the mth order. C is an arbitrary multiplicative constant. Equation (3-28) is the so-called dispersion relation to be solved, and we can rewrite it as

$$h^2 = - \frac{(k^2 - \frac{\omega^2}{A^2})^2 - k^2(k\Omega^* - \frac{\omega_i u}{A^2})^2}{k^2 - \frac{\omega^2}{A^2} - (k\Omega^* - \frac{\omega_i u}{A^2})^2} \quad . \qquad (3\text{-}28)'$$

Radial wave number h is determined from boundary conditions, about which we shall discuss in the section 3.4. Once we know C and h, the transverse components will be easily determined from the equations (3-25) and (3-26). Consequently, other fields, such as E_r and E_θ, are also obtainable, by using appropriate relations between $\vec{E}$ and $\vec{B}$.

If we assume u=0, then the resulting dispersion formula agrees with that obtained by Stix or Bernstein and Trehan, which is

$$h^2 = \frac{(k^2 - \frac{\omega^2}{A^2})^2 - k^4\Omega^4}{k^2 - \frac{\omega^2}{A^2} - k^2\Omega^2} \qquad (3\text{-}30)$$

or, in another notations,

$$\frac{c^2h^2}{\omega_{pi}^2} = \frac{\Omega^4 - \Omega^2(2\frac{k^2c^2}{\omega_{pi}} + \frac{k^4c^4}{\omega_{pi}^4}) + \frac{k^4c^4}{\omega_{pi}^4}}{\Omega^2(1 + \frac{k^2c^2}{\omega_{pi}^2}) - \frac{k^2c^2}{\omega_{pi}^2}} \quad , \qquad (3\text{-}31)$$

where

$$\Omega = \frac{\omega}{\omega_i} ,$$

$$\omega_{pi} = \frac{4\pi Z_i^2 e^2 n_i}{M} \quad \text{(ion Plasma frequency).} \quad (3\text{-}32)$$

It should be noted that the radial wave number h has no relation with the azimuthal wave number m.

3.2.3 Oscillation near Ion Cyclotron Frequency

Let us consider the case that the oscillation frequency is near ion cyclotron frequency, or $\omega \simeq \omega_i$. Furthermore, we assume that the plasma density is tenuous enough to satisfy the relation

$$\frac{\omega_i^2}{k^2 A^2} = \frac{\omega_{pi}^2}{k^2 c^2} \ll 1. \quad (3\text{-}33)$$

Relation (3-33) means that the ion plasma frequency is very low compared with the frequency of an electromagnetic wave with wavelength of $2\pi/k$.

Equation (3-30) may be rewritten in another form as

$$\frac{1}{\omega_i^2}(\omega - ku - \frac{\omega_i^2 u}{kA^2})^2 = (1 - \frac{\omega^2}{A^2 k^2})(1 - \frac{\omega^2}{A^2(k^2+h^2)}). \quad (3\text{-}34)$$

Under the condition given by equation (3-33), above equation becomes, approximately,

$$\left(\frac{\omega-ku}{\omega_i}\right)^2 \simeq 1 - \frac{\omega^2}{A^2k^2} - \frac{\omega^2}{A^2(k^2+h^2)} \quad . \qquad (3\text{-}35)$$

This is the dispersion relation of the ion cyclotron wave with an ion beam.

We have, instead of equation (3-35),

$$\omega = \frac{1}{1+\frac{\omega_i^2}{A^2k^2}\,\frac{2k^2+h^2}{k^2+h^2}} \left[ku \pm \omega_i \left\{1 - \frac{u^2}{A^2}\left(\frac{2k^2+h^2}{k^2+h^2}\right)\left(1-\frac{\omega_i^2}{k^2u^2}\right)\right\}^{1/2}\right] \quad . \quad . \qquad (3\text{-}36)$$

Therefore, if we assume k real and

$$u^2 > \frac{\omega_i^2}{k^2} + A^2\,\frac{k^2+h^2}{2k^2+h^2} \quad , \qquad (3\text{-}37)$$

then ω becomes complex. Namely, the wave grows or damps with time. This phenomenon may be considered as a kind of beam instability. However, equation (3-21) indicates that, in dilute plasma, the velocity of Alfvén wave A is very fast. Consequently, the condition of equation (3-37) may be impossible to be realized in practice. For example, ions of tenuous plasma under Joule heating (or Ohmic heating) will not be accelerated

enough to satisfy equation (3-37), due to their large mass inertia. In contrast to this ion motion, electrons will get high speed and finally grow up to runaway electrons. Equation (3-35) may be also applied to the plasma with a much shifted ion distribution, since it can be regarded as a beamlike plasma.

When u=0, equation (3-35) may be expressed by

$$\omega^2 = \omega_i^2\left(1 - \frac{\omega_i^2}{A^2k^2} - \frac{\omega_i^2}{A^2(k^2+h^2)}\right), \qquad (3\text{-}38)$$

or

$$\omega^2 = \omega_i^2\left(1 - \frac{\omega_{pi}^2}{c^2k^2} - \frac{\omega_{pi}^2}{c^2(k^2+h^2)}\right). \qquad (3\text{-}39)$$

This agrees with Stix's result for m=0 mode . When ω_i tends to ω, the axial wave number k (the axial wave length $2\pi/k$) approach to infinite (zero). And then the wave vanishes, so that the kinetic energy of the wave is converted into the thermal energy of the plasma. This mechanism may be called "Magnetic Beach" [23], because it has analogy to the collapse of Ocean waves running up on a beach.

3.2.4 Dispersion Relations in Other Special Cases

(i) When h=0, equation (3-34) becomes

$$\omega - ku = \pm\,\omega_i\left(1 - \frac{\omega_{pi}^2}{c^2k^2}\right). \qquad (3\text{-}40)$$

Equation (3-40) represents the dispersion relation of one dimensional case. Berger, Newcomb, Dawson, Frieman, Kulsrud and Lenard (1958)[24] had already obtained the dispersion relation in this case, but it is somewhat different in form from equation (3-40). However, we can easily show that they are both the same in our approximations. For large k, we have the relation

$$c^2k^2 \gg \omega_i^2 - \omega_{pi}^2$$

by using relation (3-33). Then equation (3-40) may be rewritten to be

$$\omega - ku = \pm \omega_i \left\{ 1 + \frac{\omega_{pi}^2}{\omega^2 - (c^2k^2 + \omega_{pi}^2)} \right\},$$

where we have assumed $\omega \simeq \omega_i$. Then we can readily find

$$\omega^2 - c^2k^2 - \omega_{pi}^2 \frac{\omega - ku}{\omega - ku \mp \omega_i} = 0. \qquad (3\text{-}41)$$

When many ion beams are flowing, equation (3-41) may be modified as

$$\omega^2 - c^2k^2 - \sum \frac{\omega_{pis}^2 (\omega - ku_s)}{\omega - ku_s \mp \omega_i} = 0. \qquad (3\text{-}42)$$

Equation (3-42) is just the dispersion relation obtained

by Berger et al.

(ii) When $h \neq 0$, a similar formula is also derived. Finally, equation (3-35) is written to be

$$\omega^2 - c^2k^2 - \omega_{pi}^2 \frac{i}{\omega - ku \pm \omega_i} \left\{ \omega - ku \pm \omega_i \frac{h^2}{2(k^2+h^2)} \right\} = 0 \qquad (3\text{-}43)$$

(iii) When $\omega \ll \omega_i$ and $u=0$, then equation (3-34) becomes

$$\left(1 - \frac{\omega^2}{A^2k^2}\right)\left(1 - \frac{\omega^2}{A^2} \frac{1}{k^2+h^2}\right) = 0.$$

Consequently, we have

$$\omega^2 = A^2k^2 \qquad (3\text{-}44)$$

and

$$\omega^2 = A^2(k^2 + h^2). \qquad (3\text{-}45)$$

Equation (3-44) is the dispersion relation found by Alfvèn[17] (1942). Also equation (3-43) is the dispersion relation of the extra ordinary hydromagnetic waves, which was derived by Astrŏm[25] (1950).

(iv) When $\omega \ll \omega_i$ and $u \neq 0$, a term $\omega_i^2 u/kA^2$ in equation (3-34) becomes dominant compared with ku. Hence, we get, by solving ω^2 in equation (3-34),

$$\omega^2 = A^2k^2\left(1 - \frac{k^2+h^2}{h^2}\,\frac{\omega_i{}^2u^2}{k^2A^4}\right) \qquad (3\text{-}46)$$

and

$$\omega^2 = A^2(k^2+h^2)\left(1 + \frac{k^2}{h^2}\,\frac{\omega_i{}^2u^2}{k^2A^4}\right). \qquad (3\text{-}47)$$

In this case, the velocity of Alfvèn wave becomes faster, whereas that of the extra ordinary wave slower. These facts come of the distorsion of the magnetic field by the current $\vec{J}_o = n_i Z_i e\vec{u}$.

3.3 Physical Picture

It gives detail information about physical circumstances inside the plasma to investigate the field, the ion currents, the electron motion, etc. Therefore, in this section, we shall discuss behavious of these quantites in the waves.

3.3.1 Electric Field

Substituting equations (3-25), (3-26) and (3-27) into equation (3-7), we get easily the electric field in the plasma, which is

$$E_\theta = -i\,\frac{\omega}{kc}\,\frac{1}{F^2-k^2G^2}\left[\frac{m}{r}G(F-k^2)B_z + k(F-G^2)\frac{\partial B_z}{\partial t}\right],$$

$$E_r = -\,\frac{\omega}{kc}\,\frac{1}{F^2-k^2G^2}\left[\frac{m}{r}k(F-G^2)B_z + G(F-k^2)\frac{\partial B_z}{\partial t}\right], \qquad (3\text{-}48)$$

$$E_z \simeq 0.$$

In order to examine the sense of the field rotation, we calculate iEr/E_θ . We then have

$$\frac{iEr}{E_\theta} = \frac{mk(F-G^2)J_m(hr) + G(F-k^2)hrJ_m'(hr)}{mG(F-k^2)J_m(hr) + k(F-G^2)hrJ_m'(hr)} \qquad (3\text{-}49)$$

or

$$= \frac{m(k+G)(F-kG)J_m - G(F-k^2)hrJ_{m+1}(hr)}{m(k+G)(F-kG)J_m - k(F-G^2)hrJ_{m+1}(hr)} \qquad (3\text{-}50)$$

These relations are valid for the general case. If we consider Alfvèn wave and the case u=0, we get, from equation (3-44) and (3-49),

$$\frac{iEr}{E_\theta} = 1 \ . \qquad (3\text{-}51)$$

For the ion cyclotron waves, equation (3-49) is approximately reduced to the form

$$\frac{iEr}{E_\theta} \simeq - \frac{hrJ_{m+1}(hr) - \frac{h^2}{k^2} hrJ_m'(hr)}{hrJ_{m+1}(hr) + \frac{h^2}{k^2} mJ_m} \qquad (3\text{-}52)$$

or

$$\simeq - \left[1 + \frac{h^2}{k^2} \left(1 - \frac{2m}{hr} \frac{J_m(hr)}{J_{m+1}(hr)}\right)\right] \ , \qquad (3\text{-}53)$$

where the condition u=0 is again assumed.

Therefore, the electric field in the plasma is generally elliptically polarized. Also the sense of the field rotation depends on the sign in the brackets of equation (3-53). For large k, the field may rotates around the magnetic field in the same sense as that of the ion Larmar gyration, This is clarified as follows.

If we consider the particle velocity $\vec{w}$ of an ion immersed in the magnetic field $\vec{B}_o$, the equation of motion is

$$m\frac{d\vec{w}}{dt} = \frac{Z_i e}{c}\,\vec{w} \times \vec{B}_o \ .$$

If $\vec{w}$ varies with time as $e^{-i\omega t}$, then we have

$$\frac{iw_r}{w_\theta} = -1$$

and $$\omega = \omega_i \qquad (3\text{-}54)$$

For the axisymmetric mode of the ion cyclotron waves, the polarization is expressed by, from equation (3-53),

$$\frac{iEr}{E_\theta} \simeq -\left(1 + \frac{h^2}{k^2}\right) , \qquad (3\text{-}55)$$

which agrees with Stix's result.[18)]

3.3.2 Ion Motion

Ordered motion of ions may be regarded as the mass

motion of plasma, so that $\vec{v}$ obtained from equations (3-13) and (3-17) will indicate the macroscopic ion motion.

Elliminating $\vec{J}$ from equations (3-13) and (3-17), we get, after some calculations,

$$\vec{v} \times \hat{z} + \frac{i}{\omega_i}(\omega - ku)\vec{v} - \frac{i}{\omega_e} ku\vec{v} + u\hat{z} \times \frac{\vec{B}}{B_o} + \frac{c\vec{E}}{B_o} = 0, \qquad (3\text{-}56)$$

where we have made use of equation (3-10), Each component of equation (3-56) gives the relation:

r-component:

$$i\left(\frac{\omega - ku}{\omega_i} - \frac{ku}{\omega_e}\right)v_r + v_\theta - \frac{B_\theta}{B_o}u + \frac{cE_r}{B_o} = 0 \qquad (3\text{-}56\text{-}1)$$

θ-component:

$$-v_r + i\left(\frac{\omega - ku}{\omega_i} - \frac{ku}{\omega_e}\right)v_\theta + \frac{B_r}{B_o}u + \frac{cE_\theta}{B_o} = 0 \qquad (3\text{-}56\text{-}2)$$

Combination of above two equations yields

$$v_r = \frac{1}{1-\Omega^{*2}} \frac{c}{B_o} \left[(i\Omega^* B_\theta + B_r)\frac{u}{c} + (E_\theta - i\Omega^* E_r) \right], \qquad (3\text{-}57)$$

$$v_\theta = \frac{-i}{1-\Omega^{*2}} \frac{c}{B_o} \left[(\Omega^* B_r + iB_\theta)\frac{u}{c} + (\Omega^* E_r - iE_r) \right], \qquad (3\text{-}58)$$

where we have neglected $\frac{1}{\omega_e}$ to $\frac{1}{\omega_i}$. Then we find that the macroscopic mass velocity (or ion velocity) becomes extremely large when Ω^* is near one.

Next let us consider the rotation of the velocity vector. For the sake of this purpose, we consider iv_r/v_θ , which is obtained to be

$$\frac{iv_r}{v_\theta} = -\frac{1 - \Omega^*\frac{iE_r}{E_\theta} + \frac{B_r}{E_\theta}(1+\Omega^*\frac{iB_\theta}{B_r})\frac{u}{c}}{\Omega^* - \frac{iE_r}{E_\theta} + \frac{B_r}{E_\theta}(\Omega^*+\frac{iB_\theta}{B_r})\frac{u}{c}} \quad . \tag{3-58}$$

While we have the relations:

$$B_r = \frac{kc}{\omega}E_\theta \quad \text{and} \quad -\frac{iE_r}{E_\theta} = -\frac{iB_\theta}{B_r} \quad ,$$

which are derived from equations (3-7) and (3-17). Then we get finally

$$\frac{iv_r}{v_\theta} = -\frac{1 - \Omega^*\frac{iE_r}{E_\theta}}{\Omega^* - \frac{iE_r}{E_\theta}} \tag{3-59}$$

In the case u=0, equation (3-59) becomes

$$\frac{iv_r}{v_\theta} = -\frac{1 - \Omega\frac{iE_r}{E_\theta}}{\Omega - \frac{iE_r}{E_\theta}} \tag{3-60}$$

When ω is close to ω_i and u=0, the macroscopic ion velocity rotates circularly in the same sense as would the ions. It should be emphasized that the fact above stated is valid for any finite m mode. For m=0 mode, Stix also derived the same formula as equation (3-60).

Next,we shall discuss the ion current in the wave. Multiplying the unit vector $\hat{z}$ vectorically to both sides of equation (3-13), we get

$$\vec{J}_\perp = i\Omega^*(n_i z_i e\vec{v} \times \hat{z}) + \frac{\vec{B}_\perp}{B_o} J_o \quad , \qquad (3\text{-}61)$$

where

$$\vec{J}_\perp = J_r\hat{r} + J_\varphi\hat{\theta}$$

and

$$B_\perp = B_r\hat{r} + B_\varphi\hat{\theta} \ .$$

For the cyclotron wave for sufficiently tenuous plasma, Ω^* is close to one. Whence equation (3-59) becomes

$$\frac{iv_r}{v_\varphi} \simeq -1. \qquad (3\text{-}62)$$

From the above relation, equation (3-61) is rewritten to be

$$\vec{J}_\perp = n_i Z_i e(\vec{v}_\perp + \frac{\vec{B}_\perp}{B_o} u). \qquad (3\text{-}63)$$

Thus we can say that the transverse component of the plasma current is mainly carried by the ions. The second term $\frac{B_\perp}{B_o}u$ in the parenthesis of equation (3-63) indicates the transverse bend of the ion beam in consequence of the oscillating magnetic field perpendicular to the axis, as shown in Fig. 3-2.

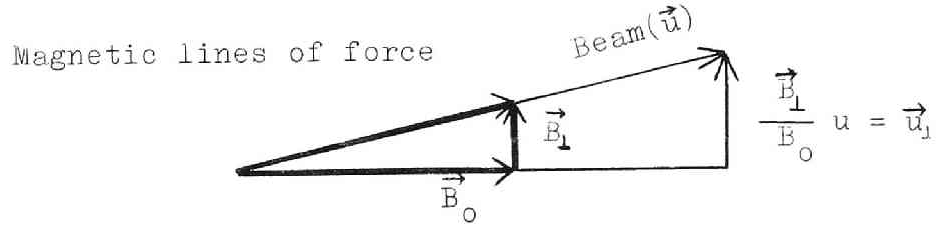

Fig. 3-2 Transverse bend of an ion beam due to the oscillating magnetic field in the wave.

3.3.3 Electron Motion

Transverse motion of the electron is a drift, which is given by

$$\vec{v}_{e\perp} = c\,\frac{\vec{E}\times\vec{B}}{B^2} \simeq c\,\frac{\vec{E}\times\hat{z}}{B_o} \qquad (3\text{-}64)$$

Then the resulting electron current is

$$J_{e\perp} = -n_e ec\,\frac{\vec{E}\times\hat{z}}{B_o}$$

$$= -\frac{n_e ecE_r}{B_o}\left(\frac{E_\theta}{E_r}\hat{r} - \hat{\theta}\right). \qquad (3\text{-}65)$$

From equations (3-56-1) and (3-7), we have finally

$$\frac{E_{r/B_o}}{v_\theta/c} = -\frac{\Omega^*\frac{iv_r}{v_\theta}+1}{(1+\frac{ku}{\omega})} \quad . \tag{3-66}$$

The numerator on the right hand side of equation (3-66) is rewritten to be

$$\Omega^*\frac{iv_r}{v_\theta}+1 = -\frac{(1-\Omega^{*2})\left[-m(k+G)(F-kG)J_m(hr)+G(F-k^2)hrJ_{m+1}(hr)\right]}{(1-\Omega^*)\left[m(k+G)(F-kG)J_m(hr)\right]+\left[G(F-k^2)-\Omega^*k(F-G^2)\right]hrJ_{m+1}(hr)} \tag{3-67}$$

where we have made use of equations (3-50) and (3-59).

For the ion cyclotron waves without the beam, equation (3-66) becomes, after some algebra,

$$\frac{E_{r/B_o}}{v_\theta/c} = -\left[\frac{\omega_i^2}{A^2k^2}\,\frac{2k^2+h^2}{k^2+h^2}\right]\times \frac{-m\frac{1+\Omega}{2}\left(\frac{h^2}{k^2+h^2}\right)J_m(hr)+hrJ_{m+1}(hr)}{-m\frac{1+\Omega}{2}\,\frac{\omega_i^2}{A^2k^2}\left[1-\left(\frac{k^2}{k^2+h^2}\right)^2\right]J_m(hr)+\frac{2k^2+h^2}{k^2+h^2}hrJ_{m+1}(hr)} \tag{3-68}$$

Therefore, combination of equations (3-65), (3-66) and (3-68) yields the transverse current of electrons. If we consider only the azimuthal component, equation (3-65) gives

$$J_{e\theta} = n_e e \frac{E_r c}{B_o} = n_e e \frac{E_{r/B_o}}{v_\theta / c} v_\theta \quad , \qquad (3\text{-}69)$$

where $\frac{E_{r/B_o}}{v_\theta / c}$ has been already given by equation(3-68). Especially for large k (resonant state and m=0 mode), equation (3-69) may be simplified as

$$J_{e\theta} = - n_e e \frac{\omega_i^2}{A^2 k^2} v_\theta \simeq -n_e e \frac{\omega_i^2}{A^2 k^2} v_{i\theta} \qquad (3\text{-}70)$$

Therefore, it becomes evident that, in the case of the ion cyclotron wave, the contribution of the electron motion to the transverse current is very small compared with that of the ion motion, since $\frac{\omega_i^2}{A^2 k^2}$ is very small.

For the case that m=0 and u=0, we can readily find

$$\vec{J}_{ei} = -n_i Z_i e \frac{\omega_i^2}{A^2 k^2} \vec{v}_{i\perp} = - \frac{\omega_i^2}{A^2 k^2} \vec{J}_{i\perp} \qquad (3\text{-}71)$$

($J_{i\perp}$: transverse ion current)

If the displacement current is negligible, it can be concluded that the charge accumulation arising from the transverse ion current is neutralized by the electron current parallel to the magnetic field.

3.4 Bounded Plasma Oscillations

In the sections 3.2 and 3.3, the radial wave number h has been assumed given for proper boundary conditions. However, the radial modes are not indispensable for investigating bounded plasma oscillations. In this section, we shall discuss nonaxisymmetric oscillations of bounded plasma for several different boundary situations. To treat the problem generally, first we consider the plasma which is immersed in a cylindrical current sheet and has a vacuum clearance between the plasma and the sheet. Fig. 3-3 shows this configuration.

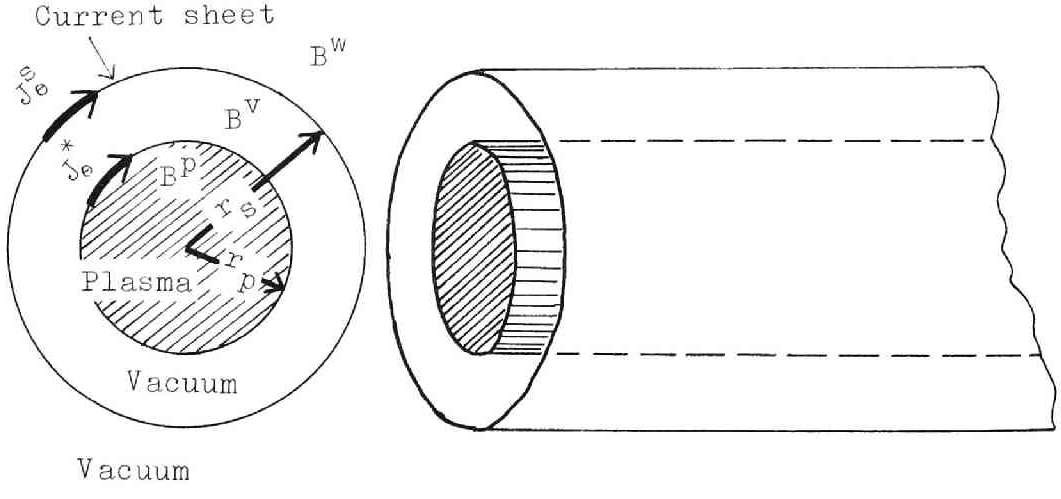

Fig. 3-3 Boundary situation of plasma.

Plasma oscillations in this general case will be treated in a section 3.4.1. If the vacuum clearance degenerates, we have a plasma wave guide discussed in a section 3.4.2. In a section 3.4.3, we consider a configuration without the current sheet, which is called natural oscillations. Bernstein and Trehan treated nonaxisymmetric natural oscillations without the beam, but this general configuration to be discussed here has not been treated up to the present.

3.4.1 General Configuration

Again the normal mode analysis is applied to following discussions, so that we assume that all quantities in equestion vary as exp $i(m\theta+kz-\omega t)$. Let the radii of the plasma and the current sheet r_p and r_s, respectively, as shown in Fig. 3-3. The surface current of the plasma is denoted by J^* and the sheet current by J^s.

We neglect the displacement current, so that the vacuum field may be similarly treated as in the chapter I. Then we can easily show that each magnetic field is approximately expressed as follows.

For $r_s < r$, (outer region)

$$\left.\begin{aligned} B_r^W &= kSK_m'(kr), \\ B_\theta^W &= \frac{im}{r}SK_m(kr), \\ B_z^W &= ikS\,K_m(kr). \end{aligned}\right\} \qquad (3\text{-}72)$$

For $r_p<r<r_s$,

(vacuum clearance region)

$$\left.\begin{aligned} B_r^v &= k\left[LI_m'(kr)+QK_m'(kr)\right], \\ B_\theta^v &= \frac{im}{r}\left[LI_m(kr)+QK_m(kr)\right], \\ B_z^v &= ik\left[LI_m(kr)+QK_m(kr)\right]. \end{aligned}\right\} \quad (3\text{-}73)$$

For $r<r_p$,

(plasma region)

$$\left.\begin{aligned} B_r^p &= \frac{-i}{F^2-k^2G^2}\left[\frac{m}{r}G(F-k^2)B_z^p + k(F-G^2)\frac{\partial B_z^p}{\partial r}\right], \\ B_\theta^p &= \frac{1}{F^2-k^2G^2}\left[\frac{m}{r}k(F-G^2)B_z^p + G(F-k^2)\frac{\partial B_z^p}{\partial r}\right], \end{aligned}\right\} \quad \begin{matrix}(3\text{-}74)\\ \text{or}(3\text{-}25)\\ \sim(3\text{-}27)\end{matrix}$$

$$B_z^p = CJ_m(hr).$$

Where we have suppressed a term exp $i(m\theta+kz-\omega t)$, and we have used superscripts p, v and w to indicate the quantities referring to the plasma, the vacuum clearance and the outer vacuum region, respectively. Constants S, L, Q and C should be related each other through boundary conditions. We shall next derive the boundary equations . From Maxwell's equations, we have

$$\Delta(\vec{r}\cdot\vec{B})=0, \quad (3\text{-}75)$$

and

$$-\Delta(\vec{r}\times\vec{B})=\frac{4\pi}{c}\vec{J}^* \ (\text{or } \frac{4\pi}{c}\vec{J}^s) \quad (3\text{-}76)$$

Also the magnetic pressure balance at the interface gives the relation

$$\Delta\left(\frac{B^2}{8\pi}\right) = 0. \qquad (r=r_p) \qquad (3\text{-}77)$$

Where $\Delta(X)$ denotes the change of some quantity X across the surface. The linearized forms of these equations are

$$B_r^p = B_r^v , \qquad (r=r_p) \qquad (3\text{-}78)$$

$$B_z^p = B_z^v , \qquad (r=r_p) \qquad (3\text{-}79)$$

$$B_r^v = B_r^w , \qquad (r=r_s) \qquad (3\text{-}80)$$

and

$$B_z^v - B_z^w = \frac{4\pi}{c} J_\theta^s \qquad (r=r_s) \qquad (3\text{-}81)$$

$$\text{or} \quad -(B_\theta^v - B_\theta^w) = \frac{4\pi}{c} J_z^s .$$

The constants S, L, Q and C can be determined from the combination of the field equations (3-72) to (3-74) and the boundary equations (3-78) to (3-81). After some straightforward reductions, we get finally

$$\left.\begin{aligned} S &= i \frac{4\pi r_s}{c} J_\theta^s \left[I_m'(kr_s) - Y K_m'(kr_s)\right] , \\ L &= i \frac{4\pi r_s}{c} J_\theta^s K_m'(kr_s), \\ Q &= -i \frac{4\pi r_s}{c} J_\theta^s K_m'(kr_s) H, \\ C &= -\frac{4\pi r_s}{c} J_\theta^s \frac{kr_s K_m'(kr_s)}{J_m(hr_p)} \frac{1}{HK_m(kr_p) - kr_p K_m'(kr_p)} , \end{aligned}\right\} \qquad (3\text{-}82)$$

where

$$Y = \frac{H\, I_m(kr_p) - kr_p I'_m(kr_p)}{H\, K_m(kr_p) - kr_p K'_m(kr_p)} , \qquad (3\text{-}83)$$

$$H = \frac{k}{F^2-k^2G^2}\left[m(F-k^2)G + k(F-G^2)hr_p \frac{J'_m(hr_p)}{J'_m(hr_p)}\right] . \qquad (3\text{-}84)$$

Thus we can write down the magnetic field in each region, and they are

$$\text{for } r_s < r, \quad \left.\begin{aligned} B_r^W &= iN^S kr_s\left[I'_m(kr_s) - YK'_m(kr_s)\right] K'_m(kr), \\ B_\theta^W &= -N^S \frac{mr_s}{r}\left[I'_m(kr_s) - YK'_m(kr_s)\right] K_m(kr), \\ B_z^W &= -N^S kr_s\left[I'_m(kr_s) - YK'_m(kr_s)\right] K_m(kr), \end{aligned}\right\} \qquad (3\text{-}85)$$

$$\text{for } r_p < r < r_s, \quad \left.\begin{aligned} B_r^V &= iN^S kr_s K'_m(kr_s)\left[I'_m(kr) - Y\, K'_m(kr)\right], \\ B_\theta^V &= -N^S \frac{mr_s}{r}\, K'_m(kr_s)\left[I_m(kr) - Y\, K_m(kr)\right], \\ B_z^V &= -N^S kr_s K'_m(kr_s)\left[I_m(kr) - Y\, K_m(kr)\right], \end{aligned}\right\} \qquad (3\text{-}86)$$

$$\text{for } r < r_p, \quad B_z^p = -N^S \frac{kr_s K'_m(kr_s)}{J_m(hr_p)} \frac{1}{H\, K_m(kr_p) - kr_p K'_m(kr_p)} J_m(hr), \qquad (3\text{-}87)$$

where $$N^S = \frac{4\pi j_\theta^S}{c} \quad , \tag{3-88}$$

and we have again suppressed the term exp i(mθ+kz-ωt). Equations (3-85), (3-86) and (3-87) give the complete solution for steady state excitation. The electric field in each region is readily obtained from Maxwell's equation (i.e. rot $\vec{E}=-\partial\vec{B}/c\partial t$) and equations (3-85) to (3-87).

3.4.2 Cylindrical Plasma Waveguide

Natural wave modes inside a conducting cylinder are discussed in this small section. Natural waves mean the oscillations without any external exciting current. Outside the completely conducting cylinder, there are no oscillating field. Then we can set $\vec{B}^W=0$ for $r>r_s$, but this solution is somewhat complicated still. For simplicity, we shall consider the case $r_s=r_p$ (i.e. the completely filled plasma waveguide), whence

$$B_z^W = -N^S kr_s \left[I'_m(kr_s) - \frac{HI_m(kr_s)-kr_p I'_m(kr_s)}{HK_m(kr_s)-kr_p K'_m(kr_s)} K'_m(kr_s) \right] K_m(kr)$$

$$\leqq 0. \tag{3-89}$$

The solution of above equation is given by

$$H = 0$$

or

$$m(F-k^2)G + k(F-G^2)hr_p\frac{J'_m(hr_s)}{J_m(hr_s)} = 0 \ , \qquad (3\text{-}90)$$

where we have used equation (3-84) and the fact that $k'_m(kr_p)$ is finite when $kr_p=0$.

For the axisymmetric mode (i.e. m=0 mode), the result is very simple, which is

$$J'_o(hr_p) = J'_o(hr_s) = 0. \qquad (3\text{-}91)$$

This gives infinite number of discrete h as the roots, which are all the radial wave number.

On the other hand, for the ion cyclotron waves, equation (3-90) is also transformed to a simple one, which is given by

$$\frac{hr_s J_{m+1}(hr_s)}{J_m(hr_s)} = -m\,\frac{h^2}{k^2} \qquad (3\text{-}92)$$

where we have used the approximation that $\frac{\omega_i^2}{A^2k^2} \ll 1$ and assumed u=0. The right hand side of equation (3-92) is very small in this case, so that the roots are approximately given by an equation

$$J_{m+1}(hr_s) = 0 \qquad (3\text{-}93)$$

Needless to say, equation (3-92) may be reduced to equation (3-91) when m=0, because $J_0' = -J_1$.

3.4.3 Vacuum Boundary

Natural modes of a plasma cylinder surrounded by vacuum can be examined by setting $\vec{J}^s=0$. The condition that $\vec{B}^p$ has a finite value when $\vec{J}^s=0$ leads to the relation

$$\frac{k}{F^2-k^2G^2}\left[m(F-k^2)G+k(F-G^2)hr_p\frac{J_m'(hr_p)}{J_m(hr_p)}\right]=\frac{kr_pK_m'(kr_p)}{K_m(kr_p)}\quad, \tag{3-94}$$

where we have used equation (3-84) and (3-87). Equation (3-94) gives infinite number of the radial wave number h, so that this equation may be called "characteristic equation". When u=0, equation (3-94) becomes

$$\frac{k^2}{(k^2-\frac{\omega^2}{A^2})^2-\Omega^{*2}k^4}\left[-m\Omega\frac{\omega^2}{A^2}+(k^2-\frac{\omega^2}{A^2}-k^2\Omega^2)\frac{hr_pJ_m'(kr_p)}{J_m(hr_p)}\right.$$
$$\left.=\frac{kr_pK'(kr_p)}{K_m(kr_p)}\right], \tag{3-95}$$

which is in agreement with Bernstein and Trehan's result.

For the axisymmetric ion cyclotron wave, equation

(3-95) can be reduced to

$$\frac{J_o'(hr_p)}{hJ_o(hr_p)} = -\frac{K_o'(kr_p)}{kK_o(kr_p)} \quad .$$

This is also rewritten as

$$\frac{hr_p J_1'(hr_p)}{J_1(hr_p)} = \frac{kr_p K'(kr_p)}{K_1(kr_p)} \quad , \qquad (3\text{-}96)$$

where we have used the relations as

$$J_o'(z) = -J_1(z), \qquad K_o'(z) = -K_1(z),$$

$$J_o(z) = J_1'(z) + \frac{J_1(z)}{z} \quad , \qquad K_o(z) = -K_1'(z) - \frac{K_1(z)}{z} \quad .$$

Equation (3-96) is in agreement with Stix's result.[26]

3.5 Application of Ion Cyclotron Waves to Plasma Heating

It has been shown in the chapter II that the efficiency of the direct ion cyclotron heating of plasma falls away as the plasma density increases. On the contrary, ion cyclotron waves are apt to be excited in such a high density. If there is a damping mechanism of the waves, we can heat plasma through two stages as follows. At first, we excite ion cyclotron

waves in a heating section. This excitation can be made with high efficiency, since the mass velocity in the waves becomes extremely high as Ω^* tends to unity as seen in equations (3-57) and (3-58). In the next stage, these excited waves are caused to damp by a damping mechanism. Thus the energy consumed by the excitation of ion cyclotron waves is finally converted into the thermal energy of plasma.

Many damping mechanisms of ion cyclotron waves (or hydromagnetic waves) may be considered, but the most effective are so-called "phase mixing" and "cyclotron damping". Possible radial and axial wave numbers h and k of the bounded waves are determined by the characteristic equation (3-90) for the configuration of a cylindrical wave guide or (3-94) for the configuration with a vacuum boundary. Therefore, there occur many waves with the same frequency. These waves are not excited equally, but the wave of the mode closest to resonant condition may be predominantly excited. In other words, one predominant wave corresponds to an ion beam. The expressions for v_r and v_θ, given by equations (3-57) and (3-58) indicate the occurence of this resonant excitation. If there are a number of ion beams in the plasma, many predominant waves may be excited. In the heating region, these waves are forced to be in phase. Generally predominant waves

corresponding to different beam velocities have different phase velocities. Therefore, as the waves propagate away from the heating region, these waves may become out of phase with each other; that is to say, a phase mixing occurs. This phase mixing gives rise to the conversion of the ordered motion of ions into random motion (or the wave energy into thermal energy of ions).

There are also configurations of coil for exciting only a hydromagnetic wave. For instance, Stix's coil excites plasma waves with a fixed axial wavelength. Similar phase mixing can also be expected even in such a case, analogously to Landau damping[27]. This mechanism is named "cyclotron damping". If the ion cyclotron wave, excited in the heating region, falls in a region where many beams are near resonance, its phase velocity becomes very slow compared with the thermal motion of ions parallel to the propagating direction (i.e. the axial direction). This situation can be seen in the dispersion relation (3-28)' for general case or (3-40) for infinite radial wavelength. The wave form is randomized by the parallel motion of ions and consequently the wave disappears or be thermalized. From the microscopic point of view, this mechanism is regarded as a cyclotron resonance absorption of ions feeling the wave field at their

own cyclotron frequencies. This damping is much effectively accomplished with damping length shorter than a wavelength. Dawson[24] and Stix[16] derived the damping length for axisymmetric mode.

The Heliotron-B device is equipped with a exciting coil of Stix's type. Excited ion cyclotron waves in this coil region are expected to be damped with the cyclotron damping at the slope of the Heliotron magnetic field, experiments on which will be described in a chapter VIII.

IV Ion Cyclotron Resonance with Collision Relaxation

4.1 Introduction

In the chapters II and III, plasma consisting of one kind of ions and electrons was considered, so that their momentum transfer to another kind of ions was not necessary to be taken into account. However, the fusion reactions between triton and deuteron (T-D reaction) can easily take place compared with deuteron-deuteron reaction (D-D reaction), since the T-D cross section has its peak at the deuteron energy of 100 keV, whereas the D-D cross section at 2 MeV. If we consider a plasma under the D-T fusion reaction, the momentum transfer must be taken into account. But this momentum transfer has a velocity dependence as w^{-2} at extremely high temperature. This fact makes it somewhat difficult to treat the problem, since the Boltzmann equation can not be linearlized in this case.

On the other hand, a weakly ionized gas governed by constant mean free time hypothesis has a linear dependence of the moment transfer on particle velocity. Then the boltzmann equation will be approximately linearlized. Furthermore, this kind of gas may be regarded as a simple model of high temperature plasma with

collision relaxation. This case is to be analyzed in this chapter.

Cyclotron resonance with relaxation was first investigated by Dresselhaus, Kip and Kittel[28] to determine the effective mass of electrons or holes in semiconductor. They observed that there are many electrons with different effective mass in germanium at 4°K and discussed the structures of the valence band of germanium and silicon. Ion Cyclotron Resonance in a weakly ionized gas has many similar points to the cyclotron resonance in solid, except for applied frequencies. When the mass is known, so-called relaxation time (i.e. collision time) of the particle may be determined.

The mechanism of the ion cyclotron resonance with collision relaxation is described as follows. Suppose a weakly ionized gas is placed in an externally applied strong magnetic field and a rf electric field perpendicular to the magnetic field, the frequency of which is near the ion cyclotron frequency. The ions are resonantly accelerated, and then they collide with the molecules of the gas and loss their energy consequently.

If we sweep the rf frequency or the magnetic field strength, then we have an absorption curve of the ion cyclotron resonance, the peak of which is

near the cyclotron frequency. As shown in a section 4.4, the half-width of this resonant absorption curve depends on the momentum collision frequency between the ions and the molecules. Therefore, we can determine the momentum collision frequency from the half-width. This method was proposed by the auther (1961)[29)30)] and will become an important one to determine the collision cross sections between ions and molecules, especially at low energy. Because Born's approximation methodis invalid for the case of low energy ions and also an experimental ion beam injection method becomes very difficult at low beam energy. The dependence of the half-width on collision frequency could be experimentally verified as described in the next chapter V.

After the auther's investigations, Wobschall, Graham and Malone (1963)[31)] carried out similar experiments in detail and determined the collision cross sections N_2^+ and Ar^+ in their parent gases.

In this chapter, we treat the case as the rf electric field for the cyclotron resonance is induced by a solenoidal sheet current flowing azimuthally and a weakly ionized gas cylinder is co-axially immersed. An external strong magnetic field is imposed parallel to its axis. Wobsnall et al used the electrostatic field produced by two plane electrodes, but this

configuration makes the phenomena in plasma very complicated, since the sheath formation on the plate will play a dominant role in the case. Therefore, it may be prudent to avoid such a configuration and adopt the axisymmetric induced field.

We derive the energy dissipation of the electric field by the ion cyclotron resonance in a section 4.2. Then the penetration of the rf field into the plasma will be discussed in a section 4.3. The proposed method to determine the collision cross section is to be described in the chapter 4.4.

4.2 Energy Dissipation into Gas under Ion Cyclotron Heating

The physical situation under consideration is as follows. An infinitely long cylindrical slightly ionized gas is immersed in a strong static field $\vec{B}_0$ parallel to its axis (the z-axis). Rf solenoidal current flows co-axially with the gas column and induces an azimuthal rf electric field. There is a vacuum gap (or clearance) between the current sheet and the gas column. The fields have no variation in the axial direction. This configuration is shown in Fig. 4-1.

The induced field in the plasma is generally different from the vacuum field, due to plasma reactions. This problem is to be discussed in the next section.

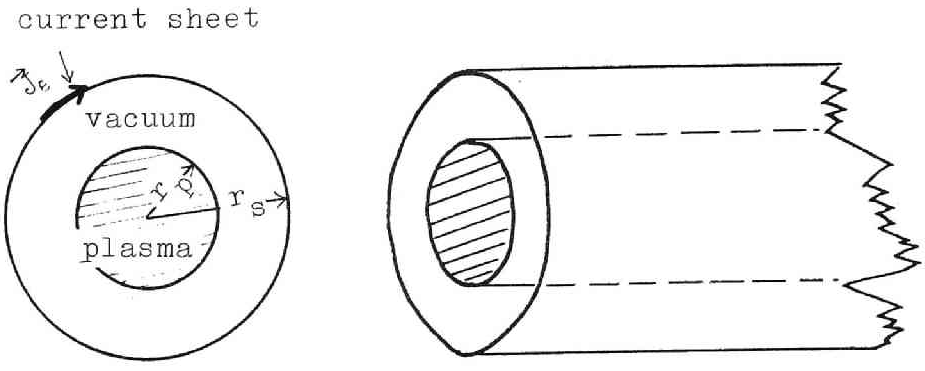

Fig. 4-1 Boundary situation of plasma.

In this section, the electric field is assumed given and the resulting ionic behaviours will be investigated self-consistently in the next section. The electric field may be expressed by complex notation as

$$\mathcal{E} = E_r + iE_\theta \tag{4-1}$$

$$= \mathcal{E}_+ e^{i\omega t} + \mathcal{E}_- e^{-i\omega t} . \tag{4-2}$$

This expression is similar to that used in the chapter II. A term $e^{-i\omega t}$ expresses a circularly polarized field in the same sense as the ion cyclotron gyration and another term $e^{i\omega t}$ in the opposite sense. As no axial dependence of fields is assumed, so $\mathcal{E}_+$ and $\mathcal{E}_-$ are functions of only the radial distance r. Furthermore, it should be noted that the axial component of the electric field does not exist in this configuration

of the sheet current.

For the sake of simplification, we shall make several approximations as follows.

i) We neglect the oscillating component of the magnetic field so that $\vec{B} \cong B_o \hat{z}$ ($\hat{z}$: an unit vector in the z-direction).

ii) We neglect the variation of the transverse electric field over the Larmor radius of the ion.

iii) The momentum transfer from the ions to the molecules of the gas is proportional to the velocity of the ions. That is,

$$\vec{P}_{in} = -\nu_m \vec{v} , \qquad (4-3)$$

where $\vec{P}_{in}$ is the rate of transfer of momentum (per cm^3 per sec) from the ions to the gas molecules and $\vec{v}$ is the macroscopic velocity of an ensemble of ions.

iv) We neglect the gravitational force and the pressure gradient of the plasma. And also we neglect the radial diffusion of the charged particles.

The basic equation for the ions in these approximations is given by

$$\frac{\partial \vec{v}}{\partial t} = \frac{q}{M}(\vec{E} + \frac{1}{c}\vec{v} \times B_o \hat{z}) - \nu_m \vec{v} . \qquad (4-4)$$

In our complex co-ordinates, equation (4-4) can be rewritten to be

$$\frac{\partial v}{\partial t} + \left(i\omega_i + \nu_m \right) v = \frac{q}{M} \mathcal{E} , \qquad (4\text{-}5)$$

where

$$v = v_r + i v_\theta \qquad (4\text{-}6)$$

and ω_i is the ion cyclotron angular frequency. Equation (4-6) can be readily solved by using Laplace transformation and then we get

$$v = e^{-\nu_m t} e^{-i\omega_i t} \left[v_+^o - \frac{q}{M} \left\{ \frac{\mathcal{E}_+}{i(\omega_i+\omega)+\nu_m} + \frac{\mathcal{E}_-}{i(\omega_i-\omega)+\nu_m} \right\} \right]$$

$$+ \frac{q}{M} \left[\frac{\mathcal{E}_+ e^{i\omega t}}{i(\omega_i+\omega)+\nu_m} + \frac{\mathcal{E}_- e^{-i\omega t}}{i(\omega_i-\omega)+\nu_m} \right] , \qquad (4\text{-}7)$$

where v_+^o is the initial velocity. Therefore, the steady solution of equation (4-5) becomes

$$v = \frac{q}{M} \left[\frac{\mathcal{E}_+ e^{i\omega t}}{i(\omega_i+\omega)+\nu_m} + \frac{\mathcal{E}_- e^{-i\omega t}}{i(\omega_i-\omega)+\nu_m} \right] . \qquad (4\text{-}8)$$

In steady state, the input power and the energy loss due to collisions are balanced each other, that is similar to the case of rain drops falling down

through the atmosphere. At the beginning, a rain drop is accelerated by the gravitational force and then finally its speed becomes constant, when the input power from the gravitational force becomes equal to the drop's work against air friction force. Therefore, the input power from the gravitational force in steady state is mg.v, where m, g and v are the mass of the rain drop, the gravitational acceleration and the velocity, respectively. Analogously to this rain drop model, we can determine the energy dissipation rate (or absorption rate), which is

$$E.D. = n_i \vec{v} \cdot \vec{F} \ , \qquad (4\text{-}9)$$

where $\vec{F}$ is a force acting on the ion. This is also rewritten as

$$E.D. = n_i (v_r F_r + v_\theta F_\theta)$$

$$= n_i Re(v \cdot f^*) \ , \qquad (4\text{-}10)$$

where

$$f = F_r + iF_\theta \qquad (4\text{-}11)$$

and X* denotes the conjugate of X.

f* is also expressed in terms of ε given in equation

(4-2) and then we have

$$f^* = q\varepsilon^* = q\left\{\varepsilon_+^* e^{-i\omega t} + \varepsilon_-^* e^{i\omega t}\right\} \qquad (4\text{-}12)$$

Thus we get

$$v\cdot f^* = \frac{q^2}{M}\left[\frac{1}{\nu_m^2+(\omega_i+\omega)^2}\left[\varepsilon_+\varepsilon_+^*\left\{\nu_m - i(\omega_i+\omega)\right\} + \varepsilon_+\varepsilon_-^*\left\{\nu_m - i(\omega_i+\omega)\right\}e^{i2\omega t}\right]\right.$$

$$\left. + \frac{1}{\nu_m^2+(\omega_i-\omega)^2}\left[\varepsilon_-\varepsilon_-^*\left\{\nu_m - i(\omega_i-\omega)\right\} + \varepsilon_-\varepsilon_+^*\left\{\nu_m - (\omega_i-\omega)\right\}e^{-i2\omega t}\right]\right] \cdots$$

(4-13)

Taking time average of E.D., then we have

$$\overline{E.D.} = \frac{n_i q^2 \nu_m}{M}\left[\frac{|\varepsilon_+|^2}{\nu_m^2+(\omega_i+\omega)^2} + \frac{|\varepsilon_-|^2}{\nu_m^2+(\omega_i-\omega)^2}\right], \qquad (4\text{-}14)$$

which is the root mean square of the dissipation power into the plasma per cm^3 per sec. If ε_+^2 and ε_-^2 are constant and ν_m is small, the second term in the braket of equation (4-14) becomes dominant when $\omega \sim \omega_i$. Then the absorption curve (or the line shape) becomes Lorentzian.

The induced ion current $\vec{J}$ is also obtained in complex form as

$$j = n_i q v$$

$$= \frac{n_i q^2}{M} \left[\frac{\varepsilon_+ e^{i\omega t}}{i(\omega_i+\omega)+\nu_m} + \frac{\varepsilon_- e^{-i\omega t}}{i(\omega_i-\omega)+\nu_m} \right] , \quad (4\text{-}15)$$

where

$$j = J_r + iJ_\theta \quad .$$

4.3 Penetration of RF Field into Plasma

We shall consider the radial variations of ε_+ and ε_- in both the plasma and the vacuum gap and discuss the penetration of the rf field into the plasma for different cases.

The fields under consideration are all axisymmetric and axially invariable. Therefore, Maxwell's equations without displacement current become in cylindrical co-ordinates

$$0 = J_r \ , \quad (4\text{-}16\text{-}1)$$

$$-\frac{\partial B_z}{\partial r} = \frac{4\pi}{c} J_\theta \ , \quad (4\text{-}16\text{-}2)$$

$$\frac{1}{r}\frac{\partial}{\partial r}(rB_\theta) = \frac{4\pi}{c} J_z \quad (4\text{-}16\text{-}3)$$

and

$$0 = \frac{\partial B_r}{\partial t} , \qquad (4\text{-}17\text{-}1)$$

$$0 = \frac{\partial B_\theta}{\partial t} , \qquad (4\text{-}17\text{-}2)$$

$$\frac{1}{r} \frac{\partial}{\partial r}(rE_\theta) = - \frac{1}{c} \frac{\partial B_z}{\partial t} . \qquad (4\text{-}17\text{-}3)$$

where we have assumed that $E_z=0$. Equations (4-16) and (4-17) correspond to $\vec{\nabla} \times \vec{B} = \frac{4\pi}{c} J$ and $\vec{\nabla} \times \vec{E} = - \frac{1}{c} \frac{\partial \vec{B}}{\partial t}$, respectively. Then we have, from equations (4-16-2) and (4-17-3),

$$\frac{\partial}{\partial r}\left[\frac{1}{r} \frac{\partial}{\partial r} (rE_\theta)\right] = \frac{4\pi}{c^2} \frac{\partial J_\theta}{\partial t} . \qquad (4\text{-}18)$$

Also we have

$$\frac{\partial J_z}{\partial t} = 0.$$

Since no constant current flow parallel to the z-axis is considered, then we get

$$J_z = 0 . \qquad (4\text{-}19)$$

Electron drift induced by the rf-field is negligible compared with the ion velocity, as described in the

chapter III. Also we have assumed that there is no radial diffusion. Therefore, it is reasonable that the radial current J_r in the plasma, if it flows, is mainly carried by the radial motion of the ions. Also the azimuthal current J_θ is in the same manner.

The radial current may be obtained from equation (4-15) and it becomes

$$J_r = Re(j)$$

$$= \frac{n_i q^2}{M}\left[\frac{1}{|d_+|^2}\left\{Re(\varepsilon_+ d_+)\cos\omega t - Im(\varepsilon_+ d_+)\sin\omega t\right\}\right.$$

$$\left. + \frac{1}{|d_-|^2}\left\{Re(\varepsilon_- d_-)\cos\omega t + Im(\varepsilon_- d_-)\sin\omega t\right\}\right], \qquad (4\text{-}20)$$

where

$$d_\pm = \nu_m - i(\omega_i \pm \omega) . \qquad (4\text{-}21)$$

Equation (4-16-1) is valid at any time, so that we have from equation (4-20)

$$\frac{1}{|d_+|^2}\left[\nu_m Re(\varepsilon_+) + (\omega_i+\omega) Im(\varepsilon_+)\right] + \frac{1}{|d_-|^2}\left[\nu_m Re(\varepsilon_-) + (\omega_i-\omega) Im(\varepsilon_-)\right]$$

$$= 0 \qquad (4\text{-}22)$$

and

$$- \frac{1}{|d_+|^2}\left[\nu_m \mathrm{Im}(\varepsilon_+) - (\omega_i+\omega)\mathrm{Re}(\varepsilon_+)\right] +$$

$$\frac{1}{|d_-|^2}\left[\nu_m \mathrm{Im}(\varepsilon_-) - (\omega_i-\omega)\mathrm{Re}(\varepsilon_-)\right] = 0 \quad . \qquad (4\text{-}23)$$

In complex form, equations (4-22) and (4-23) become

$$\varepsilon_- = -\frac{\nu_m^2 + (\omega_i-\omega)^2}{\nu_m^2 + (\omega_i+\omega)^2} \cdot \frac{\nu_m + i(\omega_i+\omega)}{\nu_m - i(\omega_i-\omega)} \varepsilon_+^* \quad . \qquad (4\text{-}24)$$

This relation gives the ratio of ε_- to ε_+^* in the plasma region.

In an extreme case $\nu_m=0$ (i.e.collisionless plasma), equation (4-24) becomes

$$\varepsilon_- = \frac{\omega_i-\omega}{\omega_i+\omega} \varepsilon_+^* \quad . \qquad (4\text{-}25)$$

Thus ε_- will be very small if $\omega \simeq \omega_i$. In other words, the circularly polarized field in the same sense as the ion gyration can not penetrate into the plasma and only the oppositely polarized field exists in the plasma region. As seen in the chapter II, both the polarized fields can penetrate into the plasma, if the field is periodic in the axial direction. This is the reason why the axially periodic field is adopted for ion cyclotron heating of plasma.

In another extreme case $\nu_m \to \infty$, equation (4-24) becomes

$$\varepsilon_- = -\varepsilon_+^* \ . \tag{4-26}$$

Infinite ν_m implies that the ions cannot move and rigidly stick to the gas, which may be regarded as solid in this case. Therefore, this state is equivalent to vacuum, since the ions do not react against the field. Equation (4-26) shows that ε_+ and ε_- are of the same order, that should be emphasized.

Next we shall discuss the radial variations of ε_+ and ε_-. From equation (4-15), the azimuthal component of the current $\vec{J}$ is found to be

$$\begin{aligned} J_\vartheta &= \mathrm{Im}(j) \\ &= \frac{n_i q^2}{M} \left[\frac{1}{|d_+|^2} \left\{ \mathrm{Im}(\varepsilon_+ d_+)\cos\omega t + \mathrm{Re}(\varepsilon_+ d_+)\sin\omega t \right\} \right. \\ &\qquad \left. + \frac{1}{|d_-|^2} \left\{ \mathrm{Im}(\varepsilon_- d_-)\cos\omega t - \mathrm{Re}(\varepsilon_- d_-)\sin\omega t \right\} \right] \end{aligned} \tag{4-27}$$

where $d_\pm$ are again given by equation (4-21). The azimuthal component of the electric field is also obtained from equation (4-2), which is

$$\begin{aligned} E_\vartheta &= \mathrm{Im}(\varepsilon) \\ &= \mathrm{Re}(\varepsilon_+ - \varepsilon_-)\sin\omega t + \mathrm{Im}(\varepsilon_+ + \varepsilon_-)\cos\omega t. \end{aligned} \tag{4-28}$$

Combination of equations (4-18), (4-27) and (4-28) yields the relations

$$D\left[\mathrm{Re}(\varepsilon_+ - \varepsilon_-)\right] = \omega_{pi}^2 \frac{\omega}{c^2}\left[-\frac{1}{|d_+|^2}\,\mathrm{Im}(\varepsilon_+ d_+) - \frac{1}{|d_-|^2}\,\mathrm{Im}(\varepsilon_- d_-)\right], \tag{4-29}$$

$$D\left[\mathrm{Im}(\varepsilon_+ + \varepsilon_-)\right] = \omega_{pi}^2 \frac{\omega}{c^2}\left[\frac{1}{|d_+|^2}\,\mathrm{Re}(\varepsilon_+ d_+) - \frac{1}{|d_-|^2}\,\mathrm{Im}(\varepsilon_- d_-)\right], \tag{4-30}$$

where

$$D = \frac{d}{dr}\left[\frac{1}{r}\frac{d}{dr}\,r\right] . \tag{4-31}$$

In complex form, equations (4-29) and (4-30) are expressed as

$$D(\varepsilon_+^* - \varepsilon_-) = \omega_{pi}^2 \frac{i\omega}{c^2}\left[-\frac{\varepsilon_+^*}{\nu_m - i(\omega_i + \omega)} + \frac{\varepsilon_-}{\nu_m + i(\omega_i - \omega)}\right] \tag{4-32}$$

Furthermore, equation (4-32) is rewritten, by using relation (4-24), to be

$$D(\varepsilon_+^*) = -\frac{b^2}{a^2}\varepsilon_+^*$$

or

$$\frac{d^2\varepsilon_+^*}{dr^2} + \frac{1}{r}\frac{d\varepsilon_+^*}{dr} + \left(\frac{b^2}{a^2} - \frac{1}{r^2}\right)\varepsilon_+^* = 0, \tag{4-33}$$

where

$$a^2 = 2\,\frac{\nu_m - i\omega}{\nu_m - i(\omega_i+\omega)}\,, \tag{4-34}$$

$$b^2 = \frac{2\omega_{pi}^2}{c^2}\,\frac{i\omega}{\nu_m - i(\omega_i+\omega)}\,, \tag{4-35}$$

Thus we have

$$\varepsilon_+^* = \varepsilon_o J_1\left(\frac{b}{a}\,r\right), \tag{4-36}$$

where ε_o is a multiplicative constant and determined from the boundary conditions.

On the other hand, ε_+^* in vacuum is found by putting $\omega_{pi}=0$, and then we have the equation

$$\frac{d^2\varepsilon_+^*}{dr^2} + \frac{1}{r}\,\frac{d\varepsilon_+^*}{dr} - \varepsilon_+^* = 0. \tag{4-37}$$

This solution is readily found to be

$$\varepsilon_+^* = \varepsilon_1 r + \varepsilon_2\,\frac{1}{r}\,. \tag{4-38}$$

In order to distinguish the field in the plasma region from that in the outer vacuum region, we shall use the superscripts p and v in bellow discussions as in the chapter III. The boundary conditions, which determine the constants ε_o, ε_1 and ε_2, are described

in this axisymmetric configuration as follows.

At $r=r_p$

$$E_\theta^p = E_\theta^v , \tag{4-39}$$

$$\frac{dE_\theta^p}{dr} = \frac{dE_\theta^v}{dr} \tag{4-40}$$

and at $r_p=r_s$

$$\frac{dE_\theta^v}{dr} = -\frac{4\pi\omega}{c^2} J_\theta^s \cos\omega t. \tag{4-41}$$

Where we have assumed that the sheet current varies with time as $J_\theta^s \sin\omega t$ (per cm). E_θ is also expressed, instead of equation (4-28), in the form

$$E_\theta = -\mathrm{Im}(\varepsilon_+^*-\varepsilon_-)\cos\omega t + \mathrm{Re}(\varepsilon_+^*-\varepsilon_-)\sin\omega t. \tag{4-42}$$

Therefore, equations (4-39) and (4-40) imply that $(\varepsilon_+^*-\varepsilon_-)$ and its radial derivative should be continuous at $r=r_p$. In the plasma, we have already introduced the relation

$$\varepsilon_+^{p*} - \varepsilon_-^p = a^2\varepsilon_+^{p*} . \tag{4-43}$$

In the vacuum gap, a^2 is 2 as above stated. Therefore we have

$$\varepsilon_+^{v*} - \varepsilon_-^v = 2\varepsilon_+^{v*} . \tag{4-44}$$

Thus we get, instead of equations (4-39) and (4-40),

$$a^2\varepsilon_+^{p*} = 2\varepsilon_+^{v*} \qquad \text{at} \quad r=r_p \tag{4-45}$$

and

$$\frac{d}{dr}(a^2\varepsilon_+^{p*}) = 2\frac{d}{dr}(\varepsilon_+^{v*}) \qquad \text{at} \quad r=r_s. \tag{4-46}$$

If the gas is assumed slightly ionized, $\frac{b}{a}r$ will be very small. Then $J_1(\frac{b}{a}r)$ is nearly equal to $\frac{b}{a}r$. In this case, we can easily determine ε_o and ε_2 in terms of ε_1 as

$$\varepsilon_o = \frac{2}{ab}\,\varepsilon_1 , \qquad \varepsilon_2 = 0. \tag{4-47}$$

Combination of equations (4-38), (4-41), (4-42) and (4-44) yields the relations

$$-2\,\mathrm{Im}(\varepsilon_1) = \frac{4\pi\omega}{c^2}\,J_\theta^s ,$$

$$\mathrm{Re}(\varepsilon_1) = 0 .$$

In complex form,

$$\varepsilon_1 = i\,\frac{2\pi\omega}{c^2}\,J_\theta^s \quad . \tag{4-48}$$

Finally we get the solution as

for $r < r_p$,

$$\varepsilon_+^p = (\varepsilon_+^{p*})^* \quad , \tag{4-49}$$

$$\varepsilon_-^p = (1-a^2)\varepsilon_+^{p*} \quad , \tag{4-50}$$

$$\varepsilon_+^{p*} = i \frac{2\pi\omega}{c^2} J_\theta^s \frac{2r}{a^2} \quad . \tag{4-51}$$

for $r_p < r < r_s$,

$$\varepsilon_+^v = \varepsilon_-^v = -i \frac{2\pi\omega}{c^2} J_\vartheta^s r \quad . \tag{4-52}$$

It is worth while noting that ε_+^v and ε_-^v are both purely imaginary; that is, there is only the azimuthal electric field.

If the plasma is collisionless, a^2 becomes 1 and we find

$$\varepsilon_-^p = 0 \quad ,$$

$$\varepsilon_+^p = 2\varepsilon_+^v \quad ,$$

at the intersurface of the plasma and the vacuum gap. As the electromagnetic energy density in the vacuum side is twice times as much as the electric energy density, so the electromagnetic energy in vacuum side

becomes just the electric energy density as one passes through the intersurface from the vacuum region.

Generally, the ε_+ field penetrates the plasma without considerable change, independently of the ion density. On the contrary, the ε_- field is also unchanged for sufficiently low ion density but is reduced by a large factor for high ion density.

4.4 Absorption Curve and Determination of Momentum Collision Frequency

In this section we shall investigate the energy dissipation due to the cyclotron resonance, by using the result in the previous sections. Then a method to determine momentum collision frequency is to be proposed.

First we shall obtain the energy absorption per unit length of the cylinder. From equation (4-24) we obtain

$$\left|\mathcal{E}_-^p\right|^2 = \frac{(\nu_m^2+\omega^2-\omega_i^2)^2+4\nu_m^2\omega_i^2}{\nu_m^2+(\omega_i+\omega)^2}\left|\mathcal{E}_+^p\right|^2 \qquad (4\text{-}53)$$

Then the dissipation power given by equation (4-14)

$$\overline{E.D.} = \frac{\pi\omega^2}{c^4}\varepsilon_{pi}(J_\theta^s)^2 r^2 \frac{\left\{(\nu_m^2+\omega^2+\omega\omega_i)^2-\nu_m^2\omega_i^2\right\}\nu_m\omega^2}{(\nu_m^2+\omega^2)\left\{\nu_m^2+(\omega_i+\omega)^2\right\}}\left[1+\frac{(\nu_m^2-\omega_i^2+\omega^2)^2+4\nu_m^2\omega_i^2}{\left\{\nu_m^2+(\omega_i+\omega)^2\right\}\left\{\nu_m^2+(\omega_i-\omega\right.}\right.$$

(4-54)

where we have used equations (4-34), (4-51) and (4-53). Thus we can derive the dissipation power per unit length of the cylinder E.D.U. from the integration of equation (4-54) with respect to r from 0 to r_p. Then we get

$$\overline{E.D.U.} = \frac{\pi\omega_{pi}^2}{3c^4}(J_\theta^s)^2 r_p^3 \left\{ \frac{\left\{(\nu_m^2+\omega^2+\omega\omega_i)^2-\nu_m^2\omega_i^2\right\}\nu_m\omega^2}{(\nu_m^2+\omega^2)\left\{\nu_m^2+(\omega_i+\omega)^2\right\}} \left[1+ \frac{(\nu_m^2-\omega_i^2+\omega^2)+4\,\omega_i^2}{\left\{\nu_m^2+(\omega_i+\omega)^2\right\}\left\{\nu_m^2+(\omega_i-\omega)^2\right\}} \right] \right\}$$

(4-55)

where we have assumed that ω_{pi}^2 (or the ion density) is constant in the plasma region.

If we draw a curve of $\overline{E.D.U.}$ as a function of ω, this curve will have a peak near the ion cyclotron frequency ω_i. Also the half-width of the peak has a relation to the ion-molecule momentum collision frequency ν_m, according to equation (4-55). Therefore, if we can practically observe this absorption curve for a given partially ionized gas, then we can determine ν_m under the situation from the half-width.

The frequency dependence of $\overline{E.D.U.}$ given by equation (4-55) is rather complicated, but it is simplified for slightly ionized gas. Because, in this case, $|\mathcal{E}_+^p|^2$ is the same as $|\mathcal{E}_-^p|^2$ and then we can use the relation given by equation (4-14) in place of (4-55). Furthermore, if ν_m is relatively small compared with

ω_i, the second term in the brackets of equation (4-14) becomes predominant and the absorption curve will be of a Lolentzian shape. Then, the half-width $\Delta\omega$ is given by

$$\Delta\omega = \nu_m \ . \qquad (4\text{-}56)$$

This relation is shown in Fig. 4-2-a.

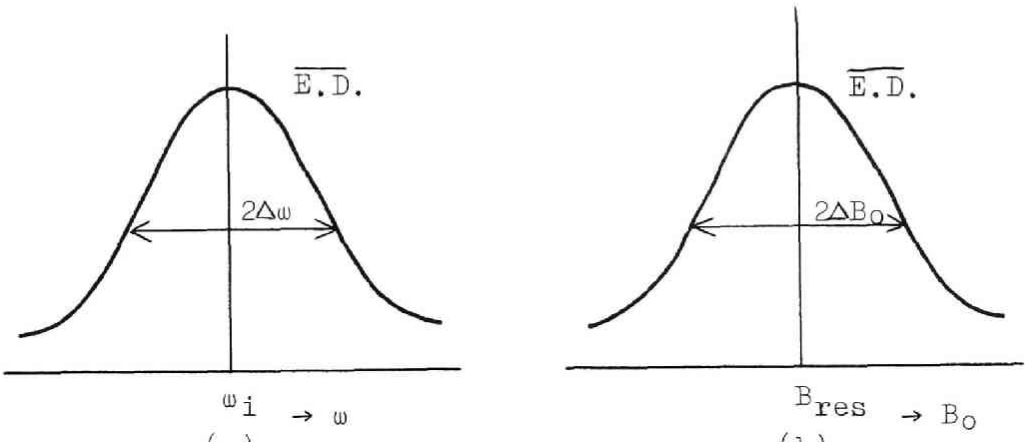

Fig. 4-2 Absorption curve of ion cyclotron resonance.
(a) Frequency sweeping.
(b) Magnetic field sweeping.

If we sweep the static magnetic field instead of the frequency sweeping, the half-width of the absorption curve as a function of B_o is also given by

$$\Delta B_o = \frac{\nu_m}{\omega} B_{res} \ , \qquad (4\text{-}57)$$

where

$$B_{res} = \frac{Mc\omega}{q} \ . \qquad (4\text{-}58)$$

In such a manner, we can experimentally determine ν_m. Such experiment was carried out by the author as described in the next chapter.

V Experiment on Ion Cyclotron Resonance with Collision Relaxation

5.1 Introduction

As explained in the previous chapter, the line broadening of the absorption curve of ion cyclotron resonance in a slightly ionized gas is mainly caused by the collision relaxation of ions with neutral gas molecules. Experiments described in this chapter were carried out so as to verify the dependence of the half-width on neutral molecule density and determine the momentum collision frequencies for different gas pressures.

Many experiments on ion cyclotron heating of plasma have been reported, but those which had pure aim to determine the collision frequency were restricted to only experiments by the auther[30] and by Wobschall Graham and Malone.[31] Also Dubovoi, Shvets and Ovchinnikov[32] observed the dependence of the line broadening on gas pressure in their experiment of ion cyclotron resonance in dense plasma, though they made experiment on plasma heating.

It is mainly attributable to the difficulty of detection of the absorption curve that there have been only a few reports concerning this problem. Becuase the resonance signal is so weak and noisy that we must begin with the development of detecting method.

The author, and Wobshall and his coworkers succeeded in the improvement on the signal to noise ratio by combining a phase-sensitive detector and a narrow band amplifier. This technique was much obliged to the development of nuclear magnetic resonance spectrometers.

Also it should be noted that Kelly, Margenau and Brown[33] had investigated electron cyclotron resonance for determining collision cross sections for low-energy electrons from the theoretical and experimental points of view. In this case, the frequency of electric field is in a microwave region and then the technique is of course quite different from that of the ion cyclotron resonance.

In the next section 5.2, several detecting methods of the absorption power and the results by them will be described. Especially, the result on the collision broadened curve observed by an autodyne oscillator method is to be given and discussed in detail in the subsequent section 5.3.

5.2 Detecting Methods for Collision Broadened Lines of Ion Cyclotron Resonance

In order to obtain the absorption curve of ion cyclotron resonance in a slightly ionized gas, two methods may be considered; that is, a magnetic field sweeping method and a frequency sweeping method, as

explained in the section 4.4. Technically, the former method is rather simple but physically the latter is more suitable, since there are apprehensions of the change in physical plasma situation during the magnetic field sweeping. Methods described in this chapter belong to the type of the field sweeping. The reason is ascribed to the difficulty to make a high gain detector for the frequency sweeping. On the contrary, as explained in a chapter VII, a frequency sweeping method could be adopted to measure the exciting power absorption of ion cyclotron waves in the Heliotron-B device, because the plasma density in the device was relatively high ($10^{12}/cm^3$) and a Franklin oscillator could be used.

The plasma and its container for the measurement of collision frequency should have properties as follows.

(i) The plasma must be quiescent as much as possible, since plasma noise has direct influence upon the S/N ratio of signals.

(ii) The plasma should be pure. For the sake, it is necessary to diminish the outgas from its gas container or discharge electrodes.

(iii) The container must be sufficiently large compared with the Larmor radius and the mean free path of ions, and otherwise the apparent collision frequency would be decided by the scale of the

container.

(iv) Currents in the plasma parallel to the magnetic field are desired to be very small.

Several detecting methods tried by the author will be described in following small sections.

5.2.1 Combination of a Magnetic Field Modulation and a Lock-In Amplifier.

The foundation of this method may be found in the technique of the detection of nuclear magnetic resonance, though there lies some differences between them. Nuclear magnetic resonance can be caused when the transition energy of the nuclei in a magnetic field between energy levels becomes equal to the quantum energy of an applied electromagnetic radiation. This relation may be written as

$$h\nu = \frac{\mu\beta_N \cdot H_o}{I} \qquad (5\text{-}1)$$

or

$$2\pi\nu = \gamma . H_o = \omega_m \qquad (5\text{-}2)$$

where I and μ are the spin number and the magnetic moment of the nuclei, β_N is a constant called the nuclear magneton, H_o the magnetic field strength, h Plank's constant and ν the frequency. Also γ is known as the gyromagnetic ratio. ω_m given by equation (5-2) is classically understood to be the precession

angular frequency of the nuclear magnet. Then we can find the correspondence of the nuclear magnetic resonance with the ion cyclotron resonance. That is, the precession angular frequency ω_m corresponds to the ion cyclotron angular frequency ω_i and γ in equation (5-2) to $\frac{q}{MC}$ of the ions. This correspondence may be schematically shown in Fig. 5-1. However, a remarkable difference between them is that the transition of the nuclear magnetic resonance is discrete

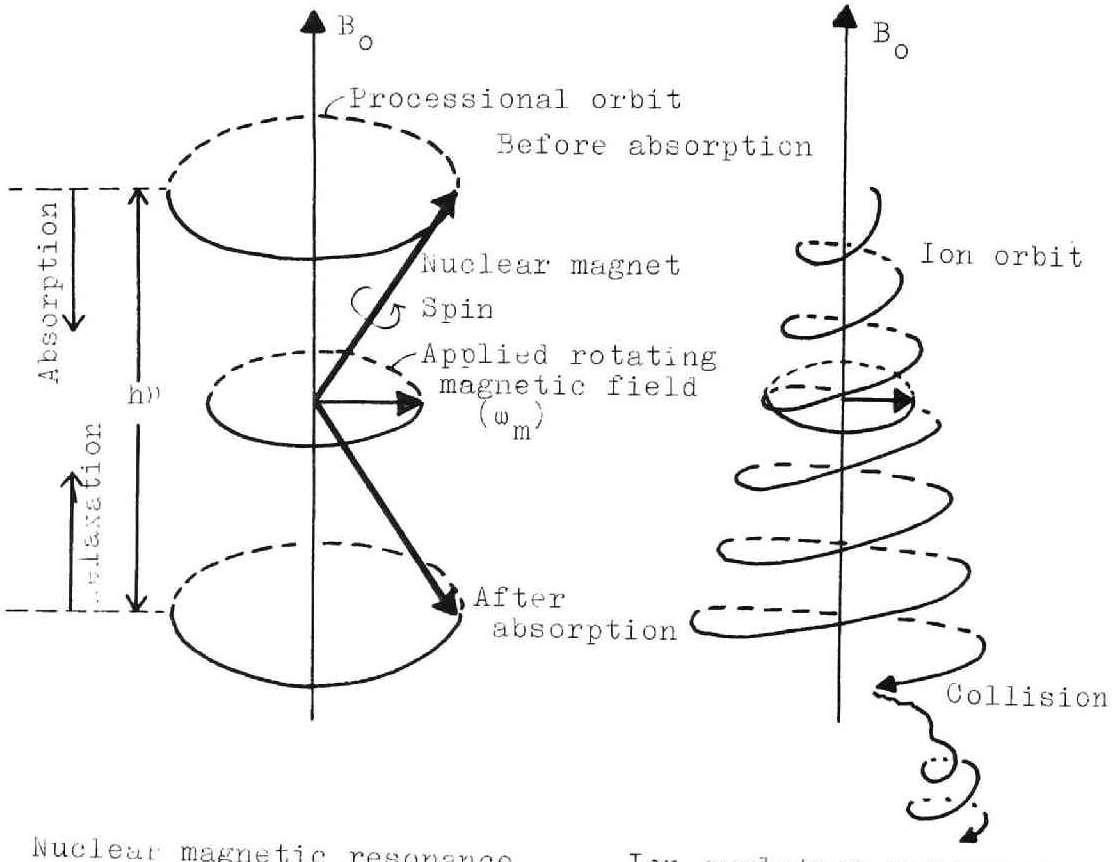

Fig.5-1 Correspondence between nuclear magnetic resonance and ion cyclotron resonance.

and, on the contrary, the acceleration by the ion cyclotron resonance is continuous, as seen in Fig. 5-1.

Nuclear magnetic resonance spectrometers are ordinarily of a field modulation type. If an oscillating magnetic field of small amplitude is imposed parallel to the static magnetic field and only a signal of the modulation frequency is detected, then the differential curve of an absorption signal can be obtained, through a phase-sensitive detector (Lock-in amplifier) as explained in Fig. 5-2.

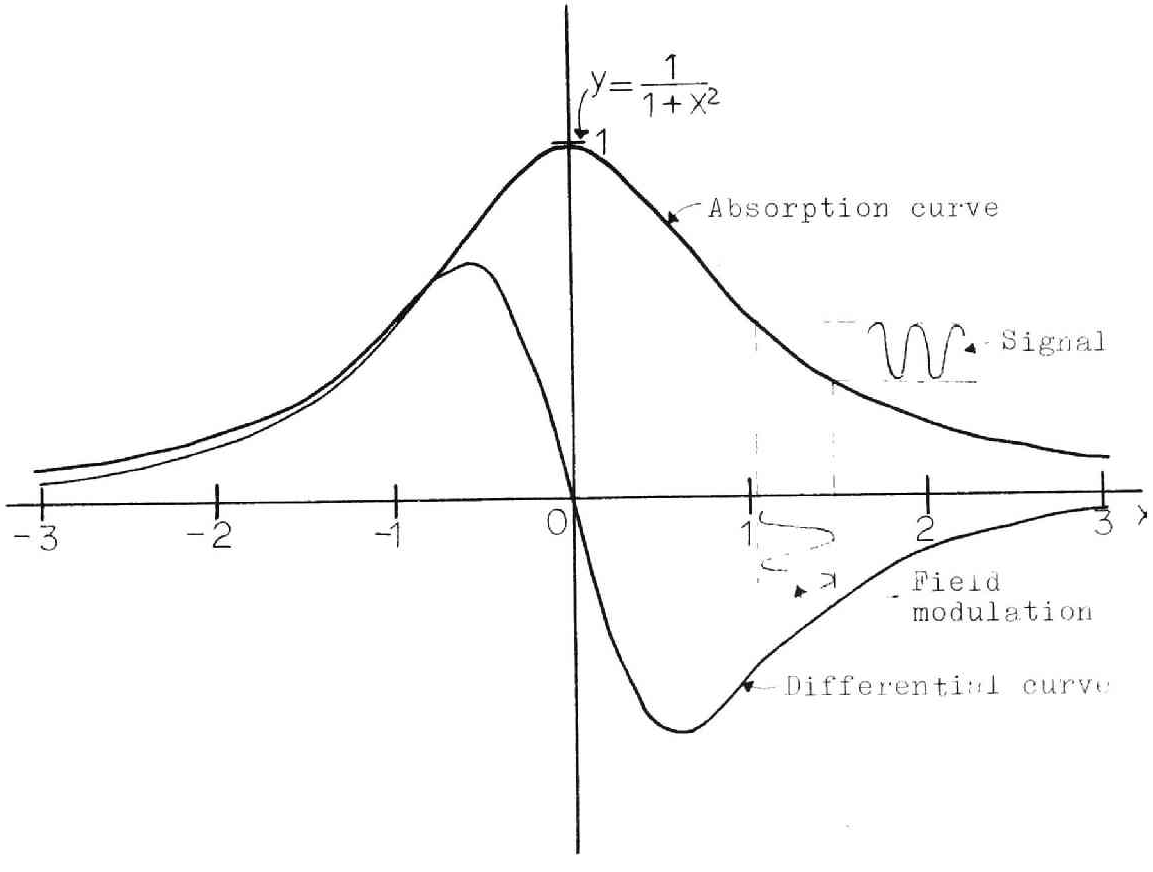

Fig.5-2 Absorption curve and its differential curve

In this case, the S/N ratio can be much improved, owing to a narrow-band amplifier and a phase-sensitive detector. This method is also available to ion cyclotron resonance spectrometers, if some attentions are paid.

The practical detecting apparatus tried by the author is shown in Fig. 5-3. A discharge tube(8 cm long and 3 cm in diameter) was mounted in the gap of poles of an electromagnet and its axis was parallel to the magnetic field. A rf work coil wound around the discharge tube formed the L-C tuning circuit of an autodyne oscillator, the circuit of which was the same as nuclear magnetic resonance spectrometer and will be again described in detail in the next section 5.3. A compensating rf coil was connected in series with the rf work coil and compensated the modulated magnetic flux passing through the rf work coil. Therefore, no signal should come from the autodyne oscillator, as far as the cyclotron resonance absorption did not occur. The ion cyclotron resonance absorption of plasma gave rise to the decrease of the oscillation level of the oscillator. The signal of this change in the level was modulated due to the magnetic field modulation and approximately proportional to the derivative of the absorption curve, which could be checked by using a dammy load instead of plasma.

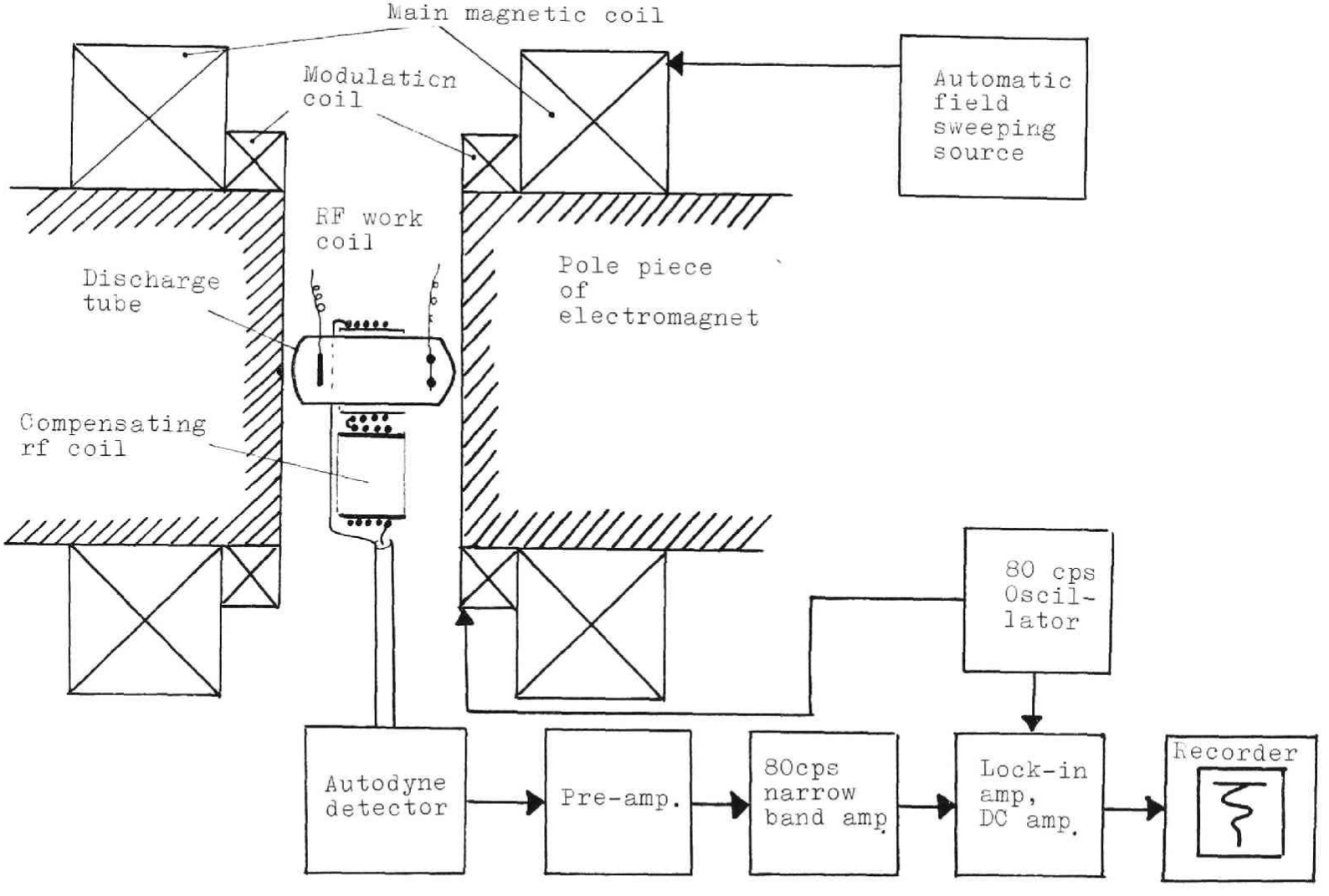

Fig. 5-3 Schematic diagram of the detecting apparatus of ion cyclotron resonance with field modulation.

The signal from the oscillator was amplified by a pre-amplifier and then put in a Lock-in amplifier through a narrow-band amplifier of the modulation frequency (80 cps), the gain of which was 60 db. The AC signal was converted into DC signal by the Lock-in amplifier and finally recorded by a pen recorder. The spacial homogeneity of the magnetic field was 10^{-5} over the plasma region, since the magnet had been made for anelectron spin resonance spectrometer. If the main static magnetic field was swept, then a differential absorption curve would be recorded.

Fig. 5-4 shows an example of the differential absorption curves obtained in such a manner. Here, the gas used was helium and the ions being subjected to ion cyclotron resonance were singly ionized helium atoms (He^+), which were produced by discharge of 100 mA. The pressure of gas was 1.6×10^{-1} Torr, that was measured by a Macleod gauge. The corresponding ordinary absorption curve could be obtained from the graphical integration of this differential curve, which is shown in Fig. 5-5. This is an absorption curve of the ion cyclotron resonance with collision relaxation. The curve is much broadened due to He^+-molecule collisions and its half-width is about 600 gausses. Then the momentum collision frequency is about 7×10^5 per second in the case.

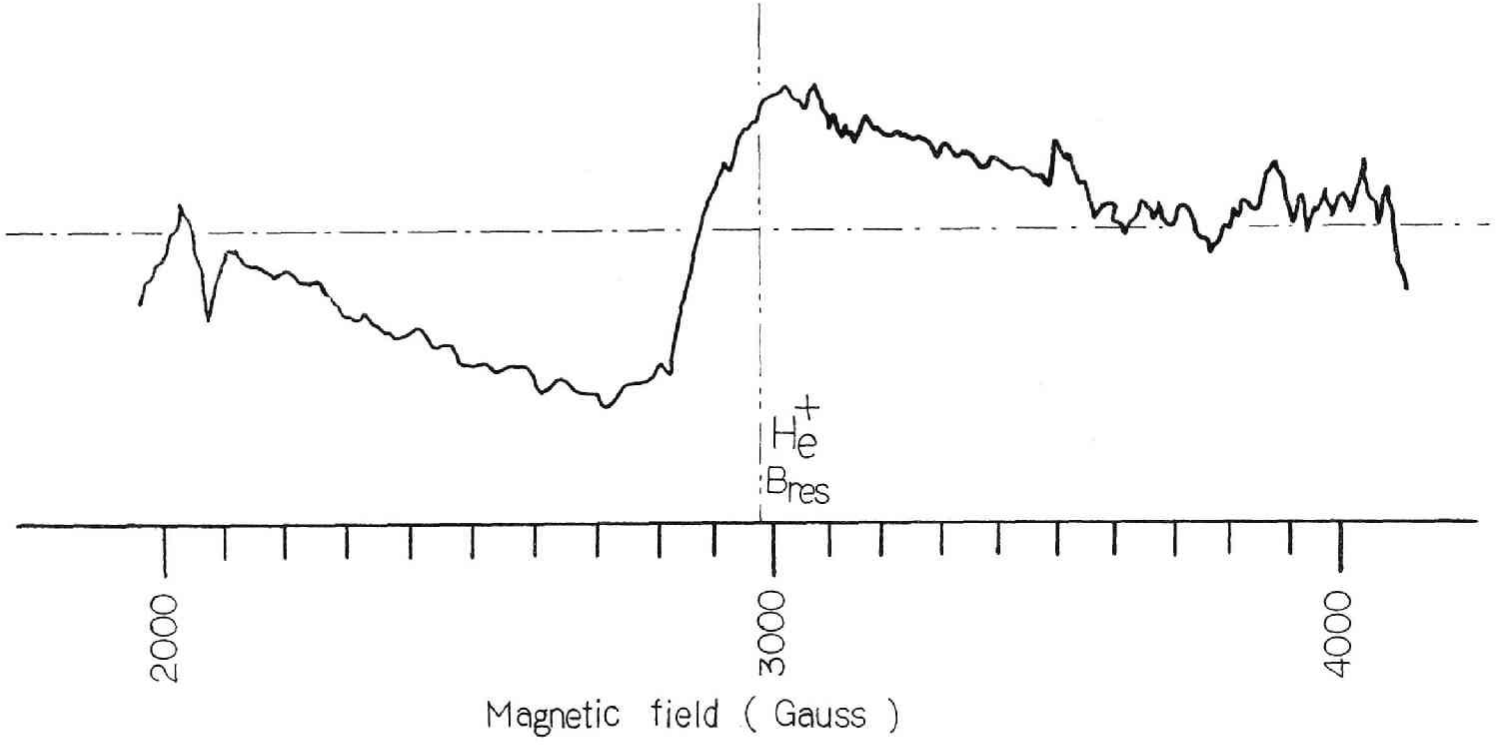

Fig. 5-4 Recorder trace of the differential absorption curve of ion cyclotron resonance with collision relaxation.
Initial pressure:0.16 Torr(He), Discharge current:100mA,
RF frequency:1.15Mc, Magnetic field modulation:15 G(p-p).

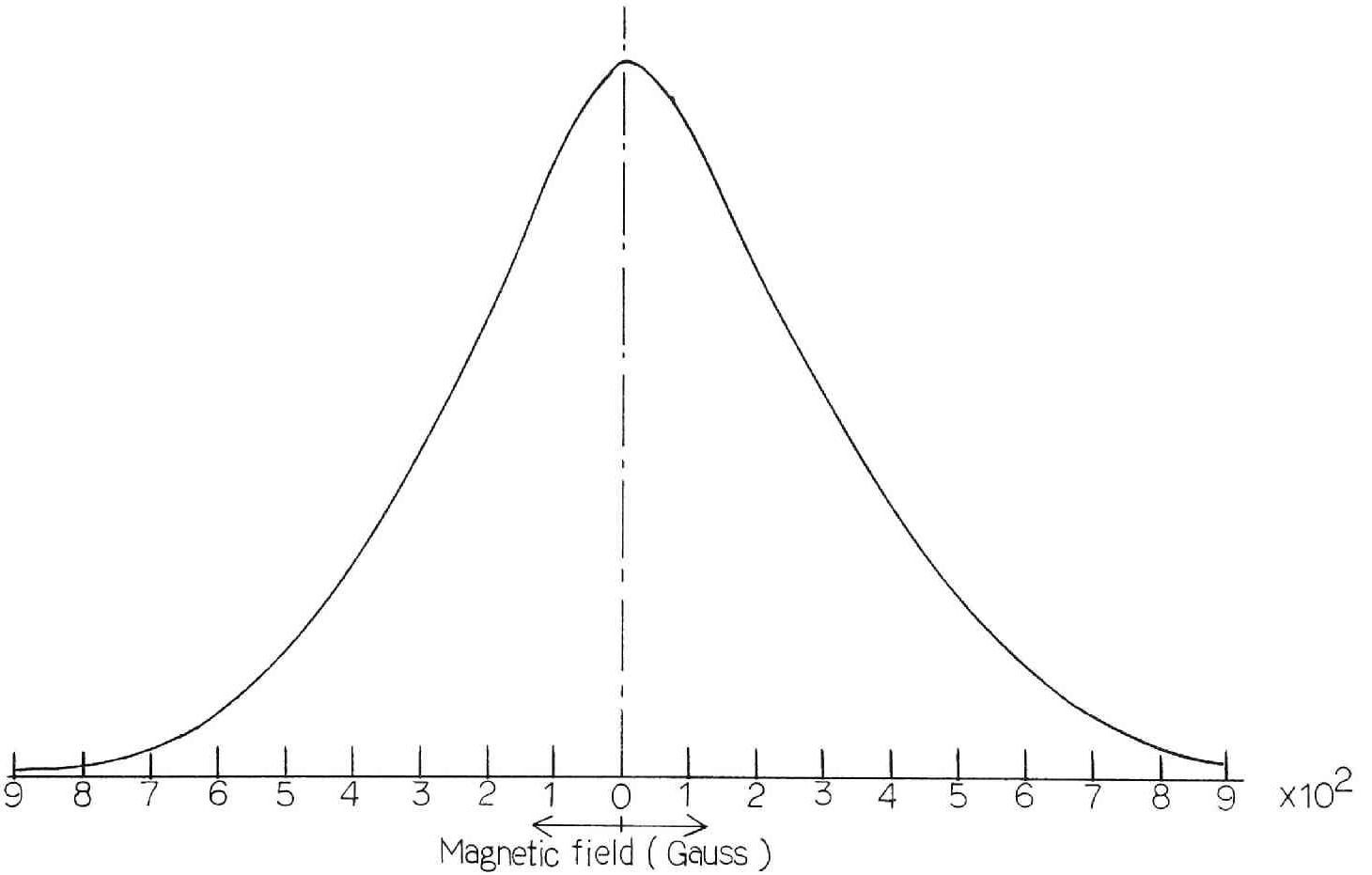

Fig. 5-5 Absorption curve of He^+ cyclotron resonance in helium discharge, obtained by graphically integrating the differential absorption curve. Initial pressure:0.16 Torr(He), Discharge current:100 mA, RF frequency:1.15 Mc, Modulating magnetic field:15 G(p-p).

This detecting method is supposed to be the most reliable one, since the S/N ratio is very large as seen in Fig. 5-4. However, long use of this electromagnet was impossible unfortunately, for it should be used for its original purpose. For the reason only a few results could be obtained by this method. Nevertheless, it became evident that rf power absorption of a slightly ionized plasma has a its peak near the ion cyclotron frequency and the shape of the line is such as expected theoretically in the previous chapter IV.

5.2.2 Direct Measurement of the Oscillation Level of Autodyne Oscillator

The direct measurement of oscillation level of the autodyne oscillator no longer needs the magnetic field modulation, though its S/N ratio becomes somewhat inferior to that of the modulation method. Therefore, the apparatus for it will be more simple.

Detail discussions of the apparatus and the results by this method are again to be given in the section 5.3.

5.2.3 Detection of Emitted Light Intensity

If radio frequency discharge in a strong magnetic field is caused by an azimuthal electric field and its frequency is near the cyclotron frequency of ionized

particles in their parent gas, the ions will be resonantly accelerated and will contribute to the ionization of the gas molecules. Then, we may observed this ionization effect of the ion cyclotron resonance from the measurement of light intensity radiated from the ionized gas. Also it will be observed that this effect is affected by the collision relaxation between the ions and the molecules.

In order to verify this effect, a simple experiment was carried out by using an apparatus as shown in Fig. 5-6. A discharge tube of Pyrex glass (40 cm long and 4 cm in diameter) was inserted in a solenoidal coil (50 cm long and 9 cm in inner diameter) co-axially with its axis. Around the discharge tube, a rf work coil was wound and induced an azimuthal rf electric field. Rf power was feeded through a matching network from a continuously working oscillator, the power and the frequency of which were 300 watts and 10 Megacycles per second. The magnetic coil was energized by a condenser bank of energy 40 kilojoule. The resulting magnetic field strength was 1.17×10^4 gausses of maximum. The total emitted light was led through a optical pipe of plastics and then detected by a photomultiplier RCA6342 . Since the homogeneity of the magnetic field was $\pm$ 2% over the plasma region, then the line width of the light intensity variation

as a function of the magnetic field strength would be expected to be observed, if the cyclotron resonance effect was present.

Experimental procedure was as follows. Hydrogen gas at pressure of 10^{-3} Torr was first put in the discharge tube and then the rf discharge produced plasma. Next, the condenser bank energyzed the magnetic coil with an ignitron switch. In such a manner, time variations of the light intensity could be observed with a synchroscope. Namely, the variation of the light intensity could be observed as a function of the magnetic field strength.

An example of the results is shown in Fig. 5-7. The light intensity increased quickly at the beginning of the magnetic field rise and then decreased slowly. Again it increased as the magnetic field was decaying. During this variation, two small peaks could be observed, which are indicated by arrows in the figure. These peaks corresponded exactly to the magnetic field where proton cyclotron frequency was equal to the rf frequency. However, these peaks became very broad 10 minutes after from the start of discharge, as seen in the second oscillogram of the figure. This may be explained as that outgassing from the tube wall raised the inner gas density gradually and, as a result , so-called collision broadening of the peak was caused. Though

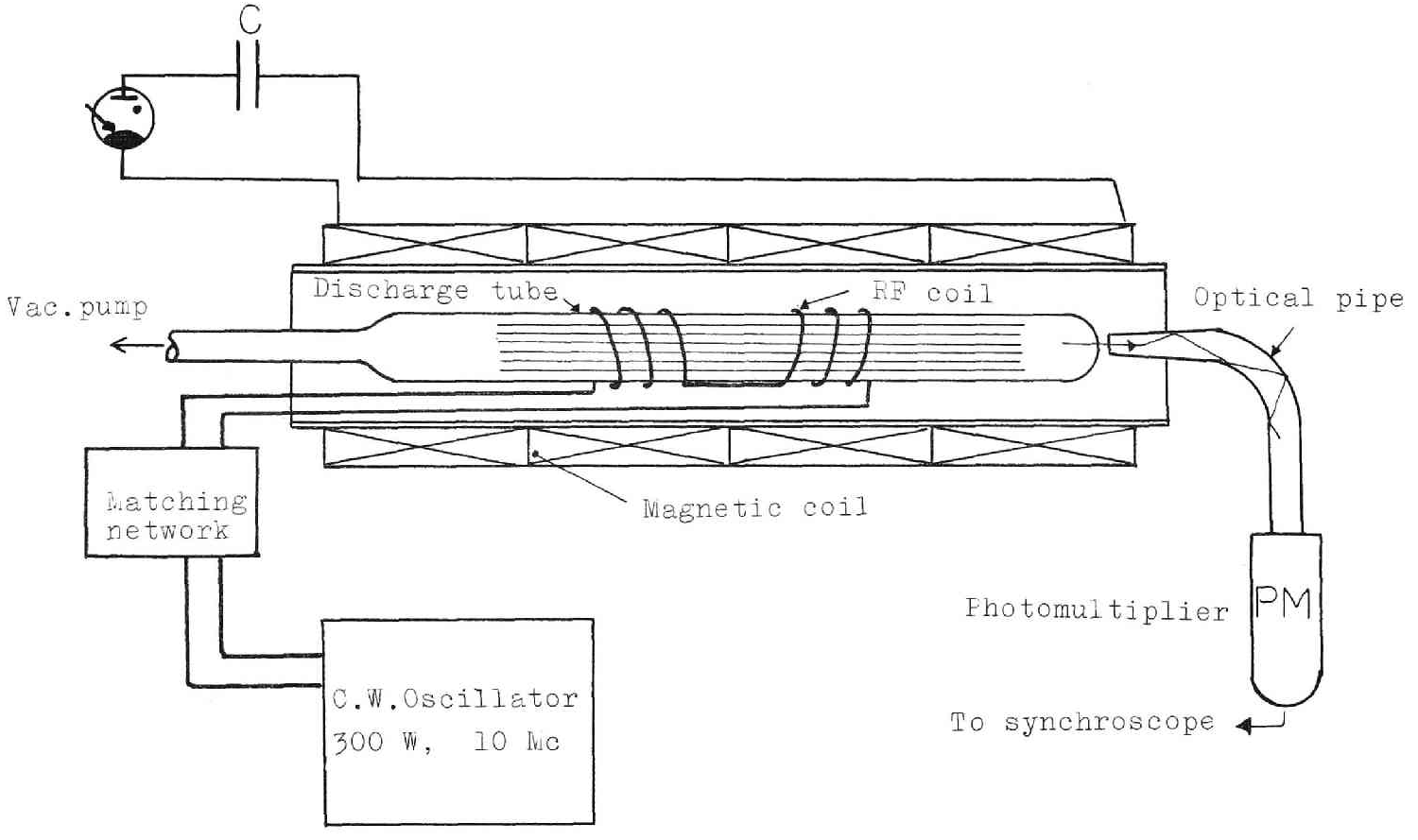

Fig.5-6 Schematic diagram of the apparatus for detecting the effect of ion cyclotron heating on the emitted light intensity.

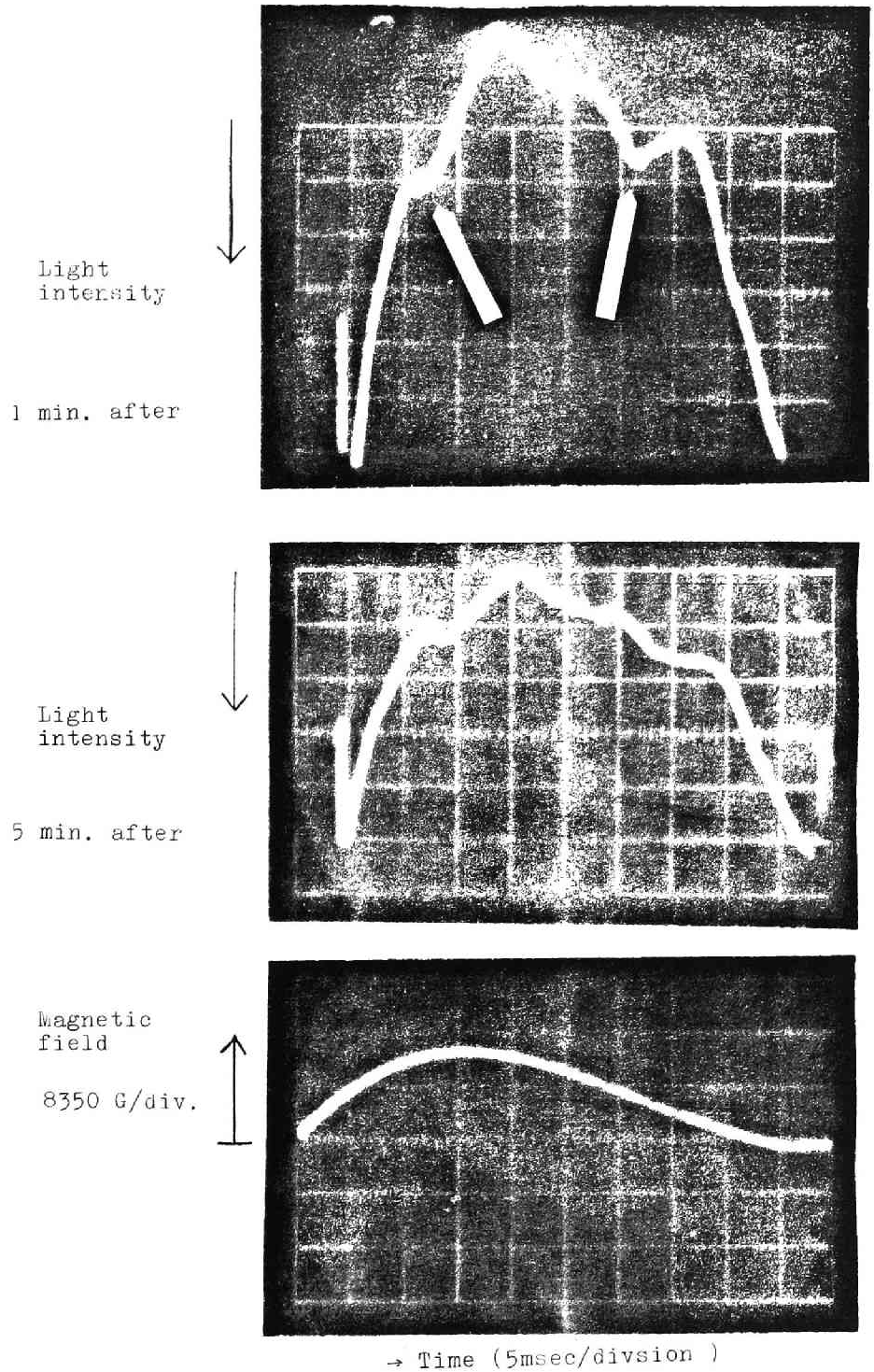

Fig. 5-7 Oscillograms of photomultiplier signal indicating the light intensity emitted from plasma. Also time variation of the magnetic field is shown.

RF frequency: 10 Mc,
Gas: hydrogen, $p_o = 2 \times 10^{-3}$ Torr.

the light was pink at the beginning, it became white 10 minutes after. This also suggested the outgas of impurities.

Therefore, it might be concluded that the ion cyclotron resonance affects the ionization mechanism of the azimuthal rf discharge and the resulting variation of light intensity is dependent upon ion-molecule collision frequency.

5.2.4 Other Detecting Methods

Other tried detecting methods for the measurement of the absorption curve were as follows.

(i) Q-meter

By measuring the Q value of the rf coil wound around the discharge tube, the absorption curves can be obtained. In practice, the resonant absorption could be detected . However, the dip of Q value due to the ion cyclotron resonance was very small and so unavailable for determining collision frequency.

(ii) Franklin Type Oscillator

A franklin type oscillator was also tried, instead of the autodyne oscillator. This oscillator has a pure sinusoidal wave form and can cover the wide frequency range with little variation of power. These characteristics make it possible to adopt a frequency plotting. Therefore, this circuit was

applied for observing ion cylotron waves of plasma in the Heliotron-B device, as described in the chapter VII.

5.3 Collision Broadened Absorption Curve and Momentum Collision Frequency

In this section, collision broadened absorption curves and momentum collision frequencies obtained by the autodyne oscillator method will be given for different gas pressures.

5.3.1 Experimental Apparatus

A discharge tube was inserted in the gap of pole pieces of a electromagnet. A rf coil wound around the discharge tube formed the L-C tuning circuit of an autodyne oscillator and induced an azimuthal electric field, so that the configuration of the field for acceleration became as discussed in the chapter IV. The power absorption of this rf field could be detected by measuring the variations of the oscillation level of the autodyne oscillator. The detail explanation of each part of the apparatus is as follows.

(i) The electromagnet

The gap and the diameter of the pole pieces was 10 cm and 25 cm, respectively. The available scanning range of its field strength was from 800 to 5400 gausses. The field uniformity was less than 10^{-4} in the discharge

region.

(ii) The discharge tube and the rf coil

Fig. 5-9 shows the sectional diagrams of the discharge tube of Pyrex glass. It was 9 cm in length and 3 cm in diameter. The discharge was caused between a copper plate anode and a hot cathod coated with barium oxide. The rf coil was wound around the discharge tube and a mica cushion was interposed between them for good fitting.

The arrangement of the discharge tube and the electromagnet is shown in Fig. 5-8. And its photograph is also given in Fig. 5-10. Fig. 5-11 shows the photograph of the discharge tube.

(iii) The detecting circuit

The circuit of the autodyne oscillator used is shown in Fig. 5-12. The frequency could be determined by adjusting the capacity of the main variable condenser. The rf work coil was connected to the oscillator with a co-axial cable hG 63/U of 1.5 m length, owing to its low capacitance as 30 pF/m. Variations of the oscillating level was detected by measuring the voltage of a terminal denoted by B in Fig. 5-12. Approximate proportionality of the variation to the apparent power loss could be verified by using a dammy load resistance. Frequency shift due to the plasma reaction was negligible, if the plasma ion

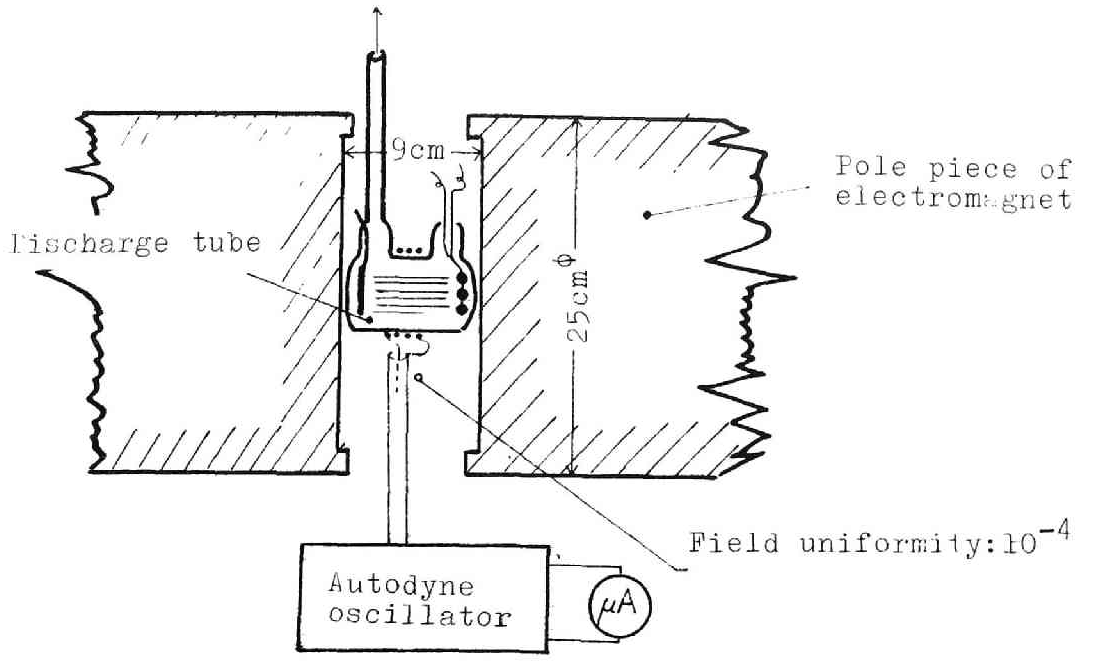

Fig. 5-8 Scematic diagram of the detecting apparatus of ion cyclotron resonance with collision relaxation.

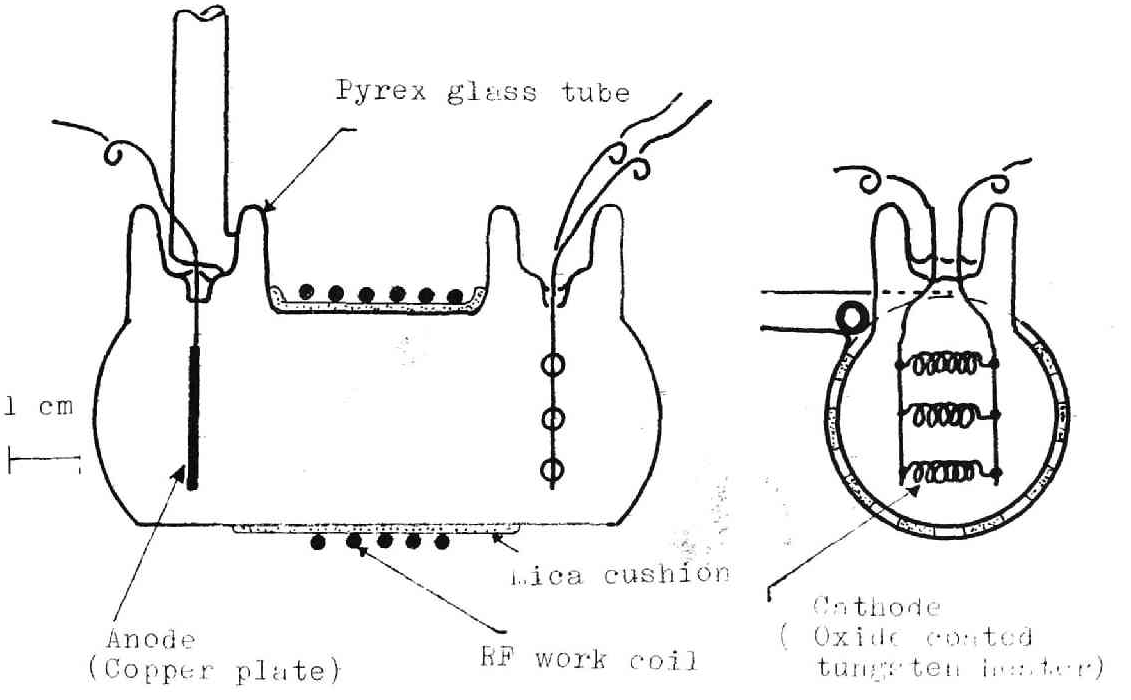

Fig.5-9 Sectional diagrams of the discharge tube for the detection of ion cyclotron resonance.

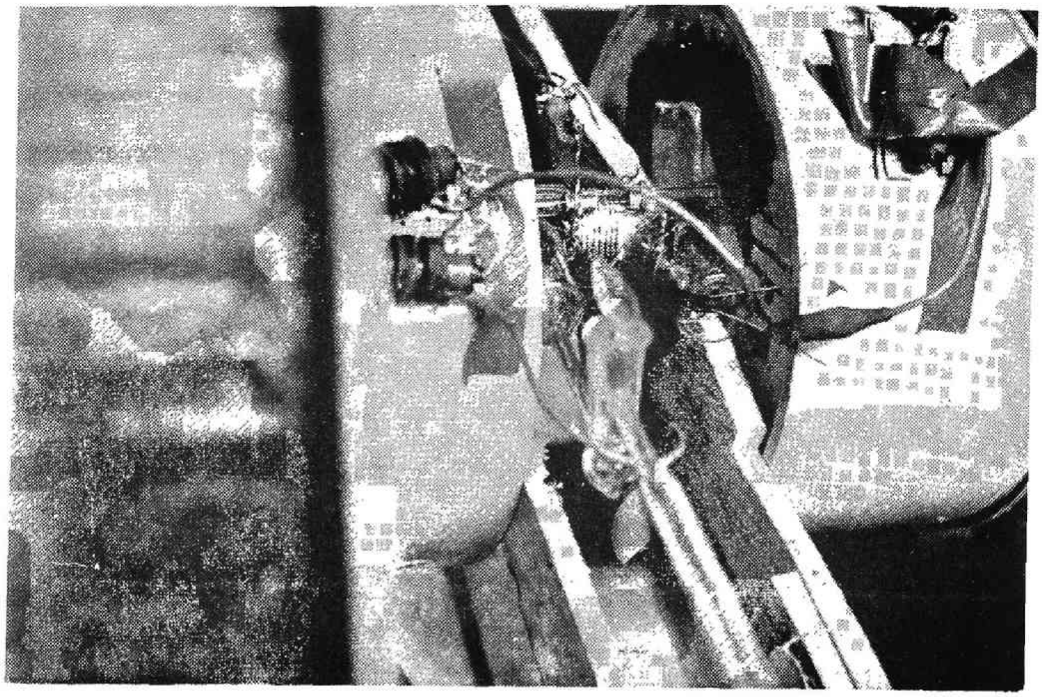

Fig. 5-10 Photograph of the discharge tube mounted in the gap of poles of the electromagnet.

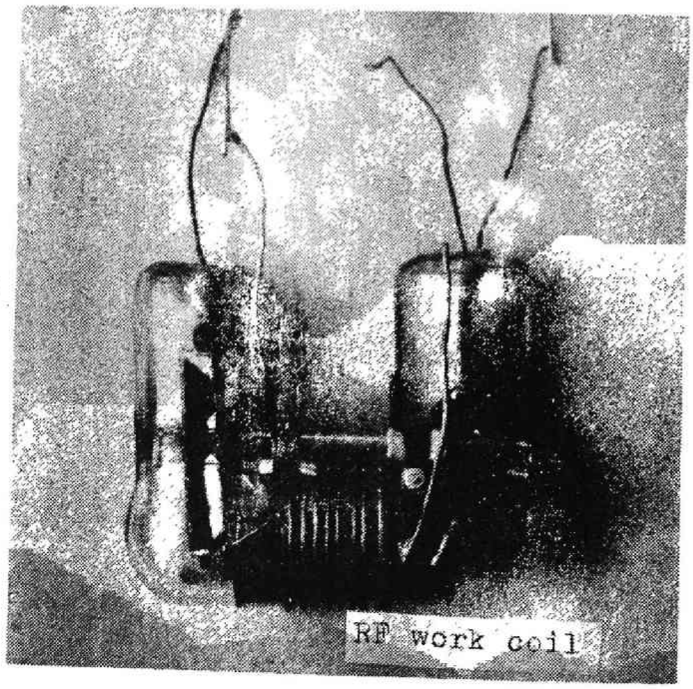

Fig. 5-11 Photograph of the discharge tube for the detection of ion cyclotron resonance.

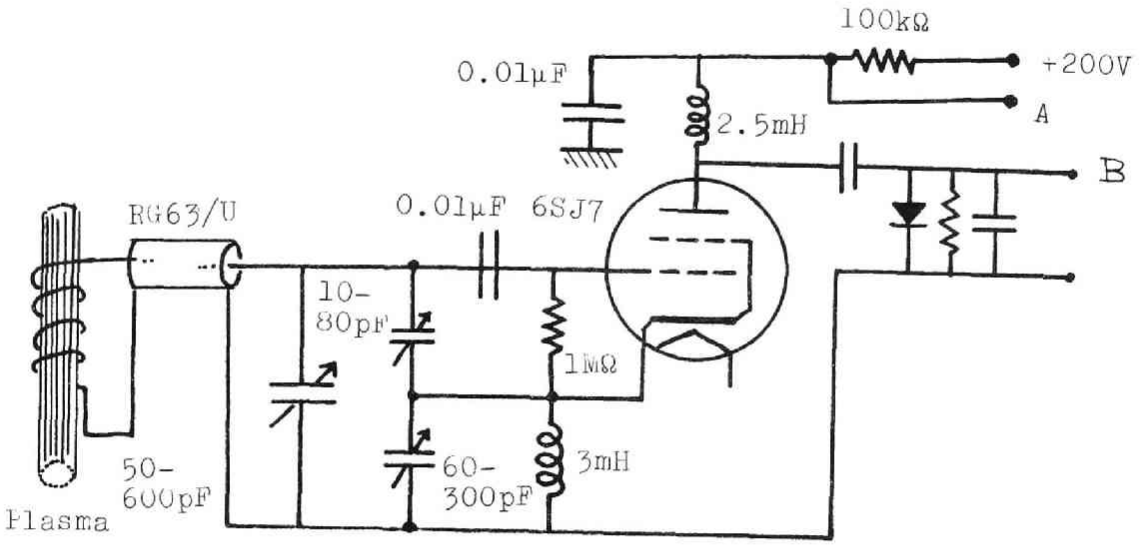

Fig. 5-12 The detecting circuit of ion cyclotron resonance with collision relaxation. (Autodyne oscillator)

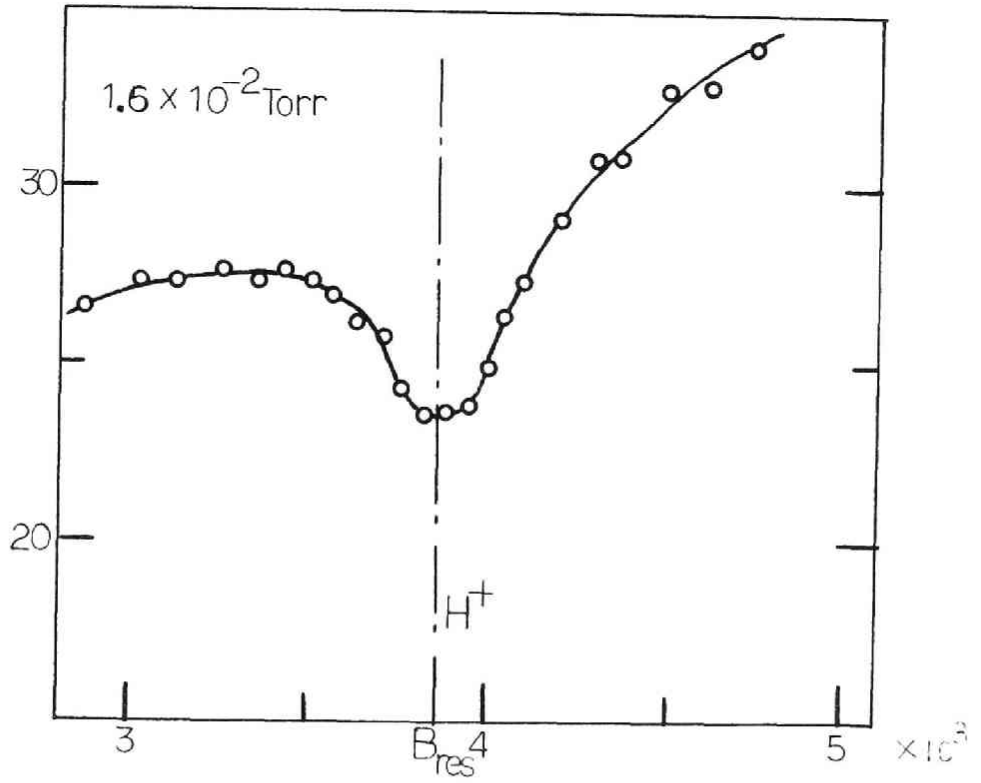

Fig. 5-13 An example of the dip of oscillation level by ion cyclotron resonance absorption.
Gas: hydrogen, Discharge current: 130mA,
Bres: Magnetic field strength where $\omega=\omega_i$.

density was very low. In this case, the frequency shift was within 10^{-3}. The oscillation power was about 10 milliwatts.

5.3.2 Obtained Results

An example of the variation of the oscillation level obtained in such a way is shown in Fig. 5-13, when the gas used was hydrogen and the objective ion was proton. The dip of the level is certainly due to the proton cyclotron resonance absorption, since the peak of the dip exactly corresponds to the magnetic field where the proton cyclotron frequency is equal to that of the rf field. If only the magnitude of the dip is considered, then one can get a absorption curve of the proton cyclotron resonance.

In order to get the pressure dependence of the line width, a series of experiments were carried out for the proton cyclotron resonance in hydrogen gas molecules. Typical results obtained are shown in Fig. 5-14. The width of the dip of the oscillation level clearly depends on the pressure of the parent gas hydrogen. The width becomes wider as the pressure increases. This dependence is such as predicted theoretically in the chapter IV. If normalized absorption curves are drawn, this dependence will be more clarified. Fig. 5-15 shows these normalized absorption curves for different gas pressures, where

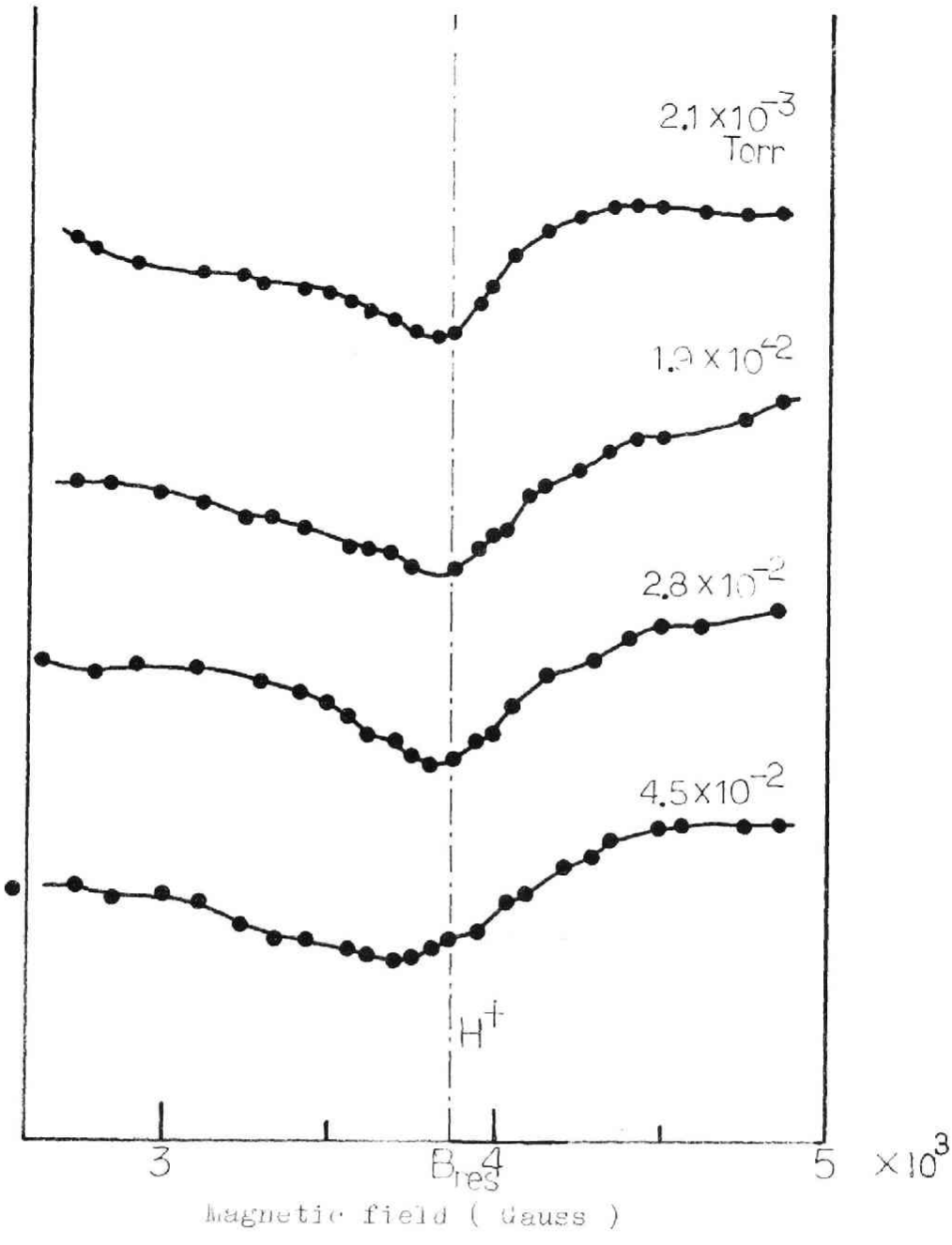

Fig. 5-14 Pressure dependences of the absorption curve of proton cyclotron resonance in hydrogen discharge. Discharge current: 130 mA.

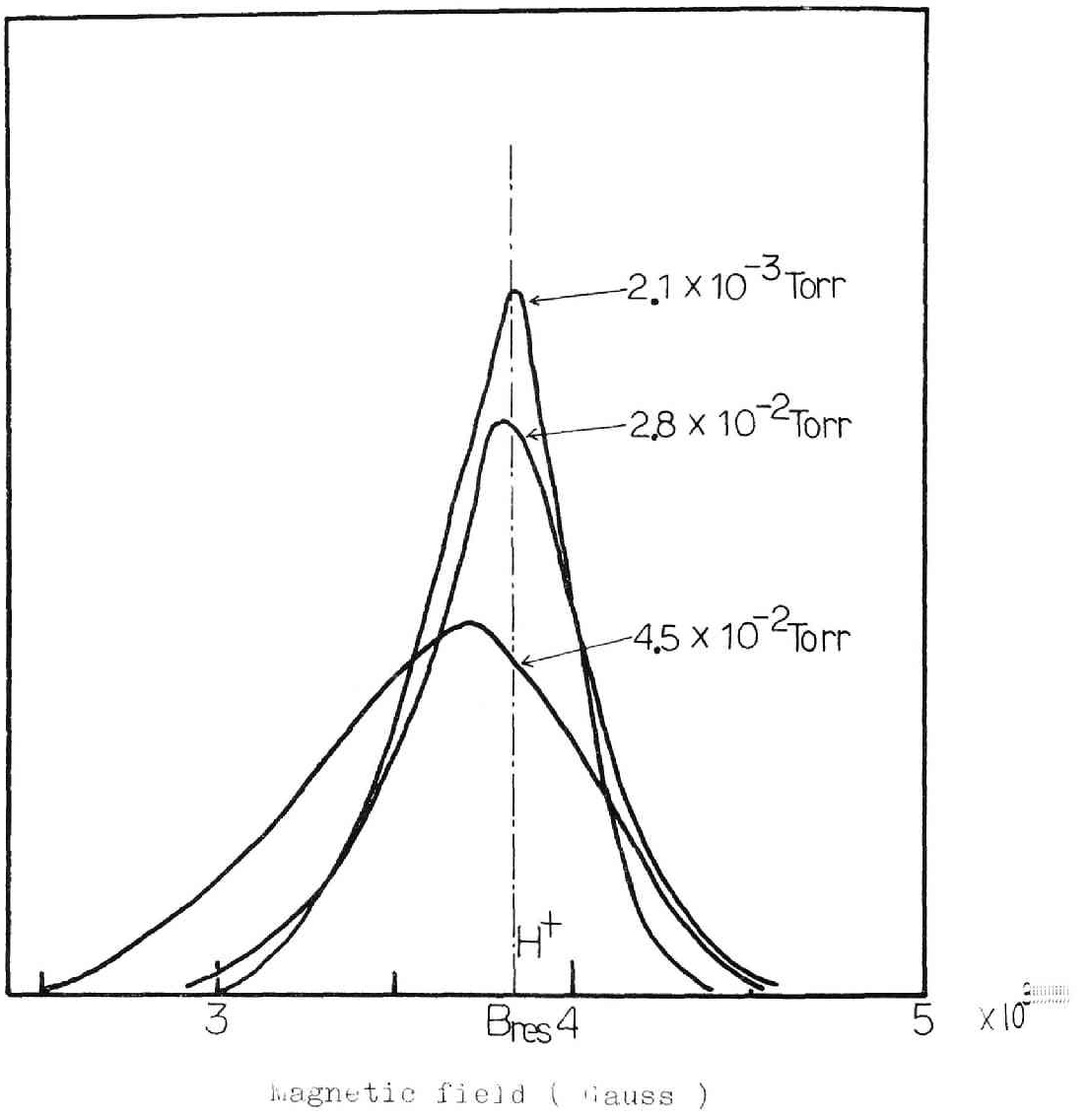

Fig. 5-15 Normalized absorption curves of proton cyclotron resonance for various initial gas pressures.
Gas: hydrogen,
Discharge current: 130 mA,
B_{res}: the magnetic field where proton cyclotron frequency is equal to the rf frequency.

the discharge current was retained constant to be 130 mA.

Thus proton's momentum collision frequency with hydrogen molecules H_2 can be determined from the half-width of the absorption curve as shown in Fig. 5-15, by using the relation (4-57). Fig. 5-16 shows the calculated results in such a way.

5.3.3 Discussion of the Results

As shown in Fig. 5-16, the collision frequency obtained is nearly constant at lower gas pressure than 2.8×10^{-2} Torr, but, beyond this pressure, it may be proportional to gas pressure (refer to dotted line in Fig. 5-16). This deviation from the proportionality between the collision frequency and the gas pressure has been observed in the case of electron cyclotron resonance by Kelly, Margenau and Brown[33] or by Dodo[34] This anticipated result below a pressure is perhaps due to the increase of the mean free path of protons, outgas from the tube wall, the rise of the proton temperature or invalidity of the relation (4-57).

If the mean free path and the mean free time of protons are assumed to be the distance between the electrodes and the reverse of the constant collision frequency in Fig. 5-16, respectively, then the resulting proton energy should be about 6 eV. This magnitude of the energy may be attainable with DC accele-

ration in the magnetic field direction by the electric field for discharge. Therefore, when the pressure is low and the discharge field is high (or at high E/p), protons will be accelerated by the DC field without collisions up to the energy of 6 eV and will directly inpact the cathod. Then the apparent collision frequency will be measured to be about 2.4×10^6 /sec. This is an explanation.

In these experiments the gas pressure was measured just before the discharge, so no contributions of the gas attaching on the tube wall and the outgas from it in the discharge were taken into account. Then the outgas might raise the molecule density and, in the result, the collision frequency might be as shown in Fig. 5-16.

Therefore, to discuss in detail, the more precise experiment must be carried out without DC electric field and outgas.

5.4 Conclusion

The experiments described in this chapter made it clear that the collision frequency of ions with molecules really affects the half-width of the absorption curve of ion cyclotron resonance, as predicted theoretically. Also the collision frequencies for different hydrogen gas pressures could be determined for protons. This method for determing the collision

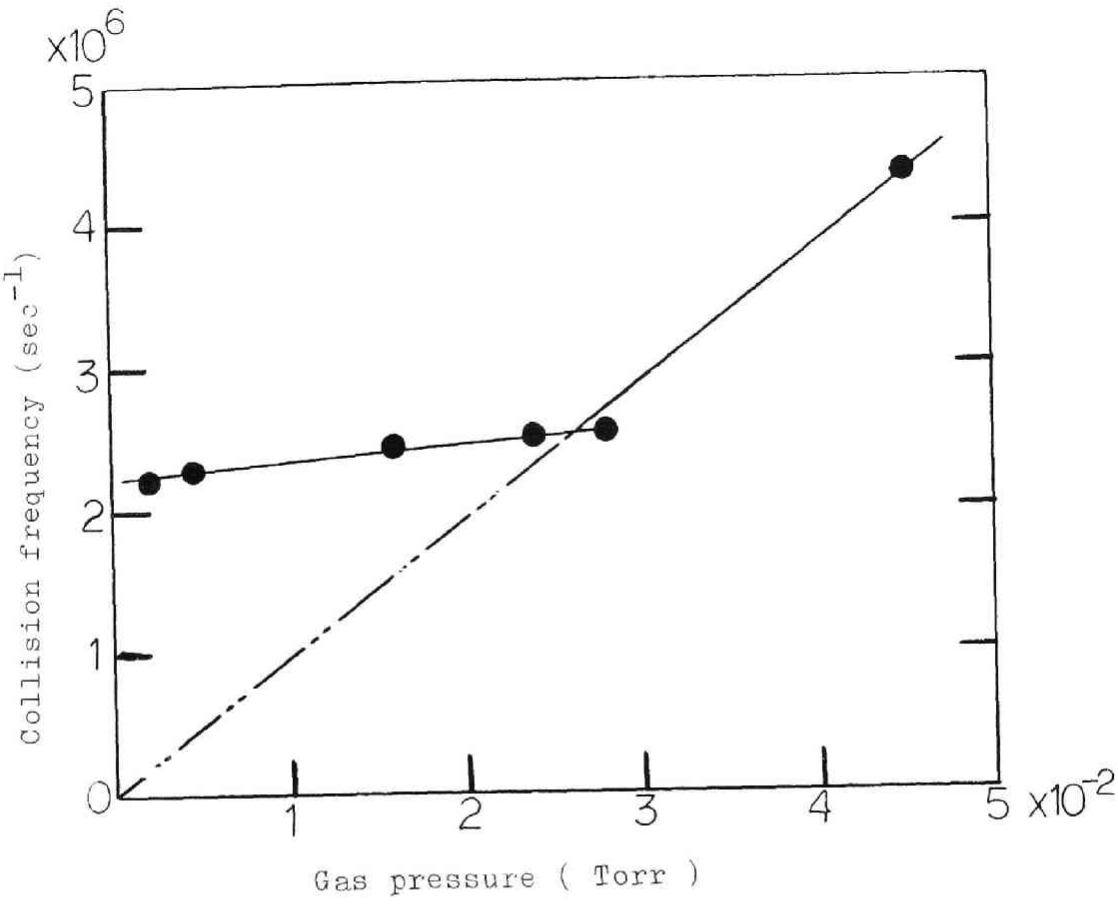

Fig. 5-16 Proton collision frequency in hydrogen gas as a function of gas pressure.
Discharge current: 130 mA.

frequency of ions with gas molecules is applicable to any kind of ions and gas. However to determine precisely the collision frequency, one must use a plasma without DC electric field and outgas.

VI Experiment on Joule Heating of Plasma in the Heliotron-B device

6.1 Introduction

In 1958 Uo proposed the Heliotron as a device for confining plasma and heating it to thermonuclear temperature and Project Helicon was organized to investigate and construct the Heliotron. Since that time the Heliotron-A and the Heliotron-B have been constructed and operated at Kyoto University. The Heliotron-A was destroyed unfortunately in 1959, due to the lack of rigidity of its discharge tube of ceramic. Next the Heliotron-B was constructed in 1960, since then the experiment on the Joule heating has been carried out. The parts for the ion cyclotron heating was equipped in 1962, and the excitation of the ion cyclotron waves and their thermalization have been also investigated.

It should be noted that the experiments described in this chapter were done in collaboration with Uo, Itatani, Mohri, Oshiyama, Kato, Kubo, Ishii and Ariga under the direction of Hayashi. However, the description of these experiments will contribute to the clear apprehension of the experiment on the ion cyclotron heating of plasma in the Heliotron-B device, which is to be described in the chapter VII and VIII. For

the sake the Joule heating of plasma in the Heliotron-B device will be briefly described in this chapter.

The Heliotron-B device has a magnetic field for confining the plasma called "Heliotron magnetic field". The concept of the field will be given in a next section 6.2. In course of the experiments, it became evident that this Heliotron-B device has several constructive defects, such as the irregularity of the coil interval, the lack of the accelerating field uniformity for Joule heating and the evil vertical magnetic field produced by the Joule heating windings. Efforts to remove these defects have been made as much as possible. For instance, a correcting winding for the Joule heating windings was tried as described in a section 6.5. Neverthless, complete improvement on them was found impossible in practice, so that a new device Heliotron-C is now under construction. In a section 6.3, the Heliotron-B device and its experimental procedure are to be explained. The results of the Joule heating are given in a section 6.4.

6.2 Heliotron Principles

The magnetic field used for the Heliotron-B was a so-called Heliotron magnetic field, as shown in Fig. 1-5. If these coils are wound around the discharge tube and the N.L. (i.e. neutral line) is present in the tube, charged particles in the tube may be classified

into two ensembles according to the characteristics of the magnetic lines of force, to which they stick. In the region near the tube axis, the magnetic lines of force undulate along the axis without crossing the tube wall, whereas those near the tube wall, namely outside the N.L. surface (the surface consisting of the lines of force intersecting the N.L.), cross the tube wall. Therefore, if the magnetic field is sufficiently strong, charged particles inside the N.L. surface can move along the lines of force without impacting the tube wall. On the other hand, particles outside the N.L. surface also run along the lines of force but finally touch the tube wall. Thus, it may be expected that we can generate the discharge only in the region inside the N.L. surface, if an axial electric field is imposed. In other words, the N.L. may act as a substitute for an aperture limiter equipped in a Stellarator[35] of Princeton University. The other distinctive characteristics of the Heliotron magnetic field are as follows.

(i) The charge separation of the plasma due to the curvature drifts of particles can be eliminated by the azimuthal drifts of the particles in the undulated field. This effect was verified from the calculation with an electronic digital computer by Amano, Murakami and Ōchi[36] (1964).

(ii) It is possible to heat the plasma by the thermalization of the ion cyclotron waves by using the beach effect at many slopes of the undulation of the Heliotron field. This thermalization effect was experimentally verified by the author as described in the chapter VIII.

(iii) By the existence of the circular cusp (N.L.) series inside the tube wall, we can satisfy the necessary condition for equilibrium of the plasma under the magnet hydrodynamical assumptions.

On the contrary, the defects of the Heliotron field may be

(i) The particles may be lost from the N.L.

(ii) Plasma oscillations may be apt to occur with the wavelength of the interval (or the axial period) of the Heliotron field.

However, the former fault will be overcome under the Joule heating, since the resultant plasma current produces an azimuthal magnetic field and, as a result, the N.L. becomes no longer the cusp.

The Heliotron-B device has the shape of a race-track. Therefore, the magnetic lines of force near the tube axis close themselves. If an electric field is induced parallel to the tube axis, the resulting plasma current can flow along the magnetic lines of force and forms the plasma column inside the N.L. surface. Ionization and preliminary

heating of gas in the Heliotron are accomplished by making a local rf discharge in the tube. Such ionized particles diffuse along the lines of force and finally the gas in the tube becomes a weakly ionized conducting gas. The Joule heating field is next imposed so as to ionize fully the gas and to heat electrons in the plasma.

Plasma instabilities, which may occur in the Heliotron, are not completely known, owing to the complexity of the field. Rotation of the plasma column around the tube axis may arise from the driving force generated by the vector product of the plasma current and the magnetic field. Some observations of these instabilities or oscillations will be explained in the section 6.4. As the conductivity of the plasma rises rapidly with temperature, so the heating rate of the Joule heating decreases. Furthermore, instability of Kulskal type[37] may arise with large plasma current. Therefore, the temperature, that can be achieved by ohmic heating, is upper-bounded.

6.3 Heliotron-B device and Experimental Procedure

The description in this section is concerning only the Joule heating of plasma in the Heliotron-B device.

The Heiotron-B has the shape of a race-track. Fig. 8-2 in the chapter VIII is its photograph, and its plane figure is also shown in Fig. 6-1. The discharge tube is made of stainless steel of 2 mm thickness and insulated by a ceramic (Zirconia) tube at one of the two linear

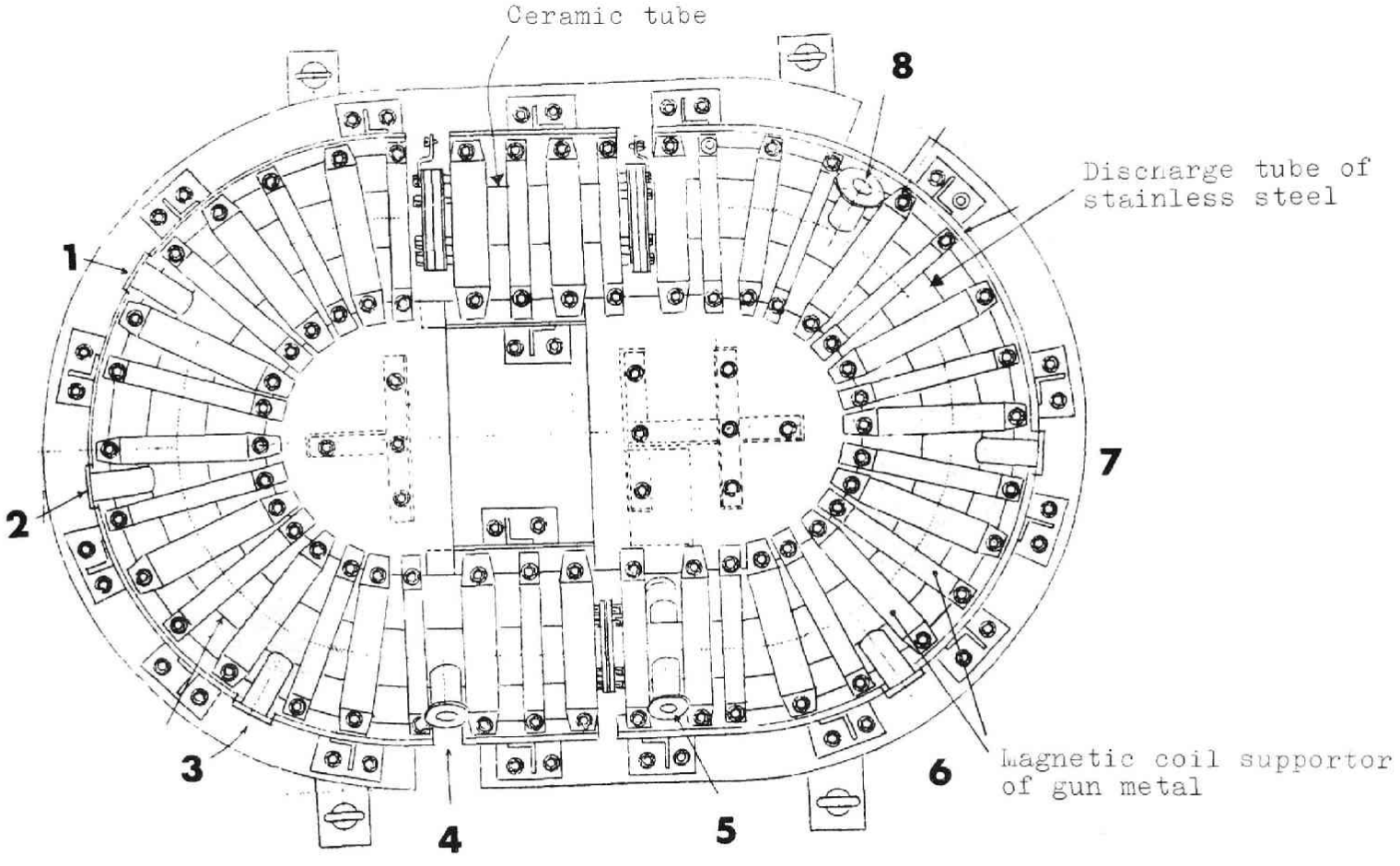

Fig. 6-1 Plane figure of the Heliotron-B without Joule heating windings.

legs of the race track shape. This ceramic break prevents the discharge tube from short-circuiting the heating transformer on the secondary side and provides a convenient section for the ion cyclotron heating. The torus radius of its curved part is 31.2 cm and the total axial length 2.96 m. The inner diameter of the discharge tube is 8.4 cm at the linear parts and 7.5 cm at the curved parts. The positive and the negative coils, which produce the Heliotron magnetic field, are supported by the gun metal supportors fixed on the angle-irons. The Joule heating windings which induce the accelerating field for the Joule heating are wound outside the gun metal supportors along the tube axis. Nine viewing ports for observation are also installed.

Pulsed confining magnetic field is used in the Heliotron-B. Energy storage for this field is obtained from a capacitor bank of 6.4×10^4 joules. This switching is performed by ignitrons M1-1200. Subsequent to the initial breakdown rf discharge, ionization is completed and the plasma is heated by means of a unidirectional axial electric field induced by the currents in the Joule heating windings. This heating current is also generated by the discharge of a condenser bank of 2×10^4 joules. The capacities and the charging voltages of condensers for the magnetic field and the Joule heating are decided according to the purpose of experiment. Fig.6-2 shows the discharging circuit of the condenser banks.

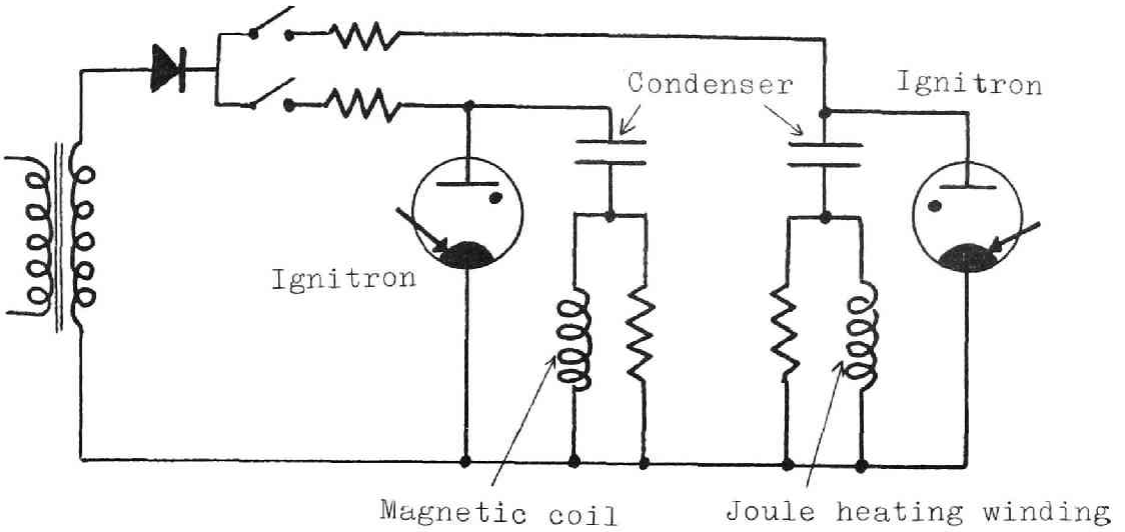

Fig. 6-2 Circuit for charging and discharging the condenser banks.

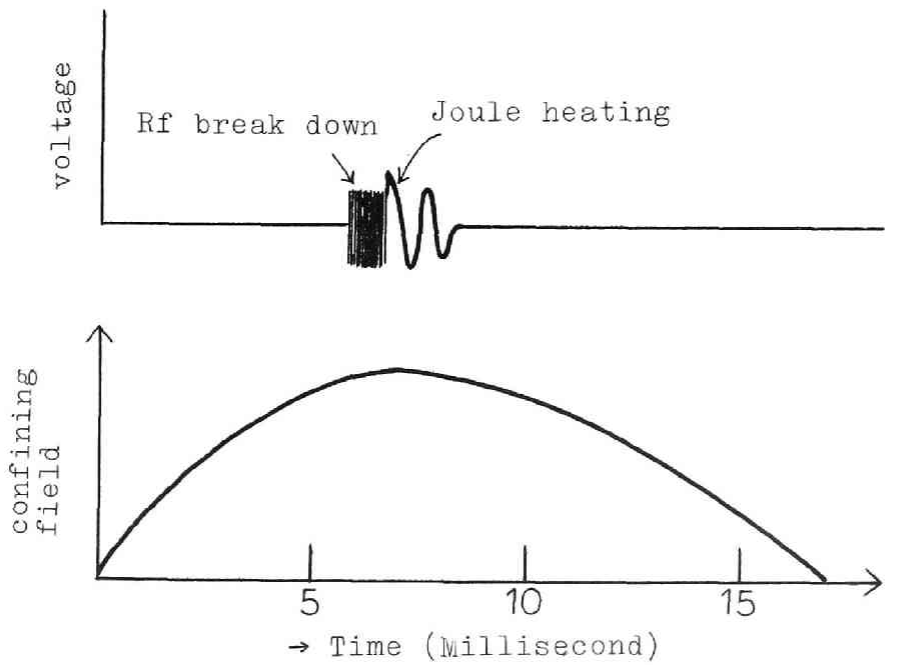

Fig. 6-3 Relative time scales of axial magnetic confining field and voltage externally applied to the Heliotron-B.

The relative time-scale and-sequence of the magnetic field confining, rf preheating and the Joule heating is shown in Fig. 6-3. Maximum current in the magnetic coil is about 500 amperes, and that in the Joule heating winding about 1.8×10^4 amperes. Slightly before the peak of the magnetic field current, the preheating rf field (10 megacycle. 1 kilowatt x 1 millisecond) is imposed. When the confining magnetic field becomes maximum, the Joule heating field is applied and produces a fully ionized gas at high electron temperature in the discharge tube. As described in the section 6.5, a collection winding for the Joule heating windings is also equipped to compensate the vertical field produced by the Joule heating windings. This correction winding is connected parallel to the Joule heating windings.

A neutral gas is let flow in the discharge tube through a controllable needle valve or a paradium leak, whereas a 4" oil diffusion pump is also continuously working. Therefore, the internal gas pressure is settled with the balancing between the gas inflow and the pumping-out speed and its range is from 10^{-2} to 10^{-4} Torr. Helium, Hydrogen and Deuterium are used. The vacuum obtainable is usually around 10^{-5} Torr. The pressure is measured with an ionization gauge for high vacuum and a pirany gauge for relatively high pressure.

The instantanuous Joule heating field is inferred from the voltage of the one turn loop along the tube axis. The plasma current is measured by means of movable Rogowski coils (toroidally wound pick up loops encircling the plasma) or fixed Rogowski coils, the output from which is electrically integrated.

Electron temperature is inferred from the relative strengths of related singlet and triplet lines in the neutral helium spectra, which is again to be discussed in the chapter VIII. Magnetic probes, Langmuir probes and a streak camera are also used for investigating oscillations and instabilities of the plasma. Electron density may be inferred from the phase-shift of a transmitted millimeter microwave beam, but this microwave method was not available to these experiments. Therefore, accurate electron density could not be measured unfortunately and only the results obtained from Langmuir probes uncertainly gave the density.

Ion temperature was measured by the author with a plane grating optical spectrometer, details of which will be described in the chapter VIII. This temperature could be inferred from Doppler broadening of spectral lines of ionized impurities.

An arrangement of these measuring apparatus and the Heliotron-E is schematically shown in Fig. 6-4. The outline of the Heliotron-E and diagnostic instruments is given in Table 6-1.

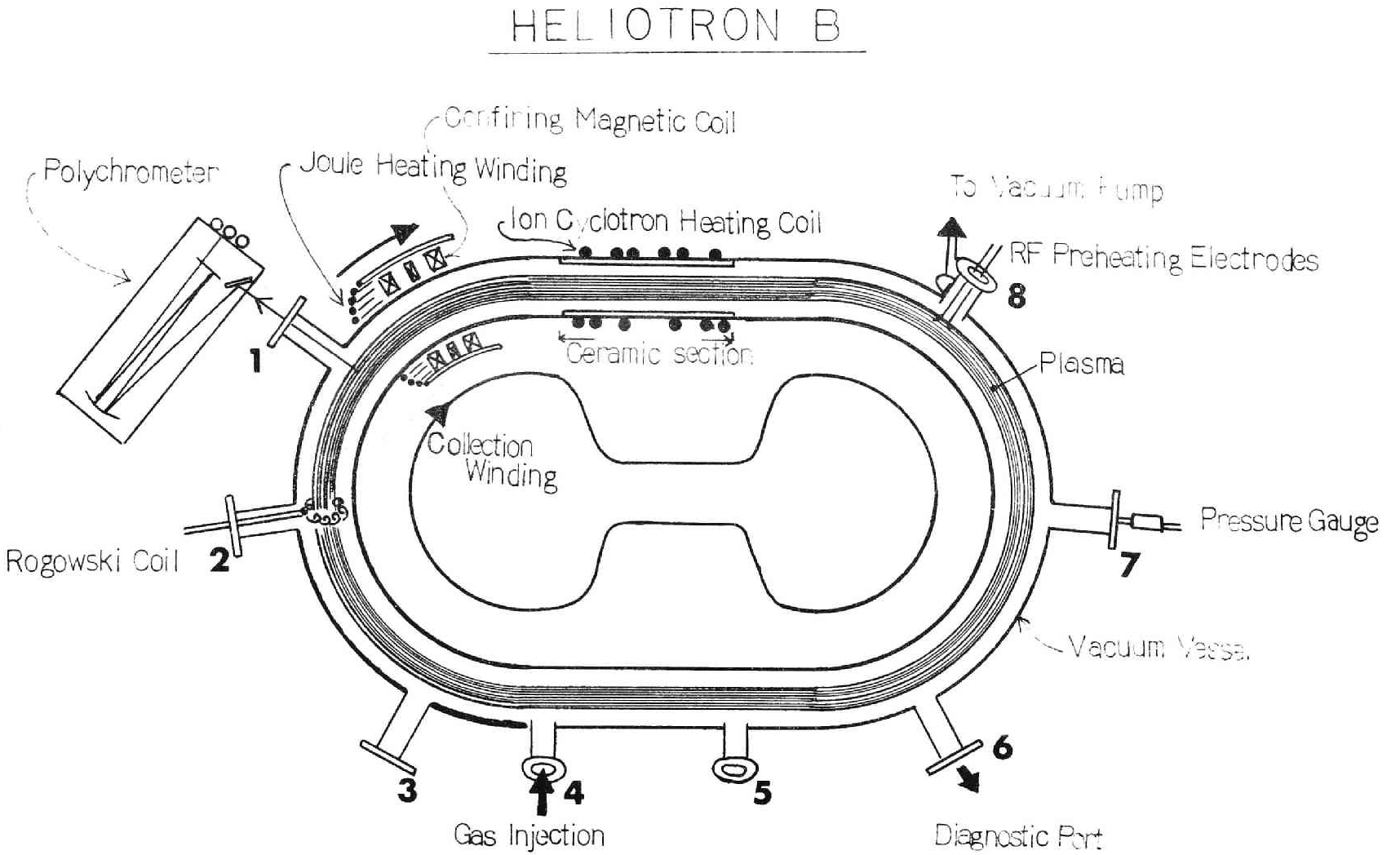

Fig.6-4 Simplified schematic drawing of the Heliotron-B.

Table 6-1 Outline of the Heliotron-B and diagnostic instruments

Heliotron-B

Magnetic coil	normal coil: 167 turns reverse coil: 84 turns } 20 pairs
Joule heating coil	10, 20, 30, 60 turns changeable
Discharge tube	race track type, stainless made linear part: 50 cm, radius of curvature: 312 mm^R, ceramic section: 330 mm, 11 obserbing ports: 40 mm^Φ
Vacuum system	Liquid oxygen trap + 4" oil diffusion pump + rotary pump
Condenser bank	1.4×10^3 μF, 84 kJ
Accelerating field	1.5 V/cm at max.
Magnetic field (on tube axis)	max: 5,000 gausses min: 500 gausses

Diagnostic Instruments

	Physical quantities or behaviours to be measured
Movable Rogowski coil	Current density (J)
Langmuir double probe	Electron density (Te)
Magnetic probe	Plasma oscillations
Double prism spectrometer	Electron temperature
Hilger qualtz spectrometer	Impurities
Small qualtz spectrometer	Survey of impurities
Plane Grating spectrometer	Ion temperature
Streak camera	Plasma oscillations

6.4 Experimental Results

In this section typical experimental observations of plasma behaviours under the Joule heating are summerized. Principal variables were the confining field, the Joule heating field (0.7 to 1.5 V/cm), and the initial gas pressure (10^{-3} to 10^{-1} Torr). Gases used were hydrogen and helium. The following discussion in this section refers to the operation without the correction for the Joule heating windings unless otherwise stated.

6.4.1 Total Plasma Current

As described in the section 6.5, the total plasma current was much affected with the confining field configuration and the correction for the Joule heating windings. The current rise, however, had little relation with the latter, since the vertical magnetic field due to the Joule primary current was weak still during the current rise. On the other hand, the current after its rise depended on the Joule heating primary current.

Rogowski coils encircling the plasma column were inserted in the discharge tube from the viewing ports and picked up the azimuthal magnetic field produced by the total plasma current. Therefore, the plasma current was inferred from the electronical integration of the Rogowski coil signal.

Upon application of the Joule heating field, the

growth rate of the plasma current depended on the heating field strength and the confining magnetic field strength. Figs. 6-5 to 6-7 show representative cases for hydrogen discharge. For helium discharge Figs. 6-8 to 6-10 are also given. The plasma current in each case was measured at the port 1 in Fig. 6-4 and the correction winding did not work. From these experiments, following facts became evident.

(i) In weak confining field, as shown in Fig. 6-5 or 6-8,
  (a) the current could grow only in high heating field;
  (b) the first peak of the current was low in its value and irreproducible;
  (c) the second peak of the current was relatively high in low heating field, but, in high heating field, it became rather lower and decayed more rapidly from its peak as indicated with an arrow in Fig. 6-5.

(ii) In strong confining field, as shown in Fig. 6-7 or 6-10,
  (a) the current could grow in relatively low heating field;
  (b) its first peak value was also large even in low heating field and the reproducibility of peak value was fairly good;
  (c) the second peak decayed more slowly than in weak confining field.

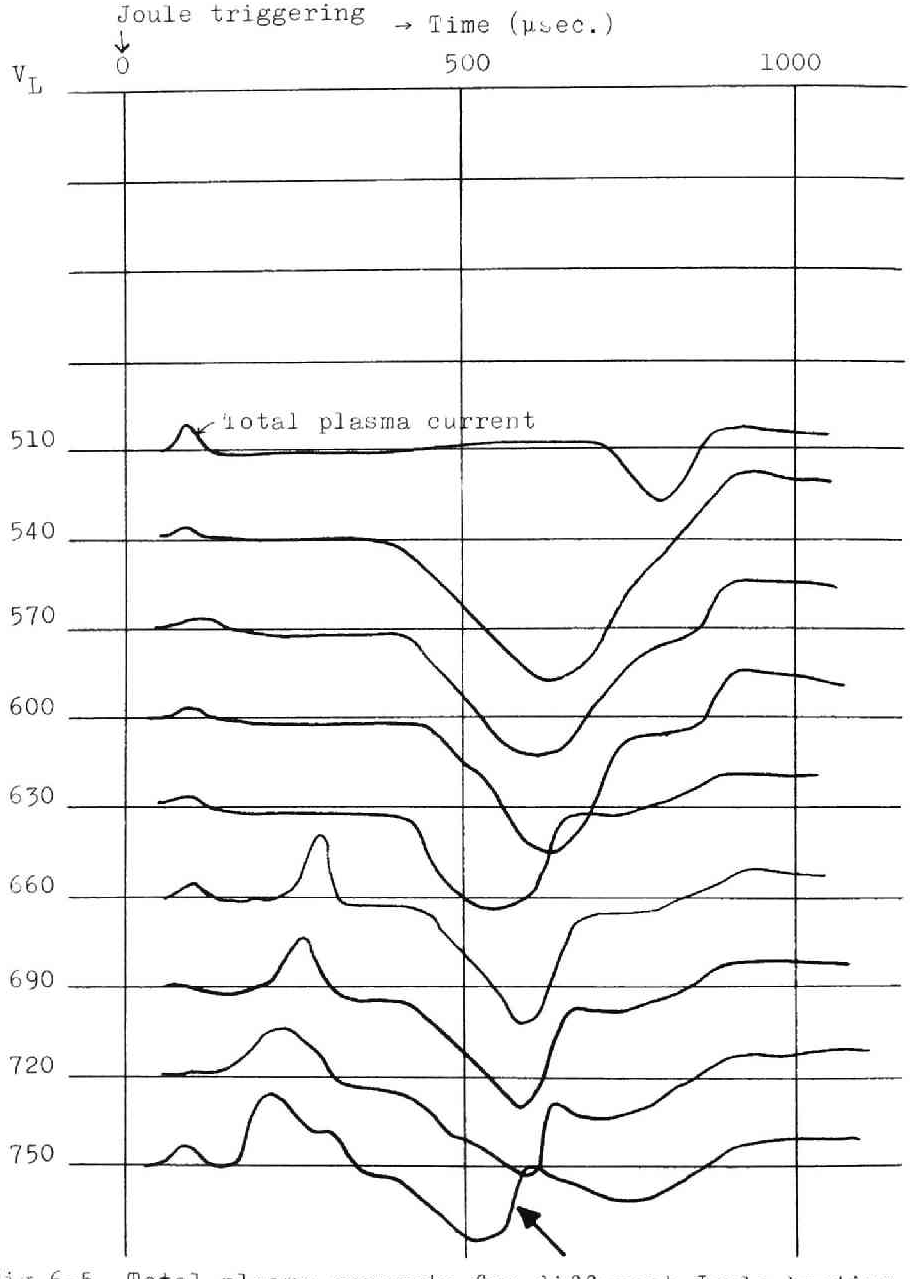

Fig.6-5 Total plasma currents for different Joule heating fields.
Average magnetic field: 1300 G,
Pressure: 6×10^{-3} Torr(H_2),
V_L: Maximum one turn loop voltage around the torus.

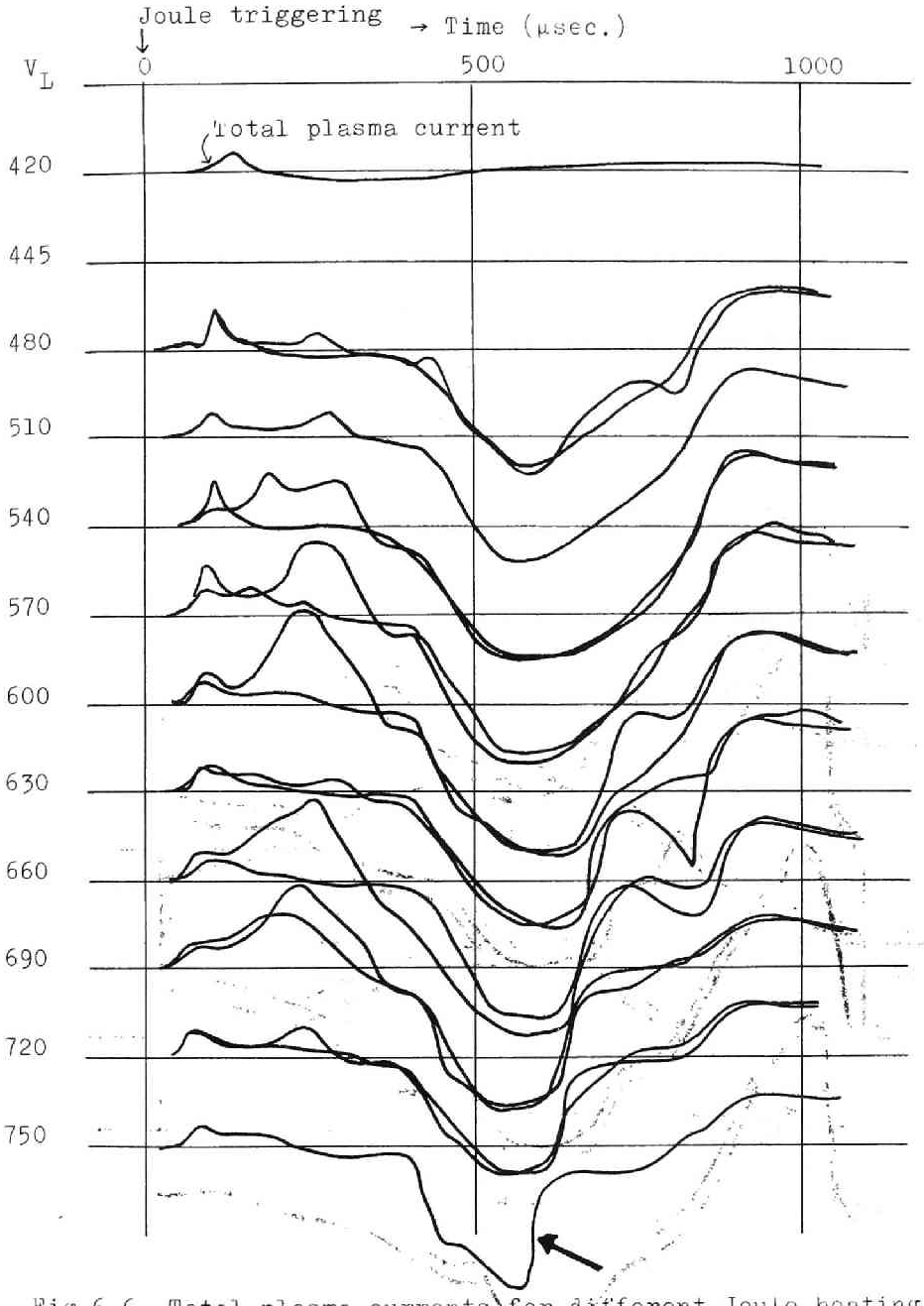

Fig.6-6 Total plasma currents for different Joule heating fields.
Average magnetic field: 2000 G,
Pressure: 6×10^{-3} Torr(H_2).
V_L: Maximum one turn loop voltage around the torus.

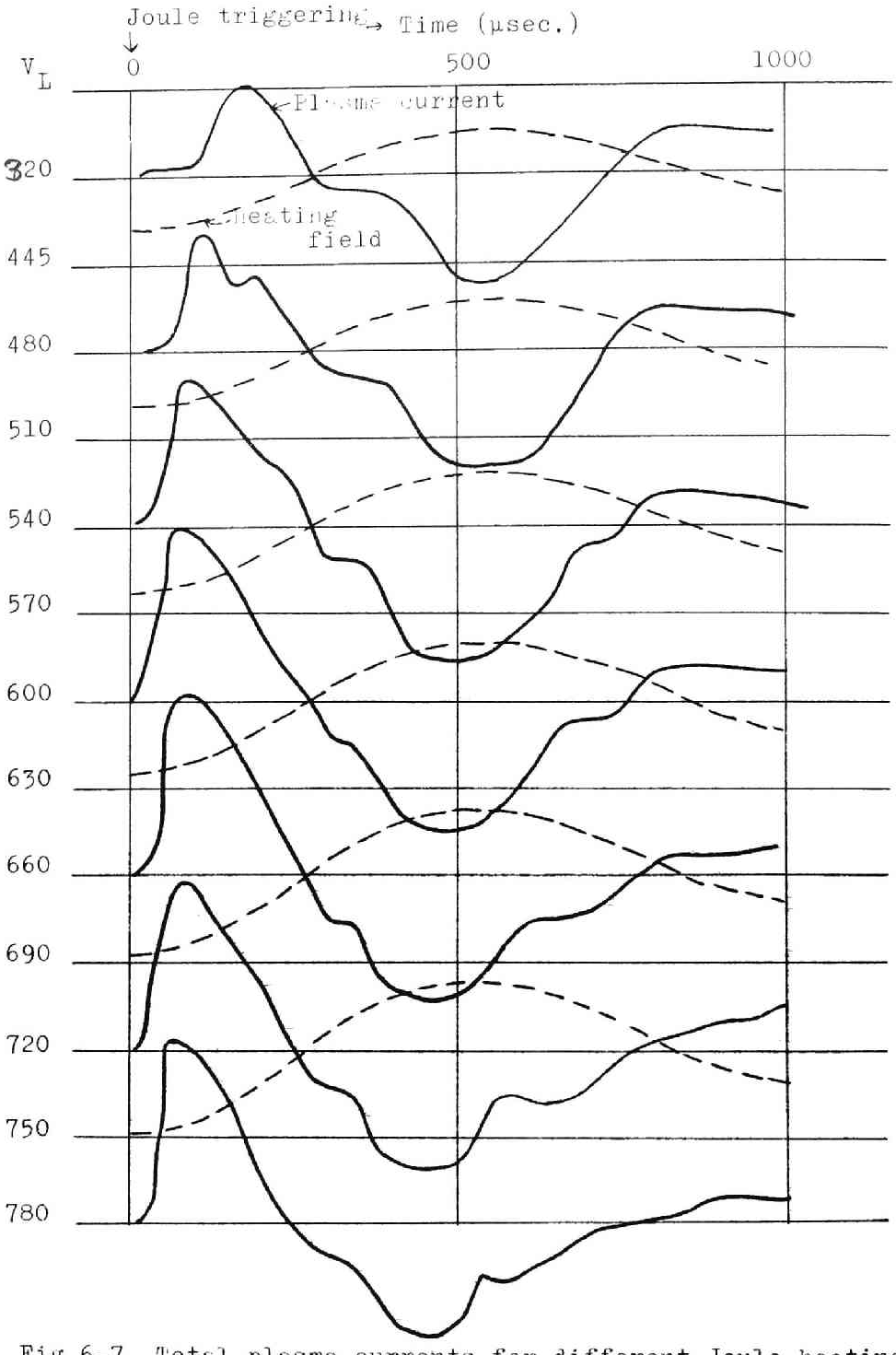

Fig.6-7 Total plasma currents for different Joule heating fields.
Average magnetic field: 3000 G,
Pressure: 6×10^{-3} Torr(H_2).
V_L: Maximum one turn loop voltage around the torus

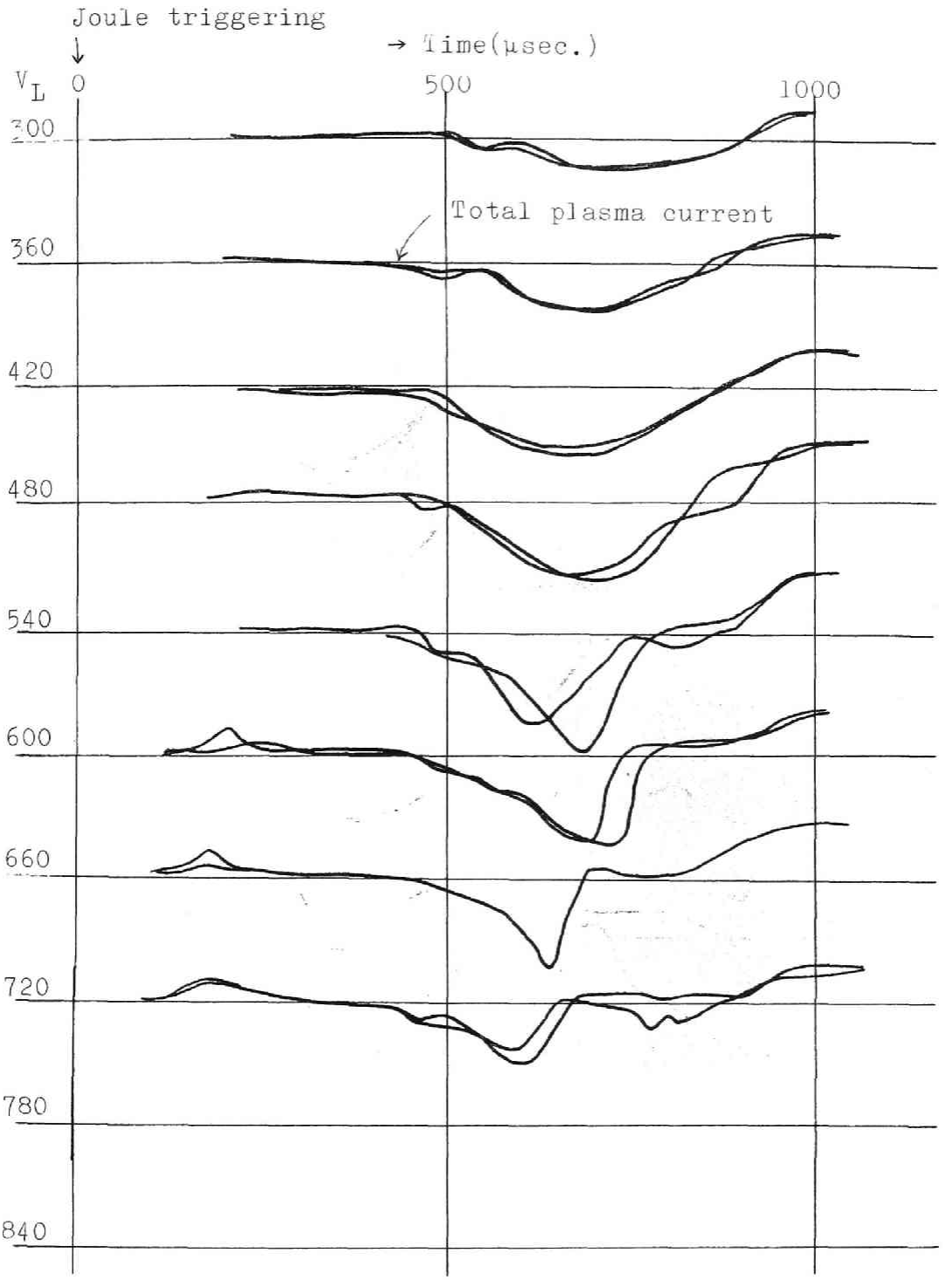

Fig.6-8 Total plasma currents for different Joule heating fields.
Average magnetic field:1300 G,
Pressure:6×10^{-3}Torr(He).
V_L: One turn loop voltage around the torus.

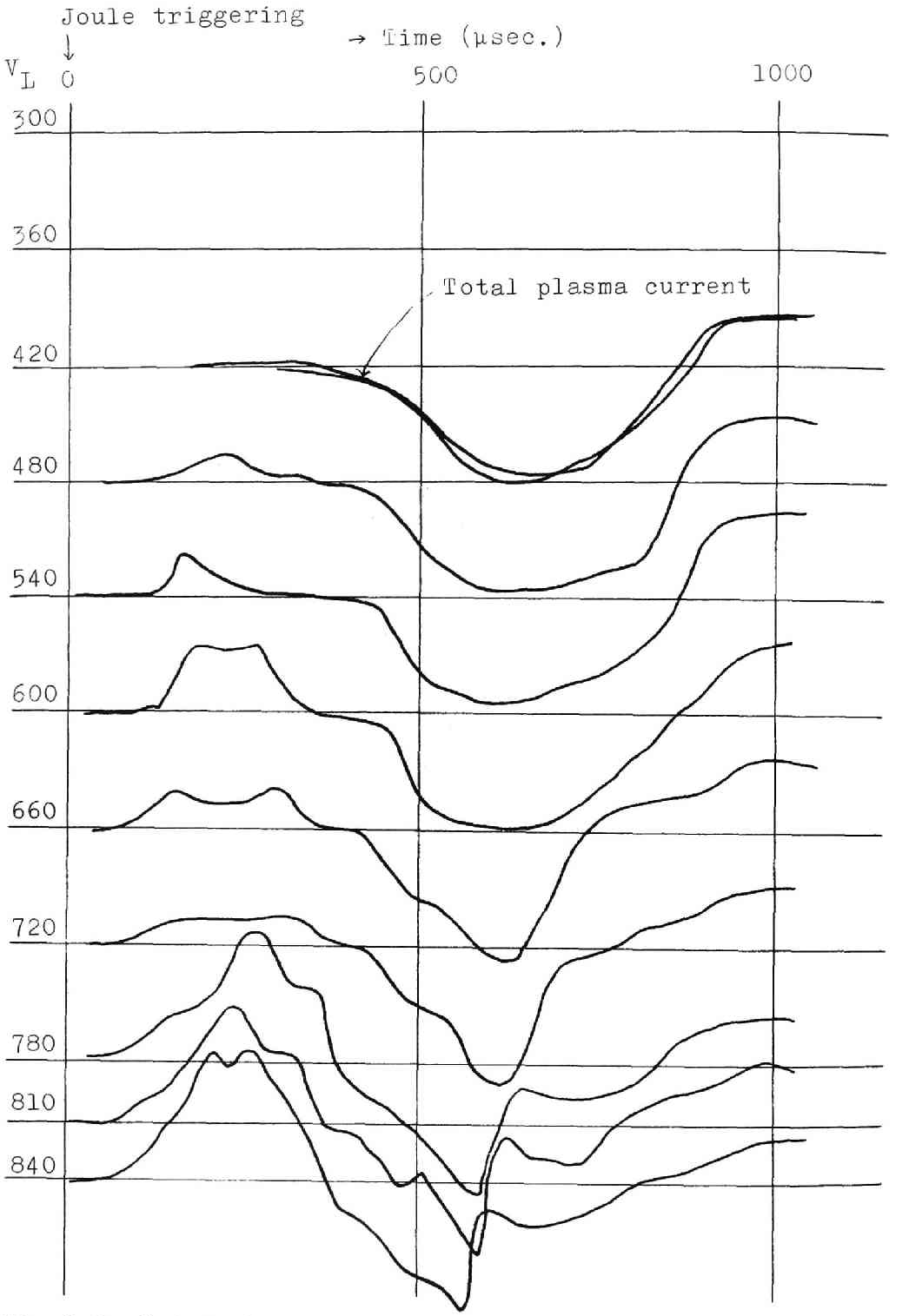

Fig.6-9 Total plasma currents for different Joule heating fields.
Average magnetic field: 2000 G,
Pressure: 6×10^{-3} Torr(He).
V_L: Maximum one turn loop voltage around the torus.

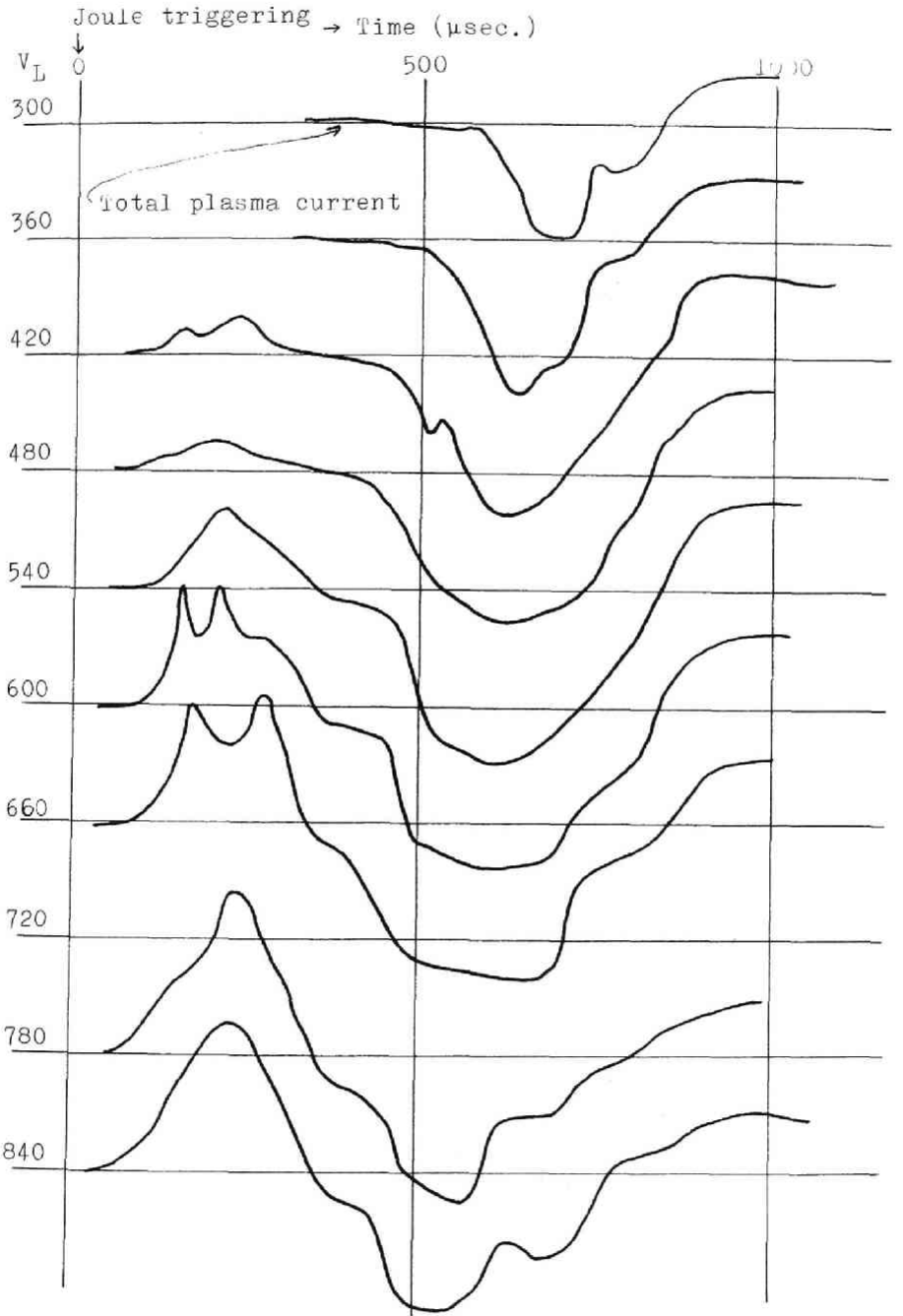

Fig.6-10 Total plasma currents for different Joule heating fields.
Average magnetic field: 3000 G,
Pressure: 6×10^{-3} Torr (He).
V_L: Maximum one turn loop voltage around the torus.

The facts (a) in both cases may be ascribed to break down conditions for discharge, which are governed by the balance of diffusion and production of charged particles. Other facts (b) may be due to the confining effect of the field. The phenomena intimated by (c) implies there may be a instability like Kruskal instability or other causes. Afterwards, this was found to be due to the vertical magnetic field produced by the primary current for the Joule heating. This magnetic field is perpendicular (vertical) to the torus plane and bends the magnetic lines of force to the tube wall. Consequently, particles moving along the lines of force impact the tube surface, especially where the confining field is weak. This leads to the inflow of the current into the stainless tube. The rapid decay of the second peak of the current may originate in such a inflow of current. Detail discussions of the vertical field will be again given in the section 6.5.

6.4.2 Average Current-Density Distribution

Movable Rogowski coils were used to measure the plasma current distribution. As shown in Fig. 6-13, the coil was wound around a vinyl tube of 3 mm diameter and inserted in a ring glass tube, whose inner and outer radii were 10 and 17 mm. The glass tube is fixed at the end of the movable probe holder. The measuring ports were 1 to 6 in Fig. 6-4.

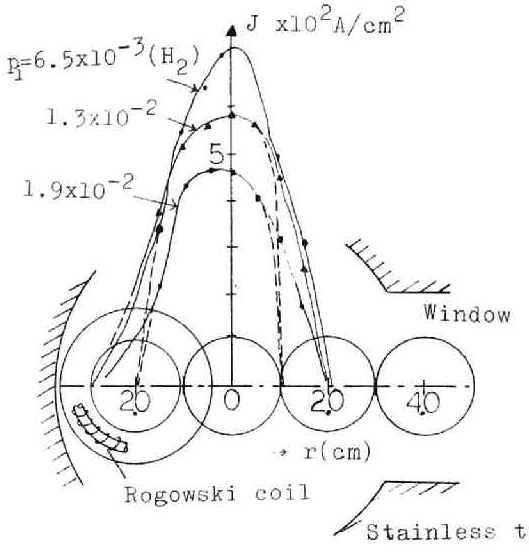

Fig. 6-11 Average plasma current density distribution in the Heliotron field.
p_i: initial gas pressure in Torr

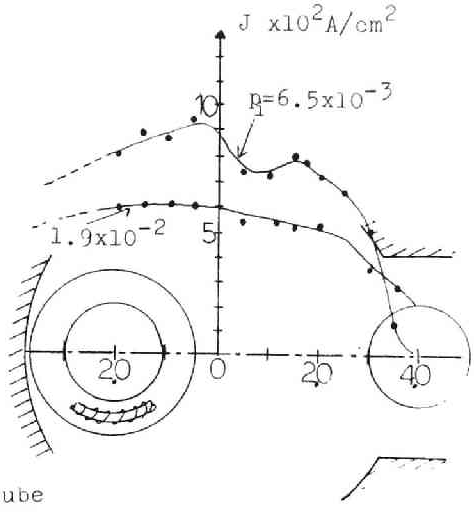

Fig 6-12 Average plasma current density distribution in the Toroidal solenoid field.

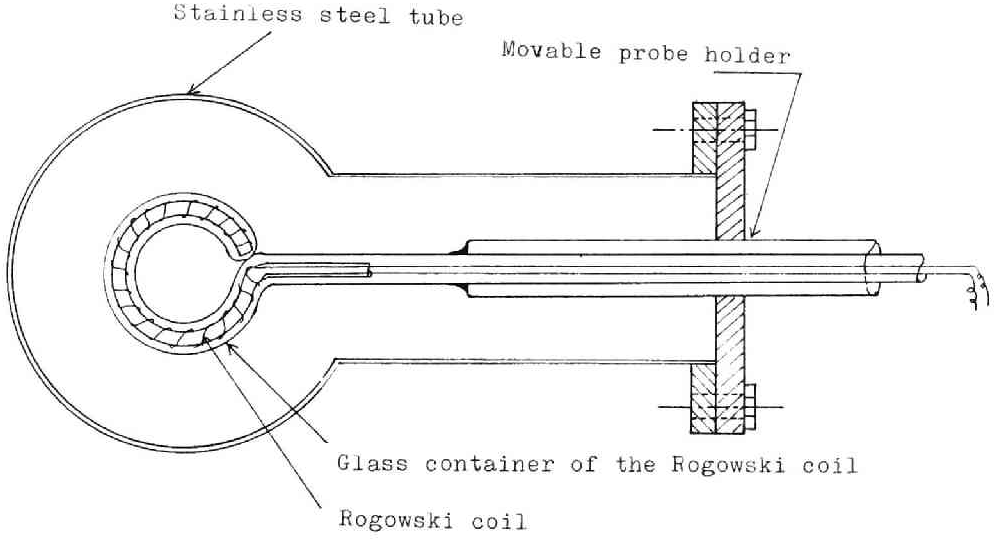

Fig. 6-13 Movable Rogowski coil detecting plasma current.

A representative result obtained is shown in Fig. 6-11. The measuring position was at the port 1. In this figure $\vec{J}$ represents the average current density in the region of the aperture of the Rogowski coil. The magnetic field intensity on the tube axis was 5000 gausses under the positive coil and 800 gausses under the negative coil. The movable Rogowski coil inserted into the plasma region detected the current passing through the aperture of the coil container.

The maximum value of the current density was near the tube axis and decreased with the radius r. Finally the current density became zero near the position r=20 mm. There was no current signal in the outer region from r≃20 mm. Therefore, the real current-density distribution can be represented by the broken lines in Fig. 6-11.

The average current-density distribution in the toroidal solenoid field is as shown in Fig. 6-12. The curves show that the current flux existed even in the vicinity of the tube wall.

Such tendency of the current-density distribution could be observed in the case with the correction for the vertical field. Therefore, it may be concluded that the concentration of the plasma current near the axis is an important characteristic of the Heliotron field.

6.4.3 Plasma Temperature

Electron temperature of the plasma Te was determined from the relative strengths of related singlet (4922 Å) and triplet (4713 Å) lines in the neutral helium spectra. This measuring technique will be explained in the chapter VIII.

The maximum value of the electron temperature was about 5×10^5 °K under the Joule heating. Time variations of the electron temperature measured at a port much depended on the direction of the plasma current and the magnetic field strength, even under working of the correction winding. This might be due to the lack of uniformity of the Joule heating field.

The ion temperature of the plasma was determined from the Doppler broadening of a singly ionized carbon line (4267 Å). A plane grating spectrometer (8 Å/mm) was used and line widths were inferred from the photographs of line images. However, this technique was difficult and only the time-integrated value could be known.

The ion temperature under the Joule heating was 1×10^5 °K or less.

6.4.4 Spectra of Impurities

In order to verify the spacial confinement of the plasma in the Heliotron magnetic field, the

impurity lines in the spectra from the plasma were investigated.

Many impurity lines could be observed, such as OII, OIII, NII, CI, CII, CIII, FeII, CrII and MnII. The spectral lines of O, N, and C are supposed to originate from the impurities in the gas or in the backflow of vapour from the oil diffusion pump, whereas the lines of Fe, Cr, and Mn from the wall material.

When the correction winding worked, intensities of these impurity lines from wall material could be reduced. Similarly, the outgas detected by an ionization gauge was reduced in this case.

Therefore, the existence of the lines of Fe, Cr and Mn might be due to the intersections of the magnetic lines of force within the N.L. surface with the tube wall. These intersections would be caused with the bend of the lines of force by the vertical field or the irregurality of the coil interval.

Impurity lines emitted from the plasma in the toroidal solenoid field discharge were stronger in intensity than in the Heliotron magnetic field. This fact may be interpreted in terms of the current distribution in the discharge tube; that is to say, high energy electrons are apt to bombard the tube wall in the solenoid field compared with in the Heliotron field.

6.5 Correction for the Toroidal Joule Heating Windings

The Joule heating windings wound around a toroidal discharge tube as shown in Fig. 6-14 had been adopted in the Heliotron-A. It is generally believed that such sorts of windings would generate a good coupling between the currents in the windings (i.e. primary currents) and the plasma current (i.e. secondary current).

However, it was found there is an inevitable defect of the field deformation in the Heliotron field: the currents flowing with a certain curvature in the toroidal windings produce a magnetic field perpendicular to the plane of the torus (vertical field). This point has been overlooked, since, in the case of a straight cylinder, the sheet currents flowing parallel to its axis produce no magnetic field inside the cylinder.

The vector force generated as the vector product of the plasma current and the transverse field pushes the plasma column to the discharge tube and disturbs the equilibrium conditions of plasma confinement.

Fig. 6-16(a) shows the magnetic lines of force produced by the currents flowing with the same magnitude in each winding. This result was obtained by an axially symmetric magnetic field simulator[38]. The dots in the figure denote the cross section of the Joule heating windings and the solid lines are the magnetic

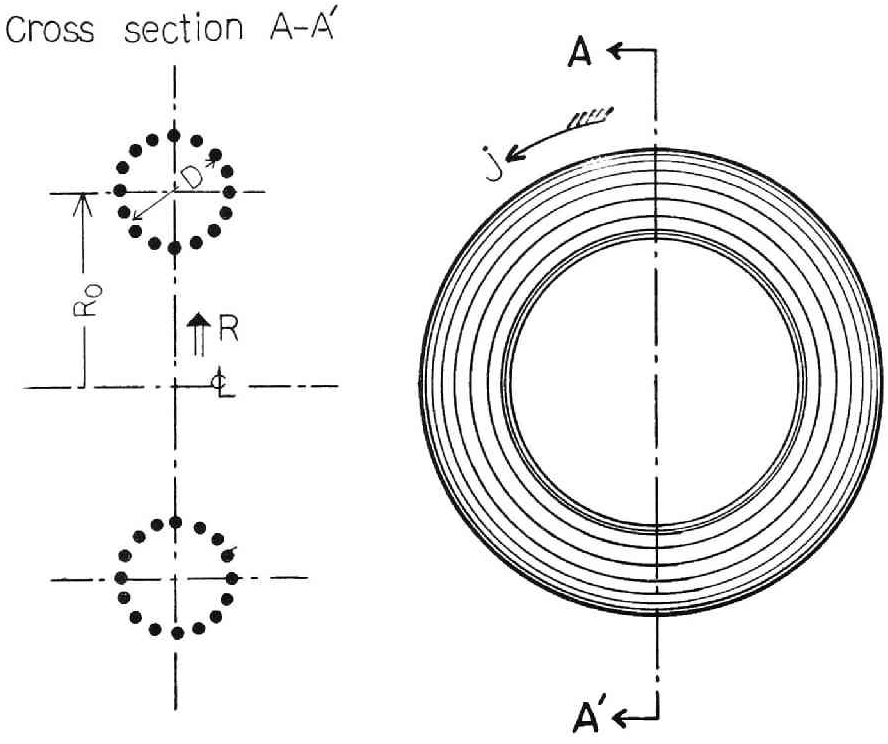

Fig.6-14 Schematic diagram of the toroidal Joule heating windings.

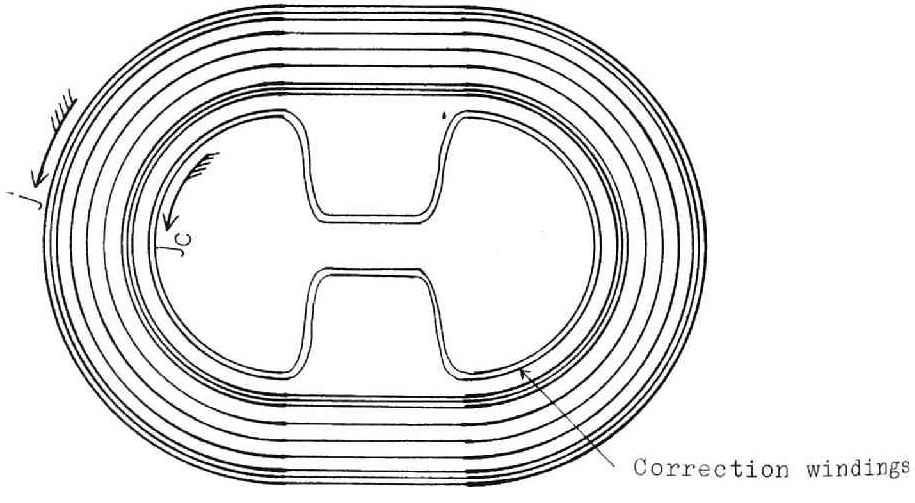

Fig. 6-15 Configuration of correction windings applied to Joule heating windings of a race-track shape.

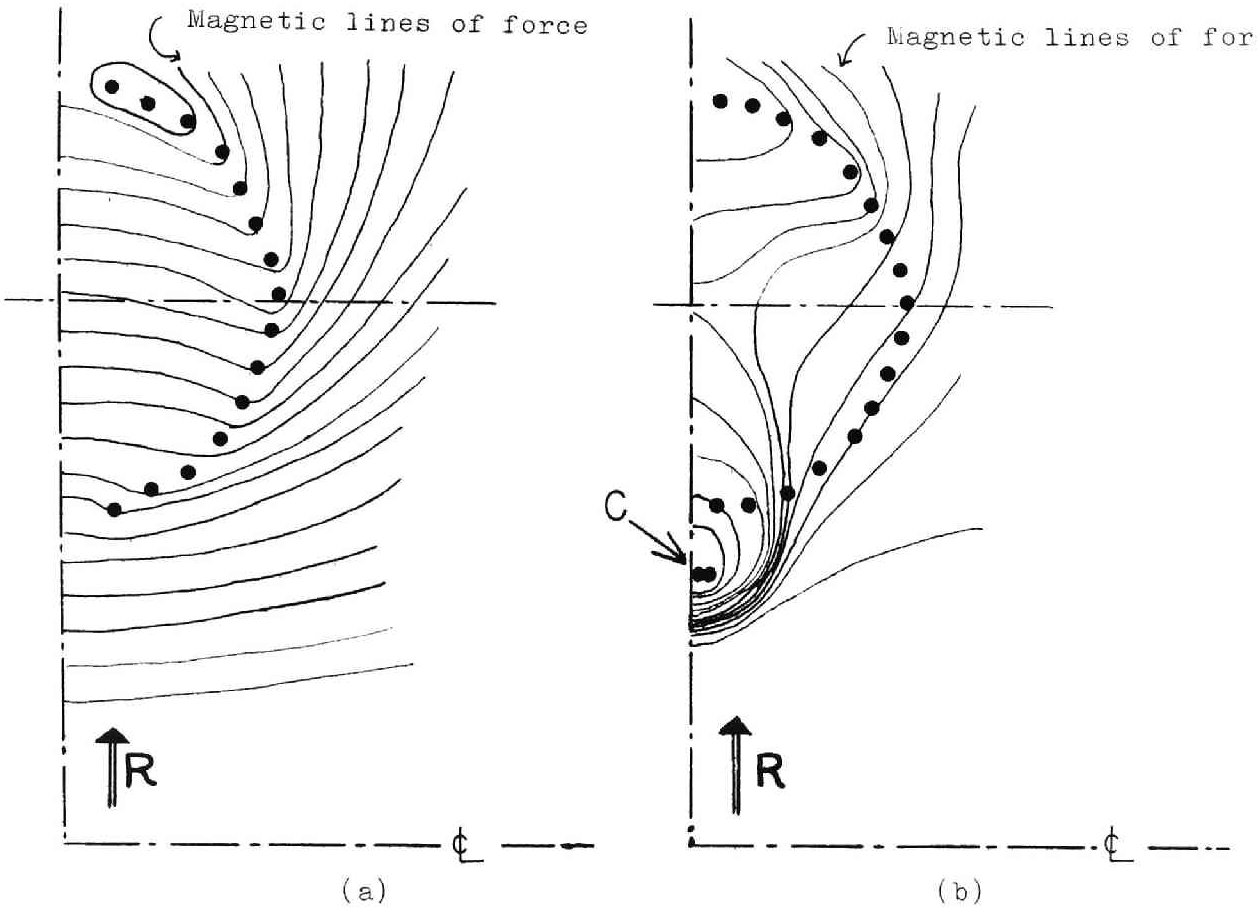

Fig.6-16 Results of the axially symmetric magnetic field simulator.
(a) without correction winding .
(b) with correction winding which is shown by point C in this figure.

lines of force. For example, under the condition that Ro=30 cm, D=25 cm and the total ampere turns of the currents is 1.5×10^5, the field on the tube axis becomes 1.2×10^3 gausses.

To avoid the defect of this curvature effect, several methods may be considered.

(i) To add the auxiliary compensating current to the uniform configuration of the primary currents. This method was adopted in the Heliotron-B.

(ii) To use a proper distribution of primary currents such that the vertical field vanishes.

(iii) To adopt iron-cores instead of the windings on the toroidal discharge tube. This method is adopted in the Heliotron-C, which is now under construction.

The correction winding in the case (i) is shown as the point C in Fig. 6-16 (b), and the current in it should flow with appropriate magnitude in the same direction as the primary currents. It can be found that there exists a region where the transverse field vanishes, but in all region within the discharge tube the field can not be cancelled out.

If the discharge tube has a race-track type as the device Heliotron-B, the configuration of such a correction winding becomes somewhat complicated and should be shaped like a dumb-bell. This configuration

adopted in the Heliotron-B is shown in Fig. 6-15. In practice, the shape was decided by the experimental procedures, and as the final result the magnetic flux density of the transverse field could be reduced less than 10 gausses over the discharge region.

6.5.1 Effect on Impurities

Experiments on plasma confinement and heating with the Heliotron-B showed that this correction winding works very effectively and contacts of the plasma with the tube wall resulting from the vertical field becomes slight compared with the case without the correction.

In practice, spectral lines of impurities could become weak with the correction, due to the diminution of the contacts of the plasma with the tube wall. Fig. 6-17 shows the microphotometric trace of the spectrograph taken with the double-prism spectrometer, when the correction winding did not work. On the other hand, Fig. 6-18 shows the case with the correction. In both cases, a mixture of hydrogen and helium was used and their pressure components were 1.7×10^{-3} Torr (H_2) and 5×10^{-4} Torr (He). On comparison, impurity lines without the correction turned out to be more and stronger than those with the correction. Such a tendency was observed in all cases.

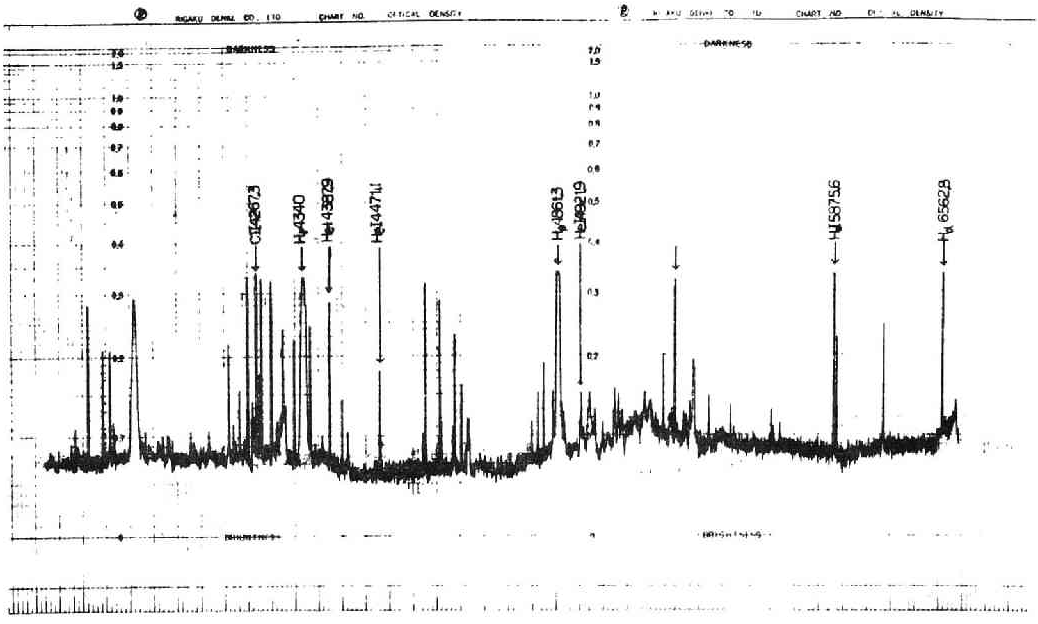

Fig. 6-17 Microphotometric trace of the spectrograph of plasma under the Joule heating. The correction winding is not working.
p_o=1.7x10^{-3}Torr(H_2)+5x10^{-4}Torr(He),E_J=1.0 V/cm.

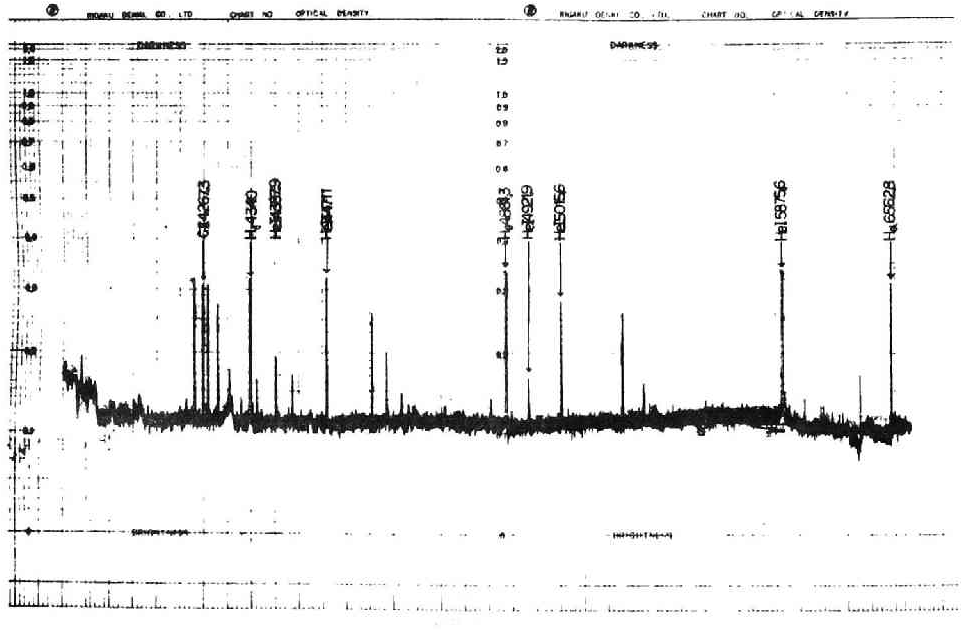

Fig. 6-18 Microphotometric trace of the spectrograph of plasma under the Joule heating. The correction winding is working.
p_o=1.7x10^{-3}Torr(H_2)+5x10^{-4}Torr(He),E_J=1.0 V/cm.

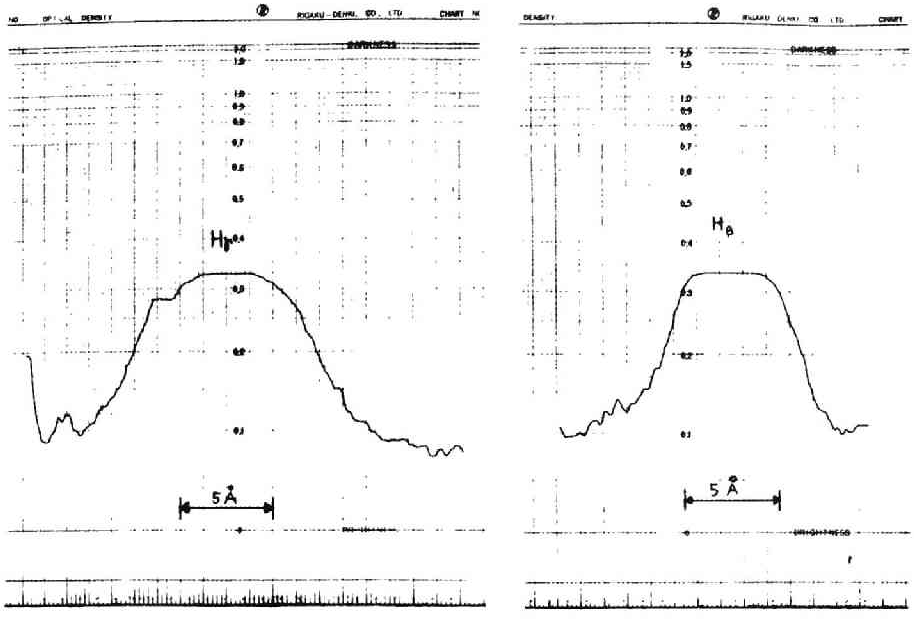

Fig. 6-19 Line profiles of H_β and H_γ under the Joule heating.. The correcting winding is not working.
p_o=1.7x10^{-3}Torr(H_2)+5x10^{-4}Torr(He),E_J=1.0V/cm.

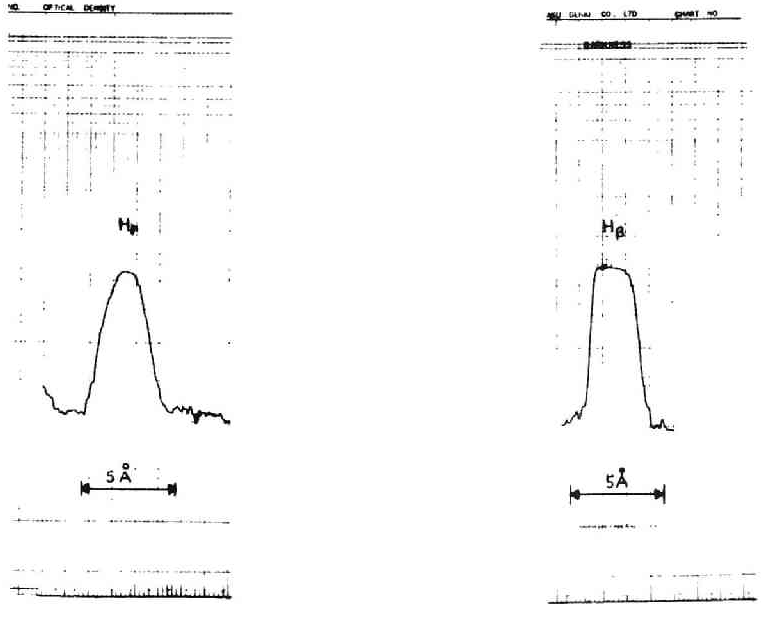

Fig. 6-20 Line profiles of H_β and H_γ under the Joule heating. The correcting winding is working.
p_o=1.7x10^{-3}Torr(H_2)+5x10^{-4}Torr(He),E_J=1.0V/cm.

6.5.2 Effect on Outgas

Another remarkable effect of the correction for the Joule windings could be seen in the outgas from the tube wall.

If a plenty of outgas of hydrogen flows into the plasma region, then the plasma density will increase and lines of Balmer series will be broadened due to Stark effect.

Even for an initial gas pressure, the widths of H_β and H_γ lines in the case without the correction became considerably broader than in the case with the correction. Figs. 6-19 and 6-20 show examples of them. Of course, this effect was fairly dependent upon the antecedents of the discharge. After many discharges, the outgas would become imperceptible.

6.6 Conclusion

In the Heliotron magnetic field, the hot plasma current is concentrated in the central region of the discharge tube. Therefore, the neutral lines (the N.L.) may be regarded as aperture limiters of the plasma.

The correction winding for the Joule heating windings works very effectively to reduce impurites and the current inflow into the stainless tube. However, perfect correction can not be expected by this correcting method.

The Joule heating in the Heliotron field can raise the electron temperature of plasma to fairly high temperature (5×10^5 °K) but cannot raise the ion temperature sufficiently.

Many oscillations of plasma are apt to be generated, but detail discussions on them cannot be made because of the constructive defects of the Heliotron-B device.

VII Experiment on Ion Cyclotron Absorption of Plasma in the Heliotron-B device

7.1 Introduction

In this chapter, experiments on excitation of ion cyclotron waves and single-particle ion cyclotron resonance are to be described.

Ion cyclotron waves with an axisymmetric mode was first observed by Stix and his coworkers[7] (1958) by using the B-65 Stellarator of Princeton University. They came to this conclusion from an asymmetry of rf absorption curves of plasma. Afterward, they gave direct evidence[19] (1960) for the existence of these waves by measuring the rf field of the waves in plasma excited by an induction coil, which was energized at 11.5 Mc with approximately 200 kilowatts of rf power. Duvovoi, Shvets and Ovchinnikov (1959)[32] observed the plasma loading of an induction coil due to ion cyclotron resonance, where the plasma was not highly ionized. Bakaev, Zaleskii, Mazarov, Ukrainskii and Torok(1962)[39] observed the generation and absorption of ion cyclotron waves in a moving plasmoid ejected from a plasma gun. Bakaev et al also observed a Doppler effect occuring from the plasmoid velocity. The author (1963)[40] found from the measurement of rf power absorption that there appear many beams of ions in the plasma under the Joule

heating in the Heliotron-B, by using such a Doppler shift.

Plasma under the Joule heating may have beam-like ions and, as a result , the ion cyclotron absorption may be shifted in frequency from the ion cyclotron frequency due to a Doppler effect, as predicted in the chapter II or III. Since the plasma density in the Heliotron-B is attainable to considerably higher value than in the Stellarators of Princeton University, the rf absorption resulting from the excitation of ion cyclotron waves is expected to be clearly distinguished from the single-particle cyclotron resonance absorption. This separation between both absorptions will give a clear evidence for the existence of ion cyclotron waves in plasma.

The experiment described herein was made so as to get basic and preliminary information on the ion cyclotron heating of plasma in the Heliotron-B. For this purpose, the following subjects were investigated.

(i) The existence of ion cyclotron waves

(ii) The distribution of ion velocity

(iii) The efficiency for exciting ion cyclotron waves

The plasma to be excited with ion cyclotron waves was generated by the Joule heating. The existence of the ion cyclotron waves may be inferred from the rf absorption curves, from which beam velocities of ions may be also

determined.

A frequency sweeping method was adopted to get such rf absorption curves, so that properties of plasma were never disturbed during the observation. On the contrary, magnetic sweeping methods adopted by Stix or Duvovoi are apt to change the plasma property itself, since it is generally much dependent of the confining field.

In the subsequent section 7.2, the experimental apparatus will be explained. Experimental results are also given in a section 7.3. The major conclusion drawn from these results will be summarized in a section 7.4.

7.2 Experimental Procedure

A rf coil for exciting ion cyclotron waves was installed to the Heliotron-B after some investigations of the Joule heating of plasma. The Heliotron-B with this exciting rf coil is shown in Fig. 6-4 with a simplified drawing. The rf coil was set on the ceramic break at one straight leg of the race track tube. The magnetic coil in this section was renewed to make uniform magnetic field. Fig. 7-1 shows the sectional diagram of these renovated parts. A detecting circuit of the rf power absorption due to the excitation of the waves is connected to the rf coil. Detail explanation of each part is given as follows.

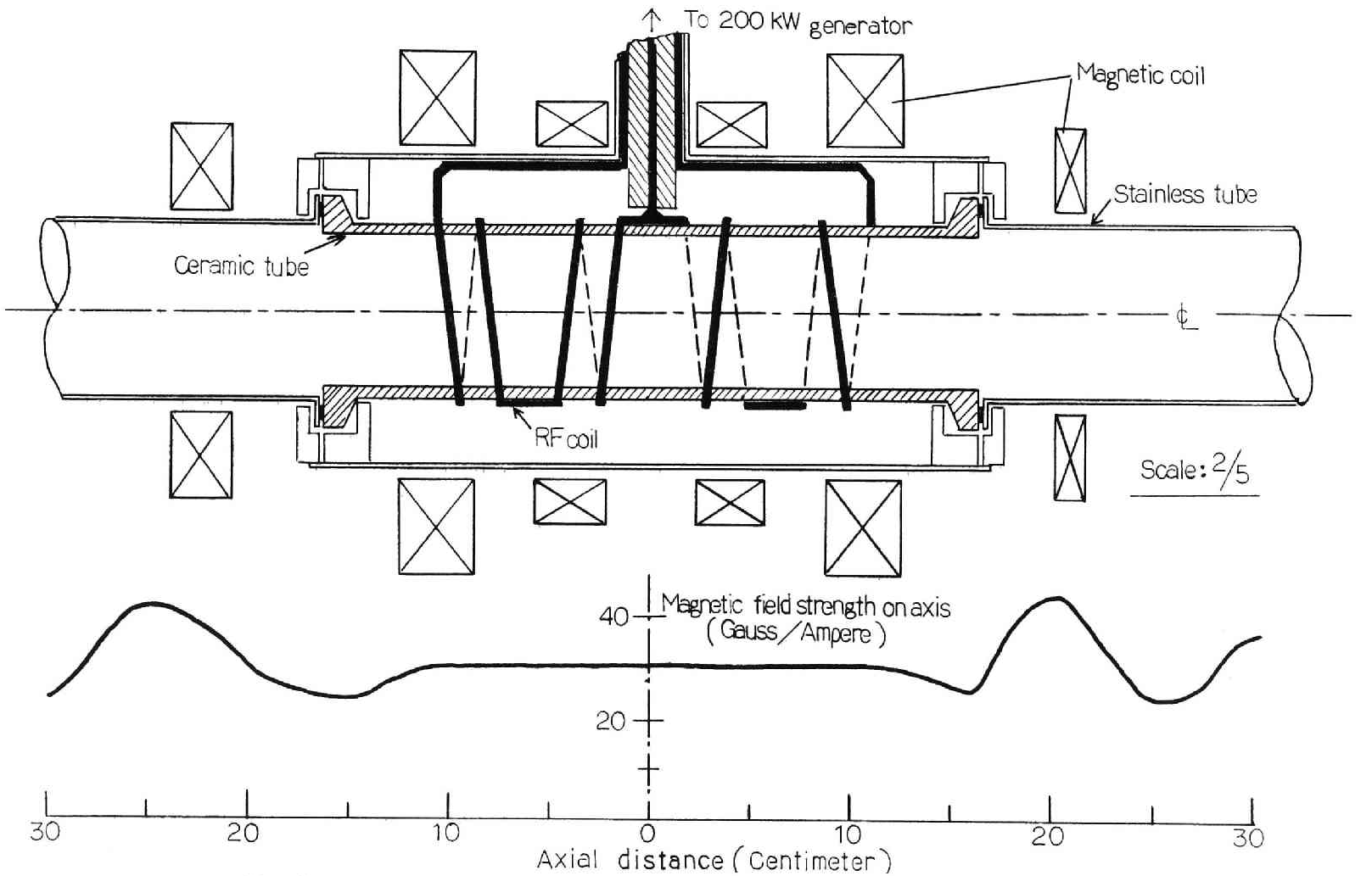

Fig. 7-1 Sectional diagram of the ion cyclotron heating section of the Heliotron-E device. Also shown is the magnetic field strength in the axial direction.

7.2.1 Rf coil and Magnetic Field

The rf coil is wound around the zircon ceramic tube, which was inserted for preventing a short-circuiting the stainless tube under the Joule heating. The rf coil is made of a gold-plated copper lod of 8 mm in diameter, and it shapes so that the azimuthal direction of the rf current alternates every 1 1/2 turns at the axial interval of 6 cm, as shown in Fig. 7-1. Thus, the coil imposes an axially periodic perturbation on plasma over a range of two wave lengths of 24 cm. The hot rf lead is connected to the centre tap of the coil, and two ends of the coil are connected to a grounded tube, which forms a co-axial line with the hot rf lead. An insulator between the hot lead and the outer tube is made of polyethylene and helps to prevent arcing at the high voltage up to 50 kilo-watts. The rf coil is enclosed with a stainless tube of thickness 2 mm for rf shielding.

In order to excite a simple axisymmetric ion cyclotron waves, the magnetic field in the rf coil region is desired to be uniform. The magnetic coils for this sake were designed with the axially symmetric magnetic field simulator[38] and their shapes and positions were determined as shown in Fig. 7-1. The coils of 2 mm copper wire are impregnated with Epoxi regin. These coils are connected in series with the other

Heliotron magnetic coils. The uniformity of the magnetic field in the rf coil region is within ± 2%. This uniform magnetic field smoothly continues the Heliotron magnetic field as shown in Fig. 7-1.

Excited ion cyclotron waves in the rf coil region propagate along the axis into the corrugated magnetic field of the Heliotron and disappear due to the phase maxing (or magnetic beach effect), as explained in the chapter III. In other words, the oscillating energy of the waves is converted into thermal energy of plasma. The ratio of the minimum value of the Heliotron magnetic field to the uniform field strength in the rf coil region is ~~above~~ less than 1/4, so that ion cyclotron waves in considerably higher density of plasma can be thermalized. This is one of distinctive characteristics of the Heliotron field.

Fig. 7-2 shows a photograph of the assembly of the rf coil, the ceramic tube, the magnetic coil and shielding stainless tube. Fig. 7-3 shows a close up of the rf coil wound around the ceramic tube. A photograph of the heating section attached to the Heliotron-B device is shown in Fig. 7-4, where the Joule heating windings are not installed.

7.2.2 Detecting Method of the RF Absorption of Plasma

As stated in the introduction, the detecting method of rf absorption of plasma in this experiment belongs